

AD-A164 056

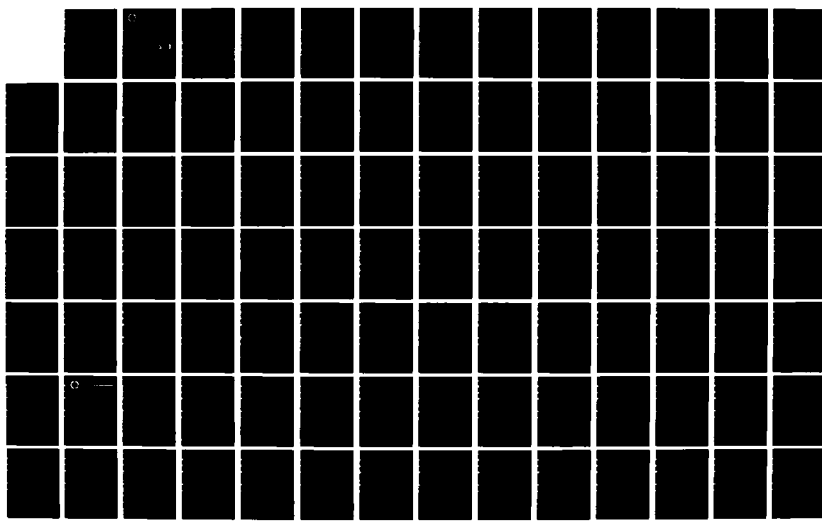
ULTRASONIC NONDESTRUCTIVE EVALUATION OF DAMAGE IN
CONTINUOUS FIBER COMPOS (U) TEXAS A AND M UNIV COLLEGE
STATION MECHANICS AND MATERIALS RE V K KINRA APR 85

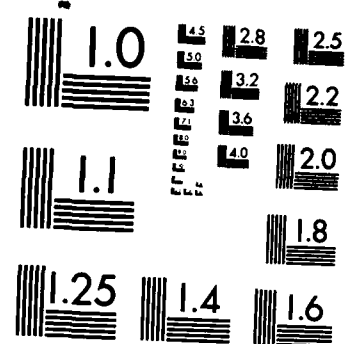
1A

UNCLASSIFIED

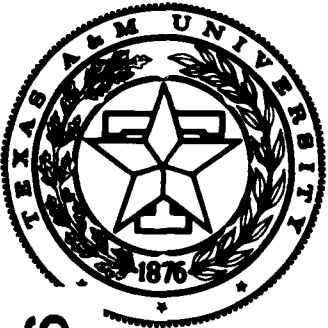
MM-5024-85-7 AFOSR-TR-85-1227 AFOSR-84-0066 F/G 11/4

NL





MICROCOPY RESOLUTION TEST CHART
NATIONAL BUREAU OF STANDARDS-1963-A



AFOSR-TR- 22-1227

7 MAY 85

(1)

**Mechanics and Materials Center
TEXAS A&M UNIVERSITY
College Station, Texas**

AD-A164 056

Ultrasonic Nondestructive Evaluation of
Damage in Continuous Fiber Composites

Annual Technical Report
by

Vikram K. Kinra
Department of Aerospace Engineering
Texas A&M University

to the
Air Force Office of Scientific Research
Office of Aerospace Research
United States Air Force

DTIC
ELECTED
FEB 12 1986
S D
D

ONE FIVE COPY

MM 5024-85-7

Grant No. AFOSR-84-0066
April 1985

Approved for public release;
distribution unlimited.

REPORT DOCUMENTATION PAGE

1. REPORT SECURITY CLASSIFICATION unclassified		1b. RESTRICTIVE MARKINGS	
2a. SECURITY CLASSIFICATION AUTHORITY		3. DISTRIBUTION/AVAILABILITY OF REPORT unlimited Approved for public release; distribution unlimited.	
2b. DECLASSIFICATION/DOWNGRADING SCHEDULE			
4. PERFORMING ORGANIZATION REPORT NUMBER(S)		5. MONITORING ORGANIZATION REPORT NUMBER(S) AFOSR-TR- 85-1227	
6a. NAME OF PERFORMING ORGANIZATION Dept. of Aerospace Engr.	6b. OFFICE SYMBOL (if applicable)	7a. NAME OF MONITORING ORGANIZATION Air Force Office of Scientific Research	
6c. ADDRESS (City, State and ZIP Code) Texas A&M University, College Station, Tx 77843		7b. ADDRESS (City, State and ZIP Code) Bolling Air Force Base Washington, DC 20332	
8a. NAME OF FUNDING/SPONSORING ORGANIZATION NA Bolling AFB, DC 20332	8b. OFFICE SYMBOL (if applicable) AFOSR/NA	9. PROCUREMENT INSTRUMENT IDENTIFICATION NUMBER Grant No. AFOSR-84-0066	
10. SOURCE OF FUNDING NOS.	PROGRAM ELEMENT NO. 611021	PROJECT NO. 2307	TASK NO. B2
11. TITLE (Include Security Classification) Ultrasonic Nondestructive Evaluation of Damage in Continuous	WORK UNIT NO. Fiber Composites		
12. PERSONAL AUTHOR(S) V.K. Kinra			
13a. TYPE OF REPORT Annual	13b. TIME COVERED FROM <u>02/01/85</u> TO <u>01/31/85</u>	14. DATE OF REPORT (Yr., Mo., Day) April 1985	15. PAGE COUNT 27 + appendix
16. SUPPLEMENTARY NOTATION <i>fr. p. 1</i>			
17. COSATI CODES		18. SUBJECT TERMS (Continue on reverse if necessary and identify by block number) Composites Automation; Fiber Reinforced Composites, Damage Ultrasonic Nondestructive Testing	
19. ABSTRACT (Continue on reverse if necessary and identify by block number) It is well known that composite materials suffer complex damage when they are subjected to either monotonic or fatigue loading. This damage affects both the velocity and attenuation of ultrasonic waves. The primary objective of this research is to correlate the damage states with the changes in the velocity and attenuation. Once this has been accomplished the pair of ultrasonic parameters becomes a measure of the damage. <i>→ to p. 1</i>			
We have developed a very fast computer-controlled technique of velocity measurement whose accuracy is about 0.2%.			
20. DISTRIBUTION/AVAILABILITY OF ABSTRACT UNCLASSIFIED/UNLIMITED <input checked="" type="checkbox"/> SAME AS RPT. <input type="checkbox"/> DTIC USERS <input type="checkbox"/>		21. ABSTRACT SECURITY CLASSIFICATION unclassified	
22a. NAME OF RESPONSIBLE INDIVIDUAL Major D. Glasgow		22b. TELEPHONE NUMBER (Include Area Code) (202) 767-4937	22c. OFFICE SYMBOL AFOSR/NA

TABLE OF CONTENTS

(i) Summary of Research Completed to Date	1
1. Introduction	2
2. Theoretical Results	2
3. Technique Development	17
4. Results	32
5. Professional Personnel	48
6. Interactions	49
7. Appendix I. A Survey of Literature Concerning Ultrasonic Nondestructive Testing of Composite Materials	
Appendix II. Propagation of Elastic Waves in Undirectional Fiber-Reinforced Composites.	

AIR FORCE OFFICE OF SCIENTIFIC RESEARCH (AFSC)
NOTICE OF TRANSMISSION OF REPORT
This technical report was transmitted to AFSC by:
Approved:
Distributed:
MATTHEW S.
Chief, Technical Information Division

(i) SUMMARY OF RESEARCH COMPLETED TO DATE

1. A survey of literature concerning ultrasonic nondestructive testing of composite materials. This is included in Appendix I.

2. A theoretical study of wave phenomena unique to the (anisotropic) composite materials has been completed. This is included in Appendix II.

3. A theoretical study of the experimental technique under development has been completed (Section 2)

4. → A very accurate computer-controlled experimental technique to measure wavespeed in a composite material has been developed. For conventional isotropic materials accuracies of two parts per ten thousand were achieved; for highly damaged Graphite/epoxy composite materials accuracies of 0.2% have been achieved. *Keywords:*

147
PL-18

Accession For	
NTIS	CRA&I <input checked="" type="checkbox"/>
DTIC	TAB <input type="checkbox"/>
Unannounced <input type="checkbox"/>	
Justification	
By	
Distribution /	
Availability Codes	
Dist	Avail and/or Special
A-1	



I. INTRODUCTION

It is well known that components made of composite materials suffer complex damage when they are subjected to either monotonic or fatigue loading. We submitted a three year proposal to develop ultrasonic nondestructive techniques to measure the damage states in fiber-reinforced composite materials (Texas A&M Research Foundation Proposal No. RF-84-34) The objective of this Annual Technical Report is to summarize the progress made during the first year of the grant period (AFOSR-84-0066).

When the damage occurs it has two effects upon the propagation of a mechanical wave through the composite: (1) It affects the stiffness, and therefore, the speed of wave propagation; (2) It increases the attenuation of the wave. Thus by measuring the speed and attenuation as functions of frequency at various known levels of damage, we propose to establish the necessary calibration curves for damage. Conversely, one can measure the ultrasonic parameters and estimate the extent of damage.

In Section 2 we summarize the theoretical results obtained to date. In section 3 we describe the development of the experimental technique. Section 4 is concerned with the implementation of the experimental techniques i.e. with the measurement of phase velocity and attenuation as the damage progresses in graphite/epoxy composite specimens

2. THEORETICAL RESULTS

In this section we describe the theoretical foundations of the experiment.

Consider a plate of a linear viscoelastic material sandwiched between two half-spaces of perfectly elastic materials. Consider a

finite-duration pulse incident at the viscoelastic plate. Because of the mismatch in the acoustic impedance of the three materials there will result an infinite series of reflected and transmitted pulses. The reflected and transmitted fields contain information about the acoustic properties of the viscoelastic material. An objective of this section is to derive expressions for the phase velocity and the attenuation of waves, given the incident and the reflected (or the transmitted) fields.

In view of the complexity of the total problem we have broken it down into the following simpler sub-problems. We will first assume that the plate is perfectly elastic. An incident pulse of arbitrary shape will be considered. The most general expressions for the reflected and the transmitted fields will be derived. Next, instead of a pulse of arbitrary shape we will consider a monochromatic wavetrain. For a perfectly elastic material the wavenumber k is real. At this point the viscoelasticity of the composite will be accounted for by letting the wavenumber k take on complex values ($k=k_1+ik_2$). A pulse of arbitrary shape can now be studied in terms of its Fourier components. Finally from this general analysis we will derive expressions for a few particular situations which will be used in the laboratory.

First, consider the reflection and transmission of a right-going displacement wave at the interface of two elastic media, see Fig. 1. The equation of motion is

$$\frac{\partial^2 u}{\partial x^2} = \frac{1}{c^2} \frac{\partial^2 u}{\partial t^2} \quad (1)$$

where u is the displacement in the x -direction, t is time and c is the speed of the longitudinal wave: $c^2=(\lambda+2\mu)/\rho$, where λ and μ are Lame's constants and ρ is the density. Let the incident pulse be given by

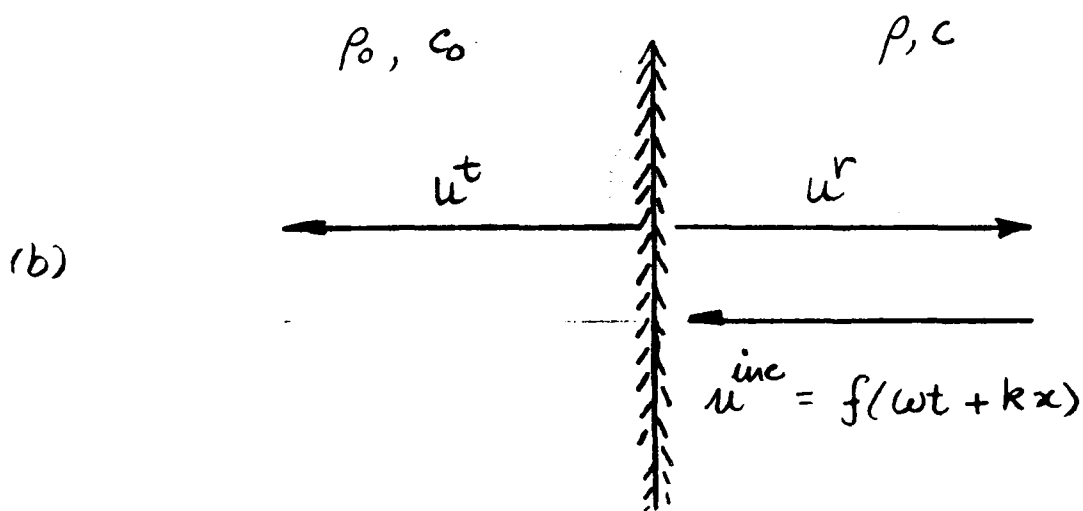
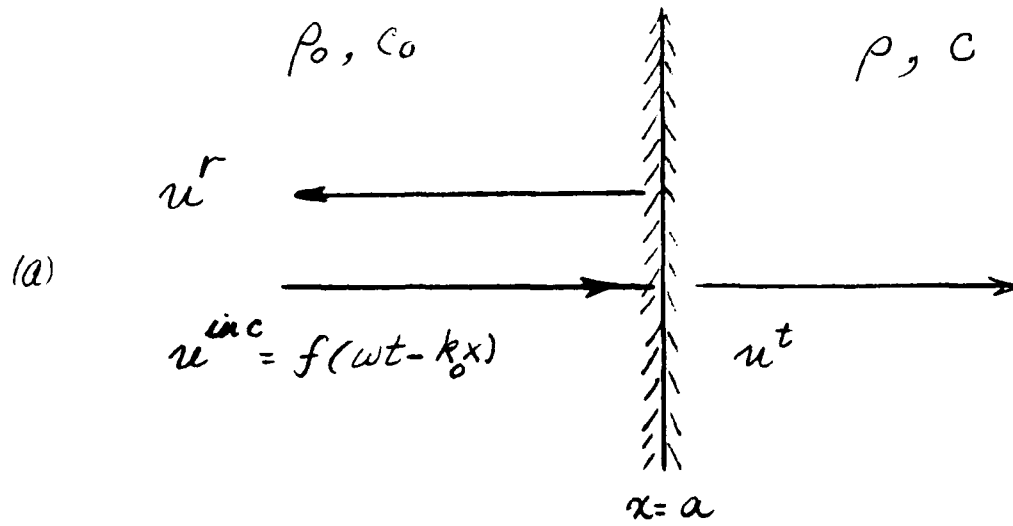


FIGURE 1

$$u^{inc} = f(\omega t - kx)$$

$$f(s) \equiv 0 \text{ for } s < 0$$

(2)

where at present ω and k are any two constants connected by $C = \omega/k$. Later, ω and k will be identified with the circular frequency and wavenumber of a monochromatic harmonic wave. The boundary conditions at $x=a$ are the continuity of displacement and stress. The reflection is given by (with $s = \omega t + k_0 x$)

$$u^r = \begin{cases} R_{12} f(s - 2k_0 a) & \text{for } s > 2k_0 a \\ 0 & \text{for } s < 2k_0 a \end{cases} \quad (3)$$

where the displacement reflection coefficient is

$$R_{12} = \frac{\rho_0 C_o - \rho C}{\rho_0 C_o + \rho C} \quad (4)$$

The transmitted field is given by (with $s = \omega t - kx$)

$$u^t = \begin{cases} T_{12} f(s - (k_0 - k)a) & \text{for } s > (k_0 - k)a \\ 0 & \text{for } s < (k_0 - k)a \end{cases} \quad (5)$$

$$\text{where } T_{12} = 2\rho_0 C_o / (\rho_0 C_o + \rho C) \quad (6)$$

Next consider a left-going displacement wave; Fig. 1b

$$u^{inc} = f(\omega t + kx) \quad (7)$$

$$f(s) \equiv 0 \text{ for } s < s_0$$

where s_0 is some arbitrary constant. With $s = \omega t - kx$, the reflected wave is

$$u^r = \begin{cases} R_{21} f(s + 2ka) & \text{for } s > s_0 - 2ka \\ 0 & \text{for } s < s_0 - 2ka \end{cases} \quad (8)$$

With $s = \omega t + k_0 x$ the transmitted wave is

$$u^t = \begin{cases} T_{21} f(s - (k_0 - k)a) & \text{for } s > s_0 + (k_0 - k)a \\ 0 & \text{for } s < s_0 + (k_0 - k)a \end{cases} \quad (9)$$

Here

$$R_{21} = -R_{12} \text{ and } T_{21} = 2 - T_{12} \quad (10)$$

We next consider an elastic plate sandwiched between two elastic half-spaces. A convenient way of following the various reflections is to draw a t-x diagram of a point of constant phase in the incident pulse; this is shown in Fig. 2. This method is also known as ray tracing. Let the displacement field along the incident ray (ray 1) be given by

$$u^{inc} = f(\omega t - k_0 x) \quad (11)$$

$$f(s) \equiv 0 \text{ for } s < 0$$

The reflection (ray 2) and transmission (ray 3) at $x=a$ are given by (in the following the superscript refer to the corresponding ray number):

$$u^2 = \begin{cases} R_{12} f(s-s_2) & \text{for } s > s_2 \\ 0 & \text{for } s < s_2 \end{cases} \quad (12)$$

where $s = \omega t - k_0 x$ and $s_2 = 2k_0 a$, and

$$u^3 = \begin{cases} T_{12} f(s-s_3) & \text{for } s > s_3 \\ 0 & \text{for } s < s_3 \end{cases} \quad (13)$$

where $s = \omega t - kx$, $s_3 = (k_0 - k)a$ and

$$R_{12} = \frac{\rho_o C_o - \rho C}{\rho_o C_o + \rho C} \quad \text{and} \quad T_{12} = \frac{2\rho_o C_o}{\rho_o C_o + \rho C} \quad (14)$$

Ray 3 now suffers a reflection (ray 5) and a transmission (ray 4) at $x=b$.

$$u^4 = \begin{cases} T_{12} f T_{23} f(s-s_4) & \text{for } s > s_4 \\ 0 & \text{for } s < s_4, \end{cases} \quad (15)$$

with $s = \omega t - k_3 x$ and $s_4 = k_0 a + k(b-a) - k_3 b$

$$u^5 = \begin{cases} T_{12} R_{23} f(s-s_5) & \text{for } s > s_5 \\ 0 & \text{for } s < s_5 \end{cases} \quad (16)$$

with $s = \omega t + kx$ and $s_5 = k_0 a + k(2b-a)$ and

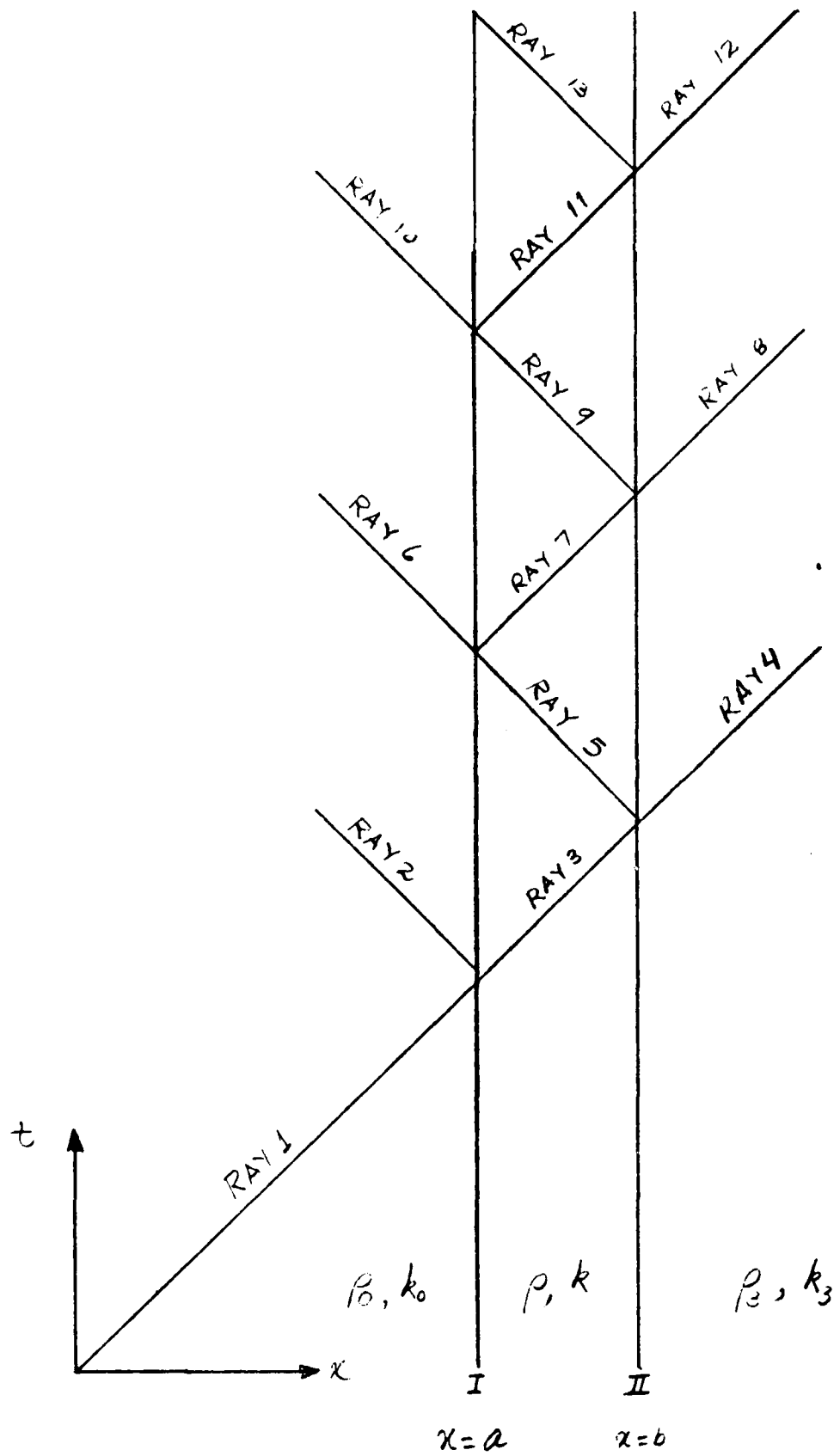


FIGURE 2.

$$R_{23} = \frac{\rho C - \rho_3 C_3}{\rho C + \rho_3 C_3} \quad \text{and} \quad T_{23} = \frac{2\rho C}{\rho C + \rho_3 C_3}$$

In a similar manner one can write down the expressions for displacement along various rays. The total reflected field is the sum of the following rays (with $h=b-a$ and $s=\omega t + k_o x$):

$$u^2 = R_{12} f(s-s_2); \quad s_2 = 2k_o a$$

$$u^6 = T_{12} R_{23} T_{21} f(s-s_6); \quad s_6 = 2k_o a + 2^{kh}$$

$$u^{10} = T_{12} R_{23} R_{21} R_{23} T_{21} f(s-s_{10}); \quad s_{10} = 2k_o a + 4^{kh}$$

.

.

.

The sum may be written as

$$u^r = R_{12} f(s-2k_o a) + T_{12} R_{23} T_{21} \sum_{m=1}^{\infty} (R_{21} R_{23}) f(s-s_m) \quad (17)$$

where $s=\omega t + k_o x$ and $s_m = 2k_o a + m^{2kh}$.

In (17) m is the number of complete round trips taken by the wave across the plate thickness h

In an exactly analogous manner one can write the expression for the total transmitted field. With $s=\omega t - k_3 x$

$$u^4 = T_{12} T_{23} f(s-s_4); \quad s_4 = a(k_o - k_3) + h(k - k_3)$$

$$u^8 = T_{12} R_{23} R_{21} T_{23} f(s-s_8); \quad s_8 = a(k_o - k_3) + h(3k - k_3)$$

$$u^{12} = T_{12} (R_{23} R_{21})^2 T_{23} f(s-s_{12}); \quad s_{12} = a(k_o - k_3) + h(5k - k_3)$$

.

.

.

The total transmitted field may be written as

$$u^t = T_{12} T_{23} \sum_{m=0}^{\infty} (R_{23} R_{21})^m f(s-s_m) \\ s_m = a(k_0 - k_3) + h[(2m+1)k - k_3] \quad (18)$$

It is emphasised that in the foregoing the plate is assumed to behave in a perfectly elastic manner. It is noted that with a slight change of detail the preceding analysis is equally valid for an incident shear wave.

Water Immersion Method

We now consider the mechanical response of a linear viscoelastic plate. If the attenuation is small this can be most easily accomplished by letting k in the expression for a time-harmonic wave, $e^{i(\omega t-kx)}$, take on complex values. Consider a basic experimental set-up shown in Fig 3(b). The piezoelectric transducer (T) and the composite specimen are acoustically coupled through water. An electrical signal is applied to the transducer which launches a longitudinal wave in the direction of the composite. The first order of business is to characterize this pulse. To this end we measure the reflection from a homogeneous medium of known properties (ρ and c); Fig 3(a), Let the incident field be

$$u^{inc} = f_0(\omega t - k_0 x). \quad (19)$$

The reflection is given by

$$u^r = R f_0 (\omega t + k_0 x - 2k_0 a); R = \frac{\rho_0 C_0 - \rho c}{\rho_0 C_0 + \rho c} \quad (20)$$

Let the reflected signal as sensed by the transducer be labelled $f(t)$, then

$$f(t) = f_0(\omega t - 2k_0 a) \quad (21)$$

Define

$$F^*(\omega) = \sqrt{2\pi} \int_{-\infty}^{\infty} f(t) e^{-i\omega t} dt \quad (22)$$

$$\text{and } F_0^*(\omega) = \sqrt{2\pi} \int_{-\infty}^{\infty} f_0(\omega t) e^{-i\omega t} dt, \quad (23)$$

$$\text{then } F_o^*(\omega) = e^{i2k_o a} F^*(\omega) \quad (24)$$

Note that $F^*(\omega)$ is the Fourier transform of a measured quantity, $f(t)$, from which, via eq. (24), we can deduce the Fourier transform of the signal launched by the transducer. Now consider a wave travelling in the positive x -direction.

$$u^{\text{inc}}(x, t) = \sqrt{\frac{1}{2\pi}} \int_{-\infty}^{+\infty} F_o^*(\omega) e^{i(\omega t - k_o x)} d\omega \quad (25)$$

Here k_o is pure real. In comparison with eq (19)

$$f_o(\omega t - k_o x) = \sqrt{\frac{1}{2\pi}} \int_{-\infty}^{+\infty} F_o^*(\omega) e^{i(\omega t - k_o x)} d\omega. \quad (26)$$

Hence

$$f(s) = \sqrt{\frac{1}{2\pi}} \int_{-\infty}^{+\infty} F_o^*(\omega) e^{is} d\omega \quad (27)$$

The reflected field is given by eq. (17). Setting $x=0$ (since the transducer is located at $x=0$) the total reflected field is given by

$$u^r(o, t) = \sqrt{\frac{1}{2\pi}} \int F_o^*(\omega) d\omega e^{i\omega t} \left[R_{12} e^{-i2k_o a} + \sum_{m=1}^{\infty} \beta_m e^{-i\{2k_o a + 2mkh\}} \right] \quad (28)$$

$$\text{Here } \beta_m = T_{12} R_{21} T_{21} R_{21}^{2(m-1)}$$

Let $u^r(o, t)$ be labelled as $g(t)$ and let

$$G^*(\omega) = \sqrt{\frac{1}{2\pi}} \int_{-\infty}^{+\infty} g(t) e^{-i\omega t} dt,$$

$$\text{then } \sum_{m=1}^{\infty} \beta_m e^{-i2mkh} = \left[\frac{G^*}{F^*} e^{2ik a} - R_{12} \right] \quad (29)$$

By observing that

$$1 + Z + Z^2 + \dots = \frac{1}{1-Z} \quad \text{for } |Z| < 1$$

the foregoing expression can be recast in the form

$$R_{21}^2 e^{-i2kh} = \frac{\beta}{1 + \beta}$$

$$\beta = \frac{R_{21}}{T_{12} T_{21}} \left[R \frac{G^*}{F^*} - R_{12} \right] \quad (30)$$

This is the key result of this section. By measuring F^* and G^* one can extract the complex-valued $k(\omega) = k_1 + ik_2$ from eqs. (30)

Measurement of $k(\omega)$ from the transmitted field

An alternative method of measuring $k(\omega)$ is from the transmitted field. With reference to Fig. 3 a matched ultrasonic transducer is used as a receiver (R). The reference signal $f(t)$, is obtained by removing the specimen from the wave path. The incident field is given by $f_o(\omega t - kx)$. Therefore

$$f(t) = f_o(\omega t - k_l) \quad (31)$$

Let $F^*(\omega)$ and $F_o^*(\omega)$ be defined as in equations (22) and (23), respectively, then

$$F^*(\omega) = e^{ik_0 l} F_o^*(\omega) \quad (32)$$

Let $g(t)$ be the total transmitted field, ray 4, 8, 12, ..., ∞ . Let

$$G^*(\omega) = \frac{1}{\sqrt{2\pi}} \int_{-\infty}^{+\infty} g(t) e^{-i\omega t} dt \quad (33)$$

Then from eq. (18)

$$G^*(\omega) = T_{12} T_{21} F^*(\omega) e^{-ihk} \cdot e^{ihk_0} \sum_{m=0}^{\infty} z^m \quad (34)$$

$$\text{where } z = [R_{21} e^{-ihk}]^2$$

observing that $\sum_{m=0}^{\infty} z^m = \frac{1}{1-z}$, eq (34) reduces to

$$\frac{-ih(k-k_0)}{e^{\frac{2}{1-R_{21}} - i2kh}} = \frac{G^*(\omega)}{T_{12} T_{21} F^*(\omega)} \quad (35)$$

$F^*(\omega)$ and $G^*(\omega)$ are measured quantities, therefore, eq. (35) is viewed as an equation to evaluate $k(\omega)$.

For very thin composites it is frequently impossible to separate the various rays (Fig. 2) in the time domain. The preceding discussion deals with that general case. Occasionally it is possible to isolate

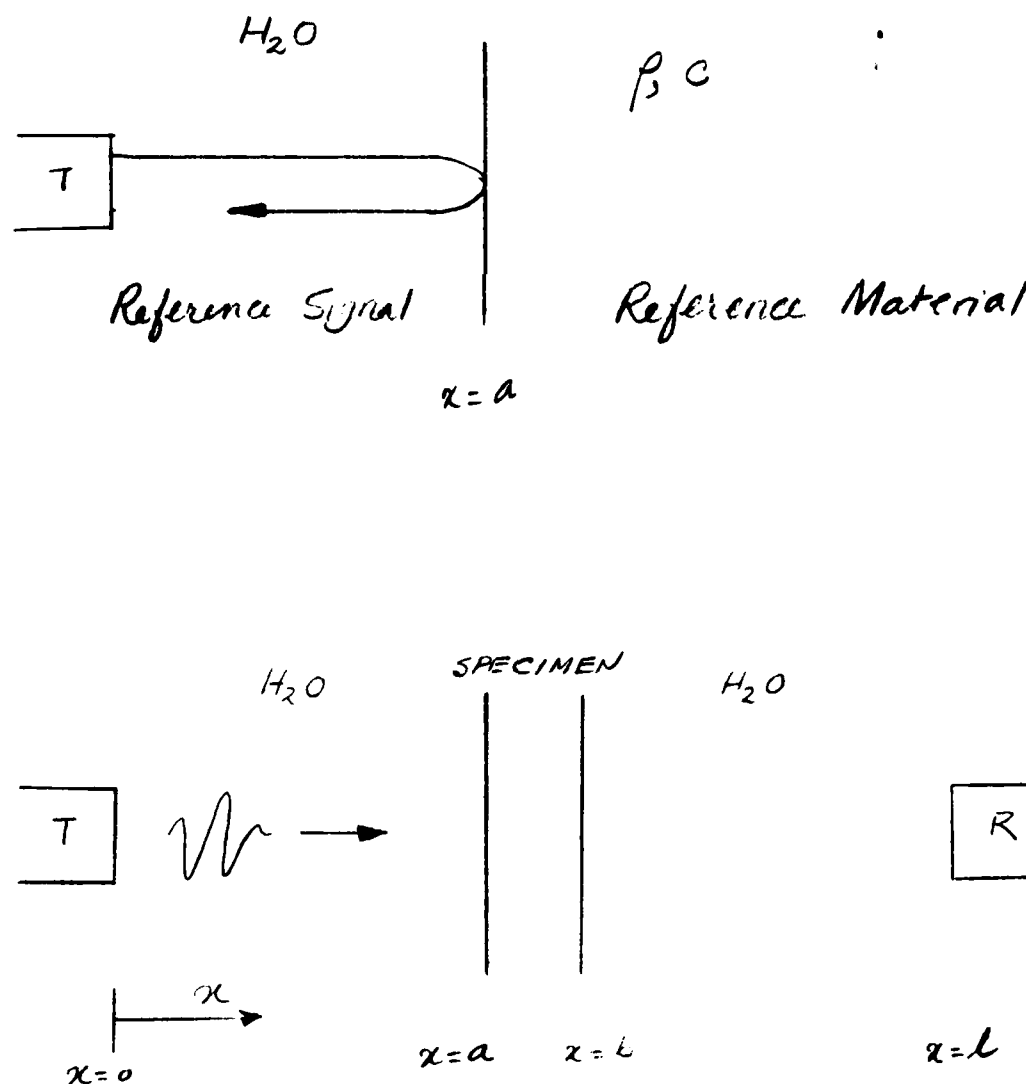


FIGURE 3

various rays. When that happens certain simplifications result. In particular let us suppose that it is possible to isolate the front surface reflection (ray 2) from the remaining reflected field. Then it is more convenient to use ray 2 as the reference signal i.e.

$$f(t) = R_{12} F_0(\omega t - 2k_0 a) \quad (36)$$

$$\text{and } F_0^*(\omega) = \frac{1}{R} e^{i2k_0 a} F^*(\omega) \quad (37)$$

Define $g(t)^{12}$ as the total reflected field after ray 2 i.e. ray 6, 10,..... ∞ . Then the results of a calculation similar to the one described in the foregoing yield:

$$\frac{1}{R_{21}} e^{i2kh} = \frac{H^3}{B}, \quad (38)$$

$$\text{where } B = \frac{R_{21} R_{12}}{T_{12} T_{21}} \frac{G^*}{F^*},$$

which is the equation for calculating $k(\omega)$.

Finally, we treat the case when the damage is large and therefore, the damping is high. When that happens Rays 10, 14,...become of insignificant amplitude. The wavespeed and attenuation are best measured by convolving Ray 2 with Ray 6. If $f(t)$ is the transducer response to Ray 2, $g(t)$ the response to Ray 6, $F^*(\omega)$ and $G^*(\omega)$ are the Inverse Fourier Transforms of $f(t)$ and $g(t)$, respectively, it can be readily shown that

$$\frac{G^*(\omega)}{F^*(\omega)} = T_{12} T_{21} e^{-i2kh} \quad (39)$$

Direct Contact Method In addition to the water immersion method we have used a direct contact technique in which the transducer and the specimen are acoustically coupled with a block of an isotropic homogeneous material (e.g. aluminum) rather than water. A schematic arrangement is

shown in Fig. 4. Within this arrangement we will discuss three cases which were found useful in the laboratory.

Case 1.

Reference Signal: Reflection from the back surface of the delay rod with the specimen removed.

Reflected field: Rays 2, 6, 10, 14, ..., ∞

$$u^{inc} = f_o(\omega t - k_o x) \quad (40)$$

$$f(t) = f_o(\omega t - 2k_o a) \quad (41)$$

$$g(t) = R_{12} f_o(\omega t - 2k_o a) + T_{12} T_{21} \sum_{m=1}^{\infty} R_{21} f_o(\omega t - s_m) \quad (42)$$

$$\text{where } s_m = 2k_o a + 2mkh$$

$$G^*(\omega) = R_{12} e^{-i2k_o a} F_o^*(\omega) + T_{12} T_{21} \sum_{m=1}^{\infty} R_{21} e^{-is_m} F_o^*(\omega) \quad (43)$$

After some algebraic manipulation we get

$$R_{21} e^{-i2kh} = \beta / (1 + \beta) \quad (44)$$

$$\text{where } \beta = \frac{R_{21}}{T_{12} T_{21}} \quad \frac{(G^* - R_{12})}{F^*} \quad (45)$$

which are the desired equations for calculating the complex-valued $k(\omega)$

Case 2

Reference Signal: Ray 2

Reflected Field: Rays 6, 10, 14, ..., ∞

$$u^{inc} = f_o(\omega t - kx) \quad (46)$$

$$f(t) = R_{12} f_o(\omega t - 2k_o a) \quad (47)$$

$$g(t) = T_{12} T_{21} \sum_{m=1}^{\infty} R_{21} f_o(\omega t - s_m) \quad (48)$$

$$\text{where } s_m = 2k_o a + 2mkh$$

$$G^*(\omega) = \frac{T_{12} T_{21}}{R_{21}} \sum_{m=1}^{\infty} R_{21} e^{-i\{2ko a + 2mkh\}} F_o^*(\omega) \quad (49)$$

After some algebraic manipulation, it can be shown that

$$e^{i2kh} = R_{21} (\alpha F^* + G^*) / G^*; \quad (50)$$

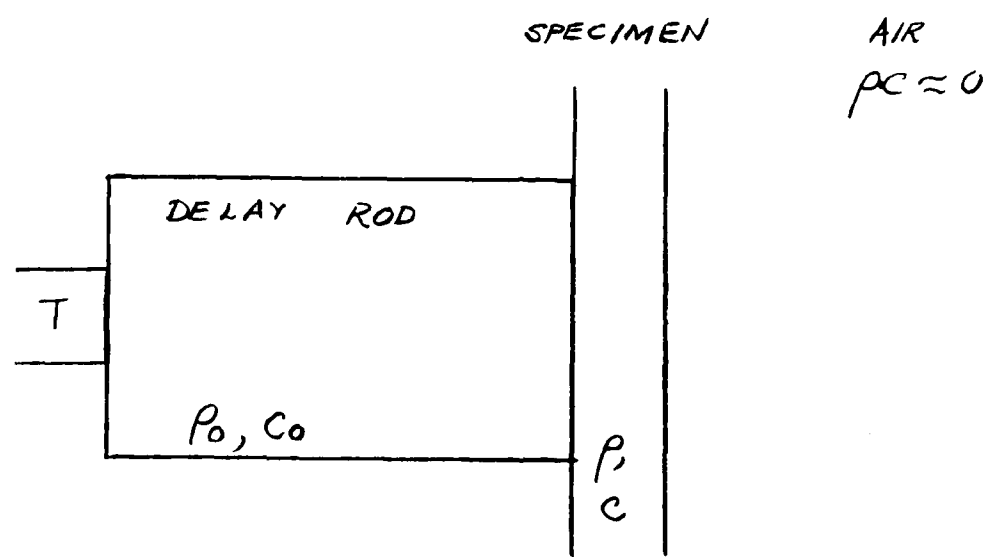


FIGURE 4.

where $\alpha = T_{12} T_{21} / R_{12} R_{21}$

Case 3

Reference Signal: Ray 6

Reflected field: Rays 6, 10, 14, ..., ∞ .

When the excitation voltage is applied to the transmitting transducer, it saturates the preamplifier in certain situations. Frequently, there is enough time for the preamplifier to have a complete recovery before the first reflection, ray 2, arrives; sometimes there is not enough time. This calculation is done for these situations.

$$u^{inc} = f_0 (\omega t - k_0 x)$$

$$f(t) = T_{12} T_{21} f_0 (\omega t - s_6); \quad s_6 = 2kh + 2k_0 a \quad (51)$$

$$F^*(\omega) = T_{12} T_{21} e^{-is_6} F_0^*(\omega) \quad (52)$$

$$g(t) = T_{12} T_{21} \sum_{m=1}^{\infty} R_{21} f_0 (\omega t - s_m); \quad s_m = 2k_0 a + 2mkh \quad (53)$$

$$G^*(\omega) = T_{12} T_{21} \sum_{m=1}^{\infty} R_{21} e^{-is_m} F_0^*(\omega) \quad (54)$$

$$R_{21} e^{-2ikh} = (G^* F^*) / F^* \quad (55)$$

3. TECHNIQUE DEVELOPMENT*

Keeping in view the tremendous speed and reliability we can achieve by using computers for collection and analysis of data, equations developed in section 2 were interpreted in a way most suitable for computer programming. The technique was developed such that the measurements could be made with least amount of operator interference.

The technique thus developed was first applied to aluminum samples as a calibration measure. The reason being, the ultrasonic waves are weakly dispersive in aluminum and the wavespeed is known apriori. The transducer was kept in direct contact with the specimen, coupled acoustically with a thin layer of mineral oil. The other end of the specimen was free, in contact with air, see Fig. 4.

When the transducer is excited by a short duration pulse, it launches a wave in the specimen and this wave reflects back and forth between the parallel surfaces of the specimen giving a signal shown in Fig. 5. The signal consists of pulses and for later discussion the pulses have been numbered. It is observed from this figure that there are regions between pulses where the signal level is very low. We can clearly define the end of one pulse and the start of the next pulse. This separation of pulses depends on the excitation frequency, sample thickness, wavespeed and dispersion in the specimen. As a first step the measurement technique is developed on thick specimen where this separation is possible. The reason why we are emphasizing on pulse width will become clear during subsequent discussions. In the case of composites we will not be able to avail this luxury and there we will use the equations in such a way that measurement will still be possible.

*Prepared by Vinay Dayal (Ph.D. Student)

Avg. A1

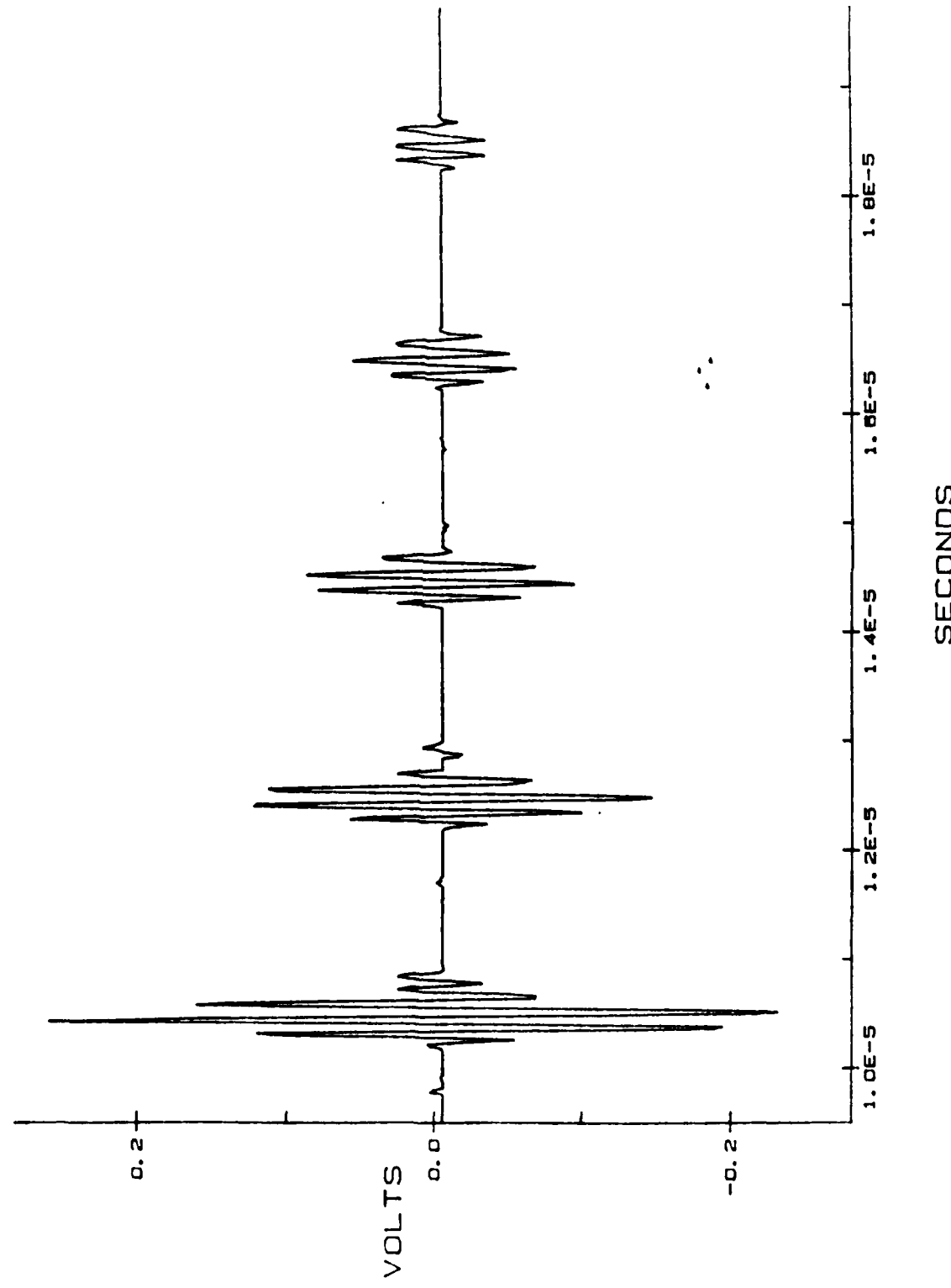


Fig. 5. Time domain signal in aluminum (direct contact, P waves)

The equation derived in section 2 for the transducer in contact with specimen is reproduced here for the continuity of discussion.

$$\frac{G^*(\omega) - F^*(\omega)}{F^*(\omega)} = R_{21} e^{-2ikh} \quad (55)$$

for aluminum k is real. We now define t_0 as the round trip time ($t_0 = 2h/C$), and the circular frequency $=kc$, then

$$G^*(\omega) = F^*(\omega) [1 + R_{21} e^{-i\omega t_0}] \quad (56)$$

here $F^*(\omega)$ is the Fourier Transform (FFT) of pulse I of Fig. 5. (Ray 6 of Fig. 2) and $G^*(\omega)$ is the combined FFT of I and II (Ray 6 & 10). Both $F(\omega) = |F^*(\omega)|$ and $G(\omega) = |G^*(\omega)|$ are plotted in Fig. 6. It can be seen that $F(\omega)$ is an inverted bell shaped curve and is essentially the transducer response. While $G(\omega)$ exhibits harmonics due to constructive and destructive interference of the first and second pulse, which is superimposed on $F(\omega)$.

If Δf is the difference in frequency between the two successive peaks, it can be readily shown that the wavespeed is

$$C = 2h\Delta f \quad (57)$$

From Fig. 6, average peak spacing on frequency scale is measured and wavespeed is calculated.

Another technique of measuring C is to recast equation (56) in the form

$$\frac{G^*(\omega)}{F^*(\omega)} - 1 = R_{21} e^{-i\omega t_0} \quad (58)$$

and plot $|\frac{G^*}{F^*} - 1|$ vs frequency. The results are shown in Fig. 7.

$$\Delta f = 0.502 \text{ MHz}$$

$$C = 6.375 \frac{\text{nF}}{\mu\text{s}}$$

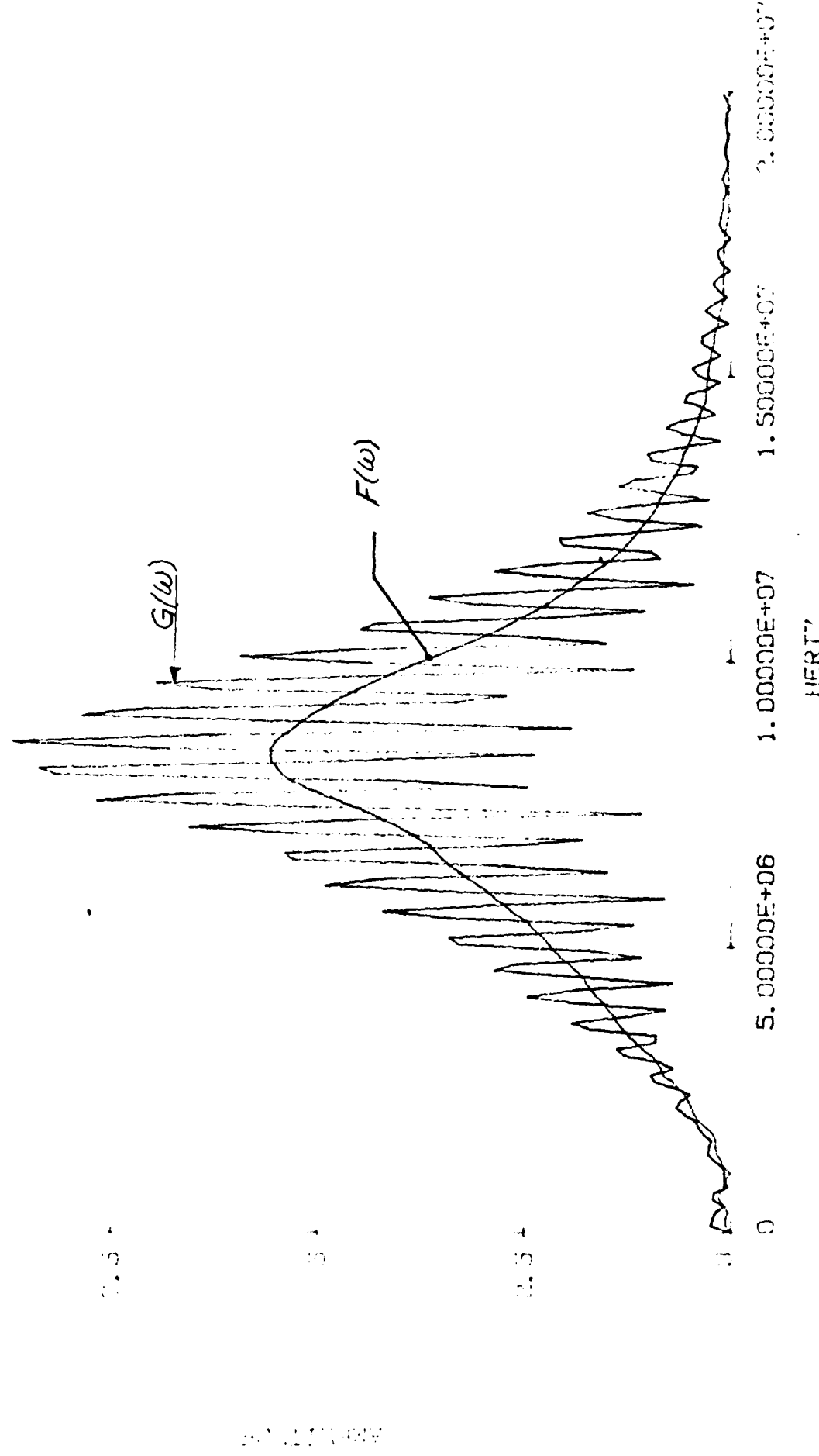


Fig. 6. $F(\omega)$ and $G(\omega)$ For Transducer In Contact With AL Specimen

$$\frac{G(\omega) - F(\omega)}{F(\omega)} = A^2 + 2A \cos(\omega t_0)$$

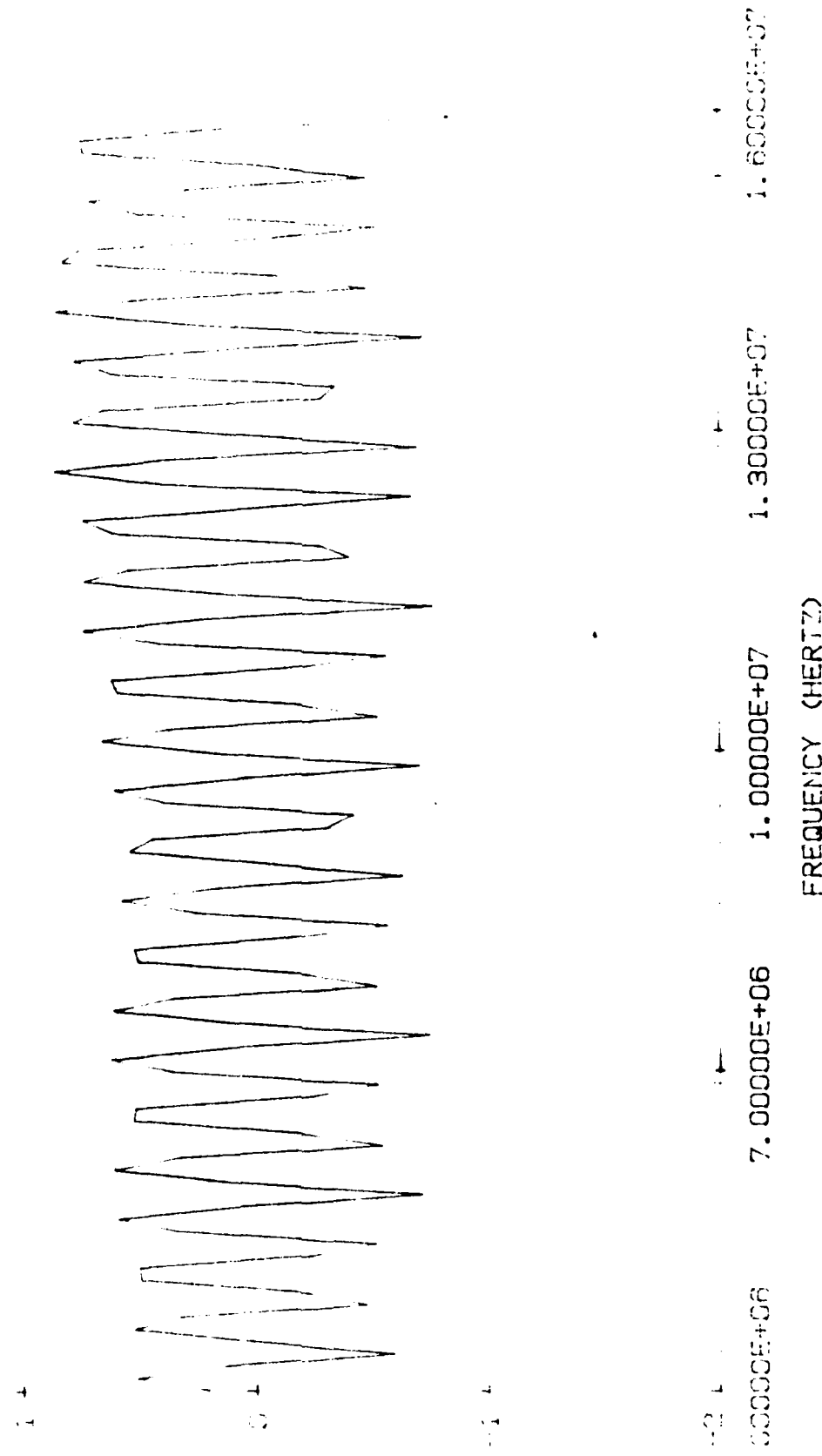


Fig. 7. Deconvolved $G^*(\omega)$ For Transducer In Contact With Al Specimen

Here we have deconvolved the system response from the interference pattern of two pulses. With Δf now interpreted as the frequency spacing between two successive zero crossings, equation (57) still holds for calculating C.

These two methods were used on aluminum specimen and wavespeed was found to be accurate to $\pm 0.5\%$. The main drawback of these techniques is that the peak spacing had to be measured manually and also in cases where the number of peaks becomes small, it will be difficult to get accurate peak spacing. As stated earlier our objective in this research effort is to develop a fully automated computer controlled measurement system. We proceed ahead and recast equation (50) in the form

$$\frac{G^*(\omega)}{F^*(\omega)} - 1 = \frac{G^*(\omega) - F^*(\omega)}{F^*(\omega)} \equiv \frac{S^*(\omega)}{F^*(\omega)} = R_{21} e^{-i\omega t_o} \quad (59)$$

where $S^*(\omega)$ is the Fourier Transform of the second pulse (Fig. 5). Both $S^*(\omega)$ and $F^*(\omega)$ are complex numbers, equation (59) can be written as

$$\begin{aligned} \frac{S^*(\omega)}{F^*(\omega)} &= R_{21} \frac{|S^*(\omega)|}{|F^*(\omega)|} \frac{e^{i\theta(\omega)}}{e^{i\delta(\omega)}} \\ &= |M| e^{i\phi} \end{aligned} \quad (60)$$

where ϕ is the phase difference between the phase of second pulse and the phase of the first pulse. Since we are interested in the difference in phase we do not care about the absolute phase and, taking the first point on the signal as the $\phi=0$ point, calculate the phase difference between the two pulses at each digitizing point.

Comparing equation (59) and (60) we get

$$R_{12} e^{-i\omega t_o} = |M| e^{i\phi}$$

$$\text{Thus } \phi = -t_o = 2\pi f \frac{2h}{c}$$

NEW. A1

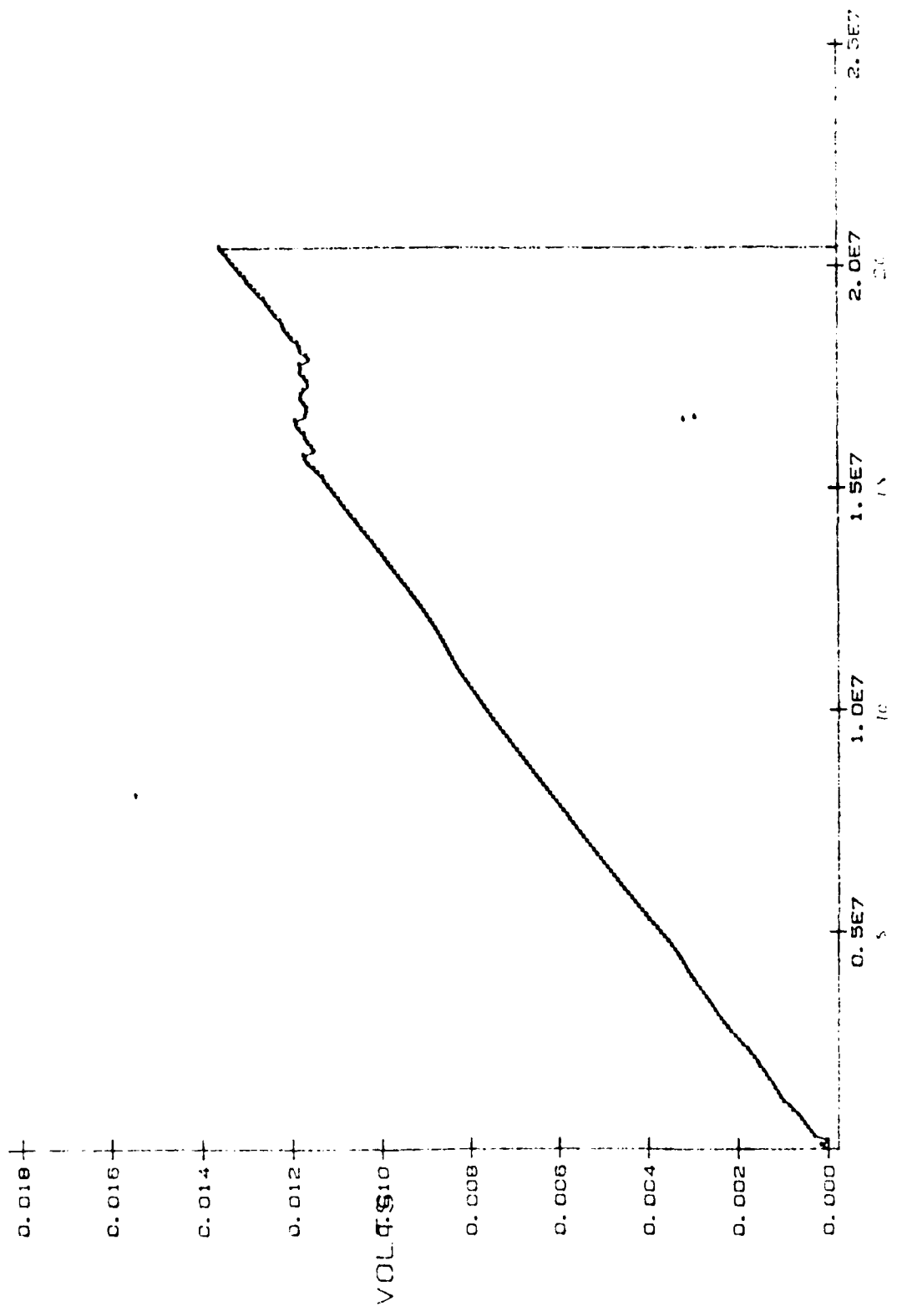


Fig. 8. Phase vs frequency plot for transducer in contact with Al specimen.

NEW. A1

$$V = \frac{4\pi t}{\text{slope}}$$

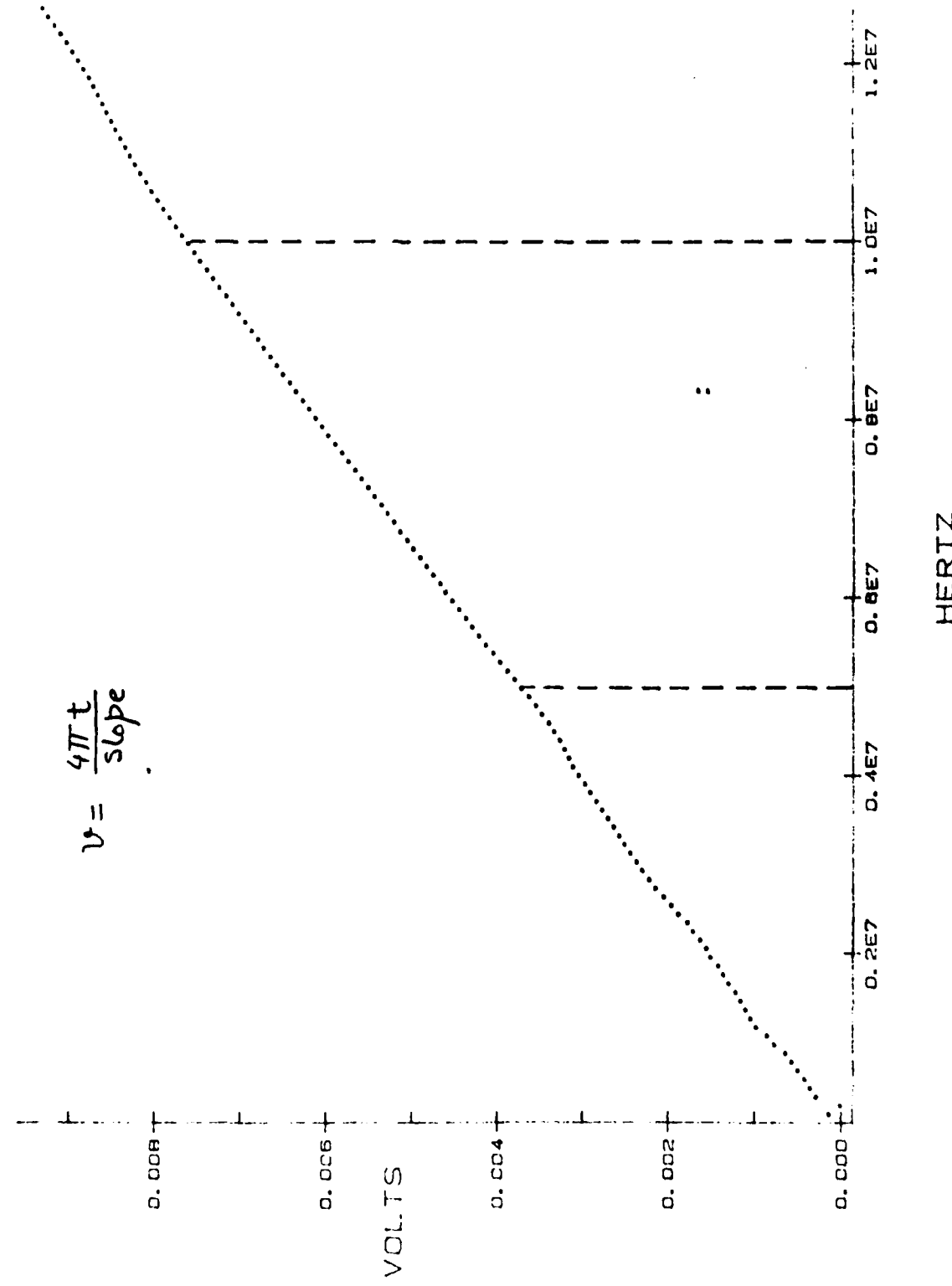


Fig. 9. Blown up portion of Fig. 8.

$$\text{or } \phi = \frac{(4\pi h)}{c} f \quad (61)$$

Now if we plot the phase difference ϕ vs the frequency we should obtain a straight line with a slope of $4\pi h/c$. Fig. 8. is the phase vs frequency plot for an aluminum specimen. It is seen that over the range of about 4.5-10 MHz a fairly straight line is obtained. This portion of the curve is expanded for clarity in Fig. 9. This straight line section of the curve is related to the frequency response of the transducer and will be discussed later. A least square fit line is passed through these points and the slope is computed from which the wavespeed is calculated. All these calculations are performed on a computer 'with no human intervention.

This form of equation (60) has been used in the development of the computer algorithm and the measurements. Now we will discuss some factors which affect the accuracy of our measurements.

The first factor is the digitizing interval for the signal. The analog signal in time domain is digitized by the oscilloscope at fixed intervals. We would like the digitization to be done at such an interval that no part of the signal is lost. If the digitizing interval is too large it would result in the loss of high-frequency components of the waveform. This effect was studied by digitizing a signal at 10, 20 and 40 nanoseconds (ns) and by comparing the FFT of the resulting data. The results are shown in Fig. 10. The response at 10 and 20 ns is very close but at 40 ns loss in amplitude and change in frequency content is observed. This shows that for the frequency range of interest in this work (~ 10 MHz) digitizing intervals of 10 or 20 ns can be safely used.

EFFECT OF SAMPLING INTERVAL ON
TRANSDUCER RESPONSE

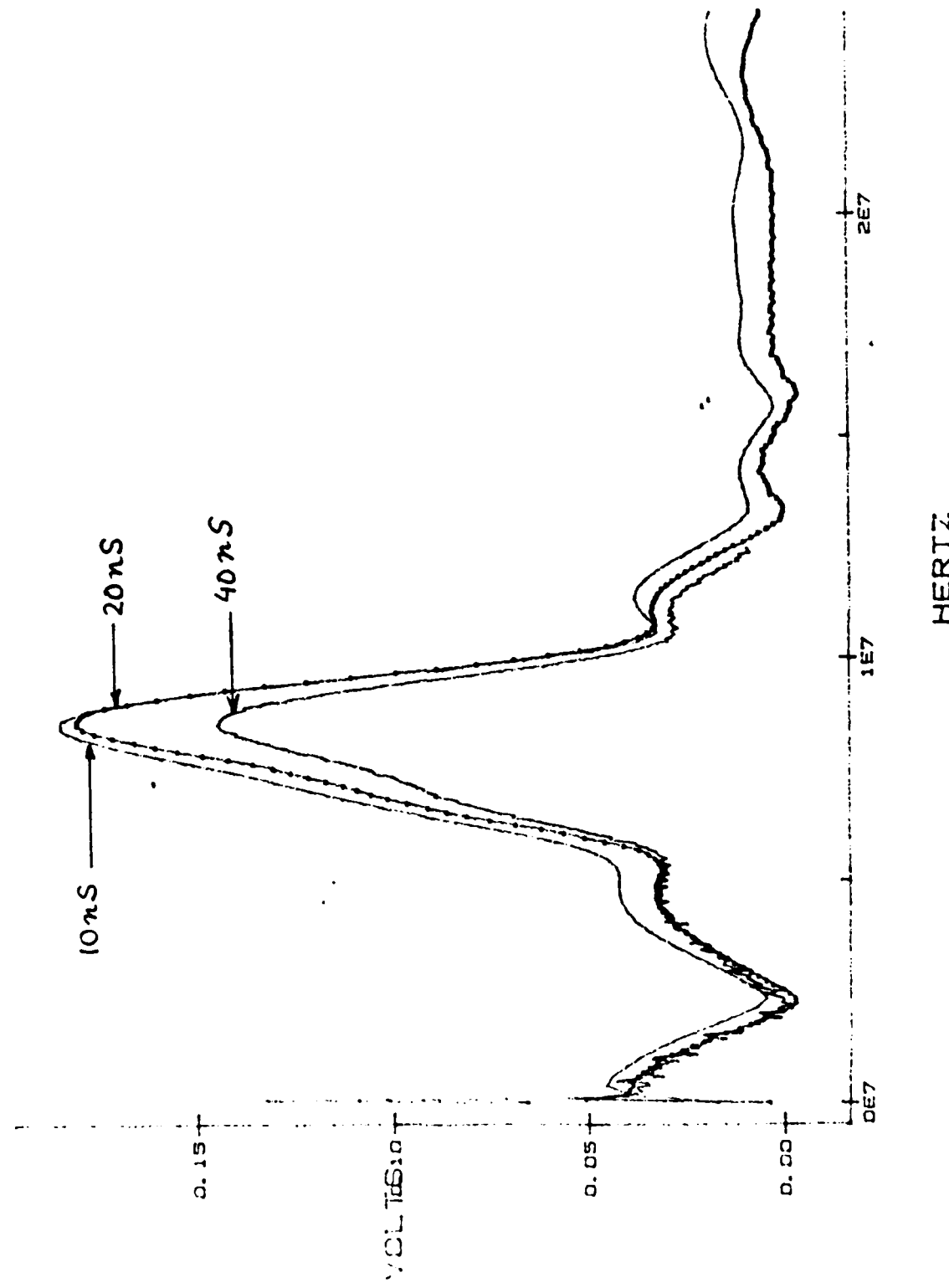


Fig. 10. Effect of sampling interval on transducer response.

In all the measurements made to date digitizing intervals of 10 or 20 ns have been used.

The second factor considered in analyzing data is the resolution of the signal in frequency domain. In the Fourier transformation the difference in frequency between the digitizing points is $\Delta f = 1/L$ where L is the signal length. The signal length can be computed by $L = N\Delta t$ where N is the total number of digitizing points and Δt is the digitizing interval. As described earlier, the digitizing interval of 10 and 20 ns is being used and is therefore, fixed. Hence we can increase L by increasing N and get a better resolution i.e. smaller Δf in the frequency domain. A resolution of $\Delta f = 0.1$ MHz was considered satisfactory and could be obtained by taking $N = 1024$ and $\Delta t = 10$ ns.

The third factor is the determination of the useful frequency range of transducer. The FFT of the time domain signal $f(t)$ in Fig. 5. is shown in Fig. 11. This is the plot of $|F^*(\omega)|$. Note also that $F^*(\omega)$ appears in the denominator of equation (60) and hence when the values of $|F^*(\omega)|$ are very small, will give rise to erroneous results. Thus, as seen in Fig. 11, the useful range of frequencies over which the calculations of equation (60) can be performed, is limited. We chose the criterion to limit $|F^*(\omega)|$ to 25% of its peak value. The range so obtained for the 10MHz transducer on an aluminum specimen is indicated in Fig. 11. It is to be noted here that the response of the transducer has some meaning when it is being used against a specimen. Hence the same transducer will respond differently against different specimens and the useful range has to be obtained for every transducer-specimen combination.

MAGCA1

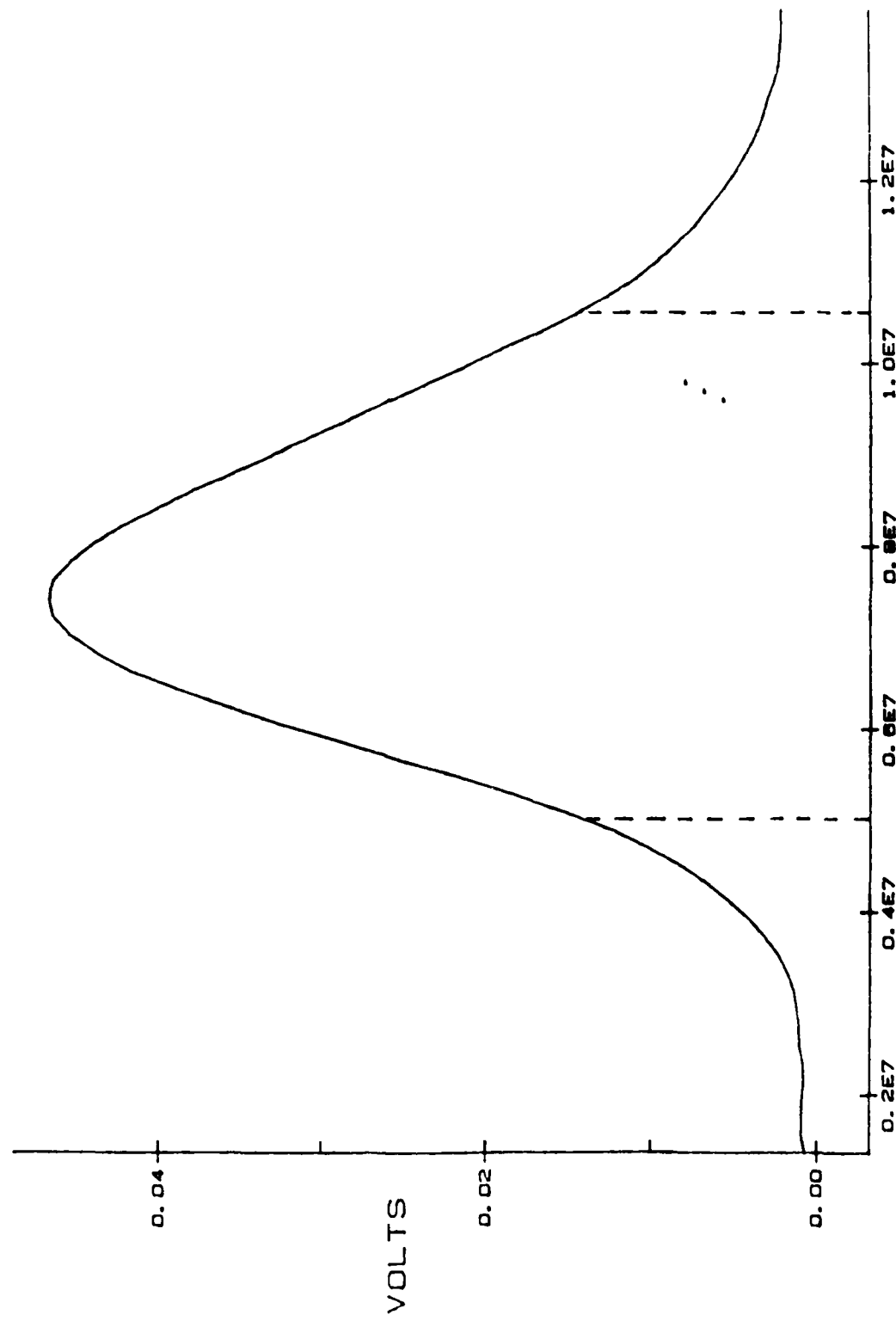


Fig. 11. Response of a 10MHz 'P' transducer in direct contact with all specimen.

The fourth factor considered is: what do we mean when we say first or second pulse? In a continuous signal where do we decide the first pulse has ended and second started? The answer to this problem is not straightforward and especially in thin samples and composite materials there is no logical way of deciding this. Hence, in the technique development stage we took aluminum samples of thickness such that one pulse dies down completely before the second arrives. Then the middle point between the pulses, where the signal is small, is taken as the end of one pulse and the start of the next.

This technique was applied to aluminum samples. Tests were conducted and wave speeds repeatable to $\pm 0.05\%$ were obtained. One very obvious source of error was the oil layer. The thickness of the oil layer could not be controlled. This source of error was eliminated by immersing the specimen and transducer in water and using water as the coupling medium. The repeatability of the tests was improved from $\pm 0.05\%$ to $\pm 0.02\%$.

In the next phase of development, the technique was applied to composite specimen. Following problems were encountered

a. Composites highly attenuate the signals being used. Hence the second pulse (Fig. 12) is very small and can not be used to get good results.

b. Composites are highly dispersive and hence as the signal passes through the specimen, it spreads in time domain. Due to this effect, the tail of one pulse and the head of the subsequent pulse begin to overlap. This phenomenon will be called the spillover of the pulses.

The first problem was solved by noting from equation (50) that the front surface reflection (Ray 2, Fig. 2), as shown in Fig. 12., can also

Avg. A1

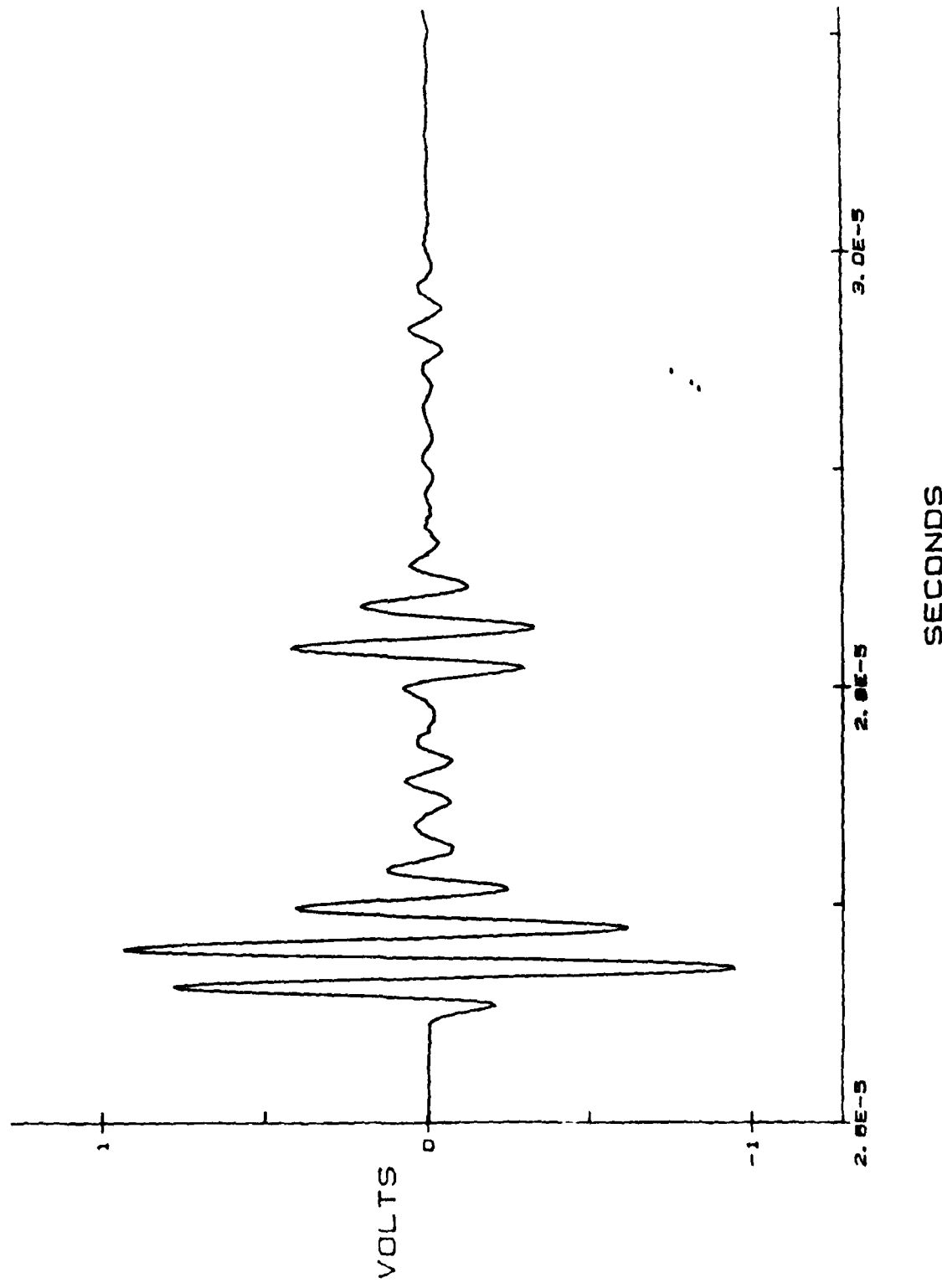


Fig. 12. Time domain signal in composite (water immersion, P waves)

be used as the reference wave in place of the first pulse. Therefore, for composites we use the front surface reflection and the first pulse to calculate the wave speed. Since front surface reflection does not traverse the specimen, it does not suffer from dispersion or broadening. It was found that the spillover problem was minimized when the front surface reflection and the first back surface reflection (first pulse) were used. Hence we were able to eliminate problem (a) and reduce problem (b) by the proper selection of pulses.

Two major problems in the implementation of this are being resolved now; these are:

- (1) The operator decides when one pulse ends and the second one starts. This slows down the process of data collection. This problem is severe and is unacceptable for thin specimen.
- (2) For dispersive medium the spillover effect becomes very profound.

Work is in progress aimed at eliminating these restrictions. As per equation (50) these problems can be eliminated by using the front surface reflection as the reference signal and then using the entire signal with all the reflections, to obtain the wavespeed. We are also in the process of calculating the attenuation of the waves through the specimen which is another important factor in assessing damage in composites.

4. Results*

Figure 13 is an overview of the equipment used. The experiment is initiated at the pulser/receiver (Panametrics Ultrasonic Analyzer Model 5052UA). The analyzer is a broadband ultrasonic device which includes a pulser, a receiver, a stepless gate, and a gated peak detector. The analyzer sends a broadband pulse of about 300 volts peak-to-peak to the transducer at a repetition rate selected by the operator. At the same instance (taken as time $t=0$) a triggering pulse is sent to the digitizing oscilloscope (Data Precision Model data 6000). The transducer launches a compressional wave in water towards the specimen. The same transducer is used to receive the reflected signals from the specimen. The signals are then sent back through the analyzer where the stepless gate is used to isolate the desired portion of the waveform from the spurious signals. From the analyzer the gated waveform is sent to the Data 6000 for signal processing. All FFT computations are performed at the Data 6000 and the results are sent to the Minc PDP 11/23 through an IEEE 488 bus line.

Longitudinal wave speed in the composite was measured by using the front-surface reflection (Ray 2, Fig. 2) and the first back-surface reflection (Ray 6, Fig. 2) and eq. (39). The initial parameters that must be determined prior to running the program are: 1) frequency range for the least squares curve fit of the phase vs. frequency plot, and 2) cursor location i.e. the point at which the two reflections will be separated.

All composite specimens were fabricated using Magnamite AS4/3502 prepreg tape. A list of specimens and associated geometry is given in Table 1.

*Prepared by J.G. Eden (M.S. Student)

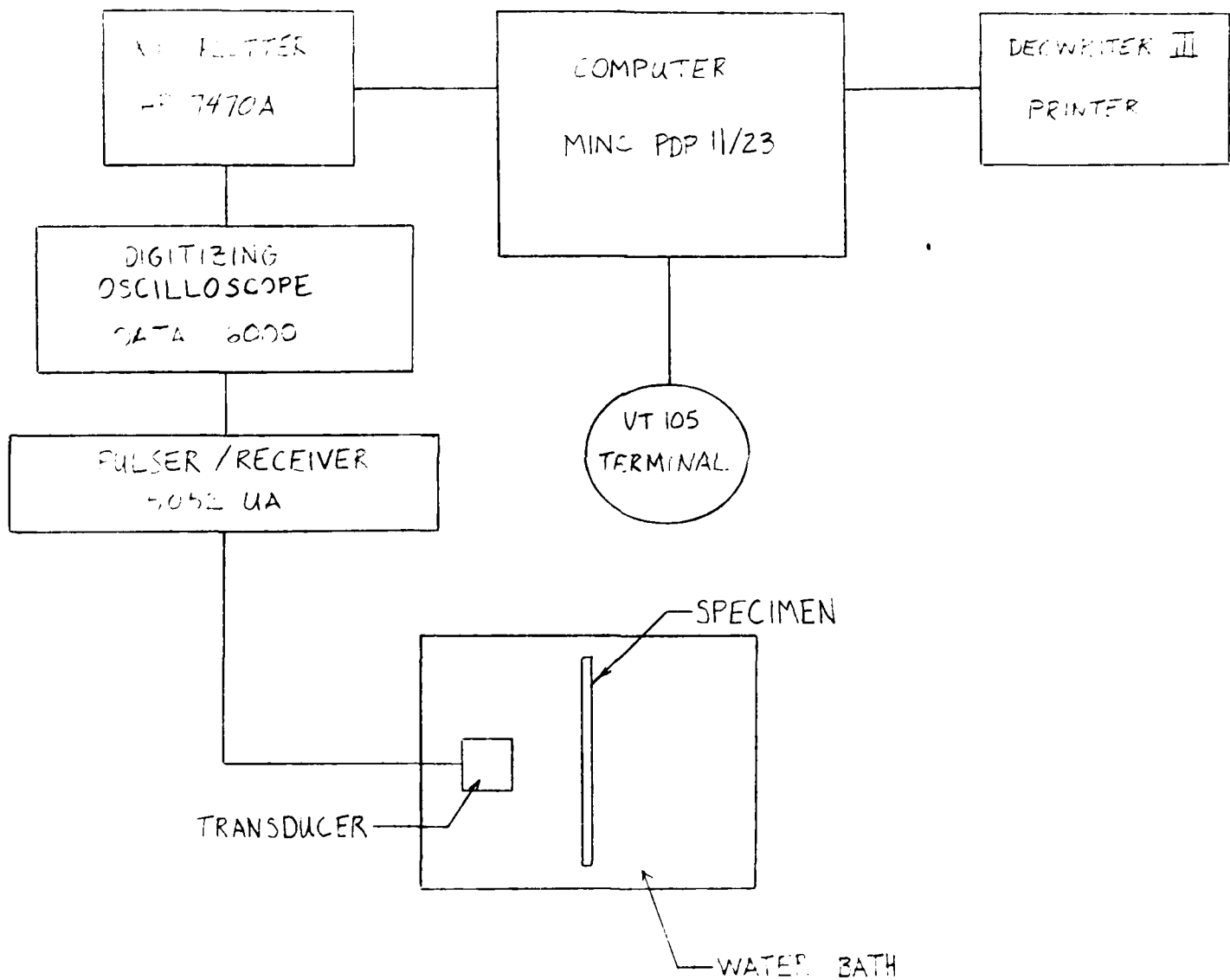


Fig. 13. Achematic of the experimental arrangement

TABLE 1

SPE MEL NUMBER	LAYER DIAMETER
16/1-10	$[O_2 / ^{\circ}C_2]_{15}$
18/1-10	$[O / ^{\circ}C]_{15}$
24/1-5	$[O_2 / ^{\circ}C_2]_{25}$

The main objective for using FFT signal processing was to achieve a very high level of precision in wave speed measurement ($\pm 0.2\%$). To date we have identified four major sources of error: 1) temperature, 2) water absorption, 3) positioning of specimen, and 4) repetition rate.

1. Temperature - It is well known that in most materials the stiffness, and therefore the wavespeed depends upon temperature. In order to carry out a well "controlled" experiment it was deemed essential to study the temperature dependence of the wave speed in a composite specimen. The temperature range studied was from 6°C to 30°C . Specimen 16-5 was used for the investigation (see Table 1). From Figure 14 it is observed that over the range of 6° to 30°C there was an approximately 2% decrease in the wavespeed. The straight line is the result of a linear least square fit. In the present set-up we have the capability to control the temperature to $\pm 0.5^{\circ}\text{C}$. From Fig. 3 it was found that a 0.5°C change in temperature corresponded to only 0.05% change in velocity i.e. the temperature contribution to the total error is about 0.05% which - in view of the overall objective of $\pm 0.2\%$ error - is an acceptable figure.

2. Water Absorption - For [0/90] geometry laminates the major form of damage created by tensile loading is transverse cracking. Since this technique involves water immersion it was of some concern that the damaged composite may be absorbing moisture via the newly created cracks. It was found that for highly damaged specimens water absorption during measurements could cause variations of $\pm 3\%$ (cf. measurement error of 0.2%). In order to eliminate this problem specimen edges were coated with a strippable coating. This precaution measurably eliminated the problem.

TEMPERATURE INFLUENCE TEST \ 16-5

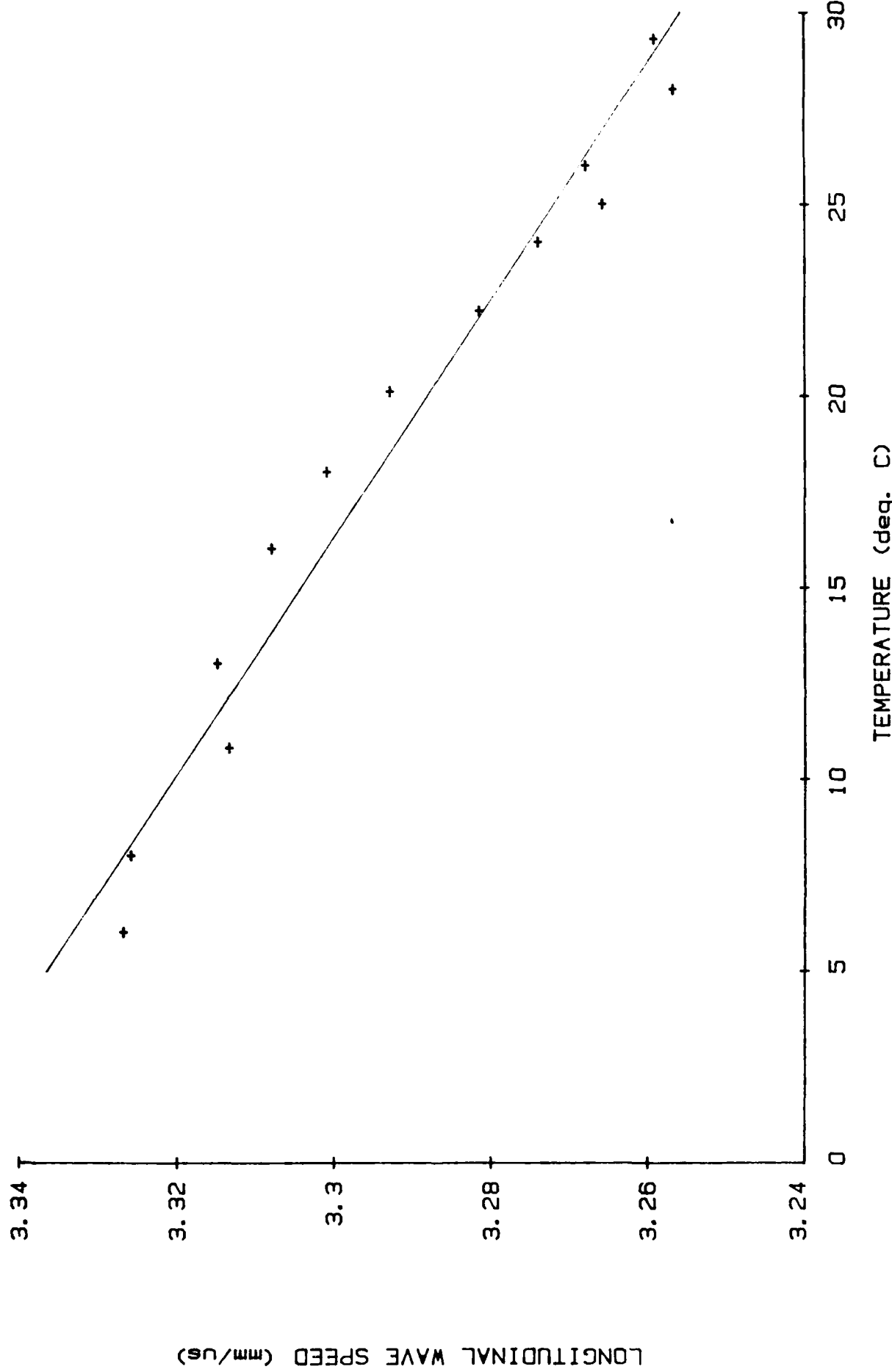


Fig. 14. The longitudinal wavespeed decreases with temperature.

3. Positioning - Due to the inconsistencies within a composite (ie. matrix or fiber rich regions, thickness variations, surface mark, etc.) a means for reproducing the same position of the transducer relative to the specimen was developed. It is estimated that the position accuracy is within ± 0.001 in.

4. Repetition Rate - As mentioned earlier a repetition rate is selected by the operator. In the early stages of this work, we selected a repetition rate of 5KHz, for no particular reason. This means that the experiment was repeated every 0.2 milliseconds (ms). Random errors as high as $\pm 5\%$ were observed. A careful examination of the experimental procedure revealed the following source of the error. Suppose the transducer is energized at time $t=0$. It will take some time (say t_0) before the mechanical energy - propagating in the form of waves - will be completely dissipated. If the subsequent experiment is initiated at some time $t < t_0$, the results will be erroneous: the waves leftover from the "previous" experiment will interfere with the waves of the "present" experiment. This phenomenon sets an upper limit on the repetition rate (lower limit on the time between two experiments). By trial and error we found the upper limit on repetition rate to be 1 KHz (i.e. time interval of one millisecond).

Technique Calibration In order to calibrate the technique the longitudinal wavespeed of aluminum was measured first. The surfaces of a block of aluminum (0.1895 in. thick) were polished to a $0.1 \mu\text{m}$ finish. The water bath temperature was held fixed to $\pm 0.1^\circ\text{C}$. A transducer with a 5MHz center frequency was used. The front-surface and the first back-surface reflections are shown in Fig. 15; the FFT of the former is shown in Fig. 16. The specimen was held fixed at one place. The results of

Avg. A1

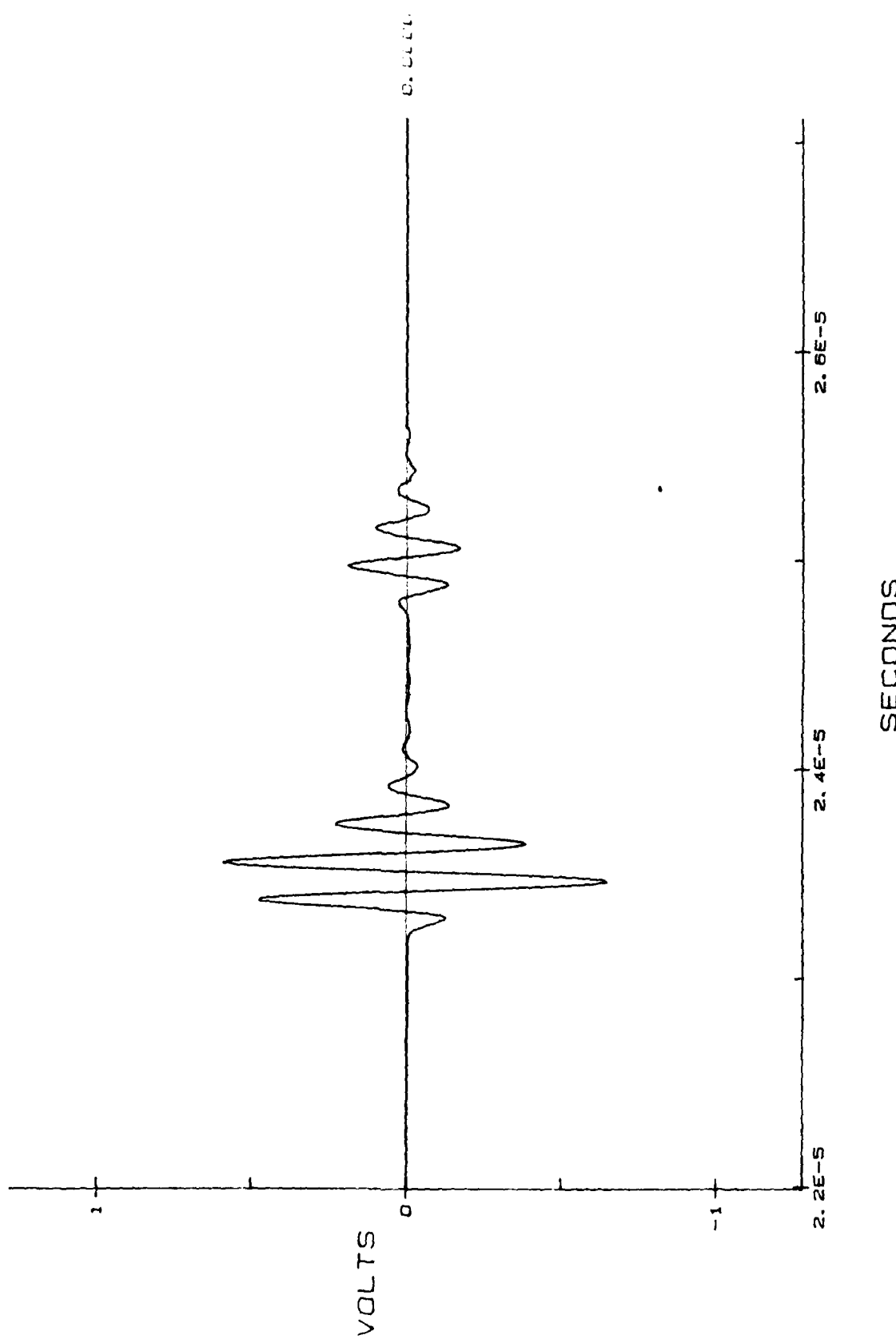


Fig. 15. Front-surface and back-surface reflections from an aluminum specimen.

MAGCA1

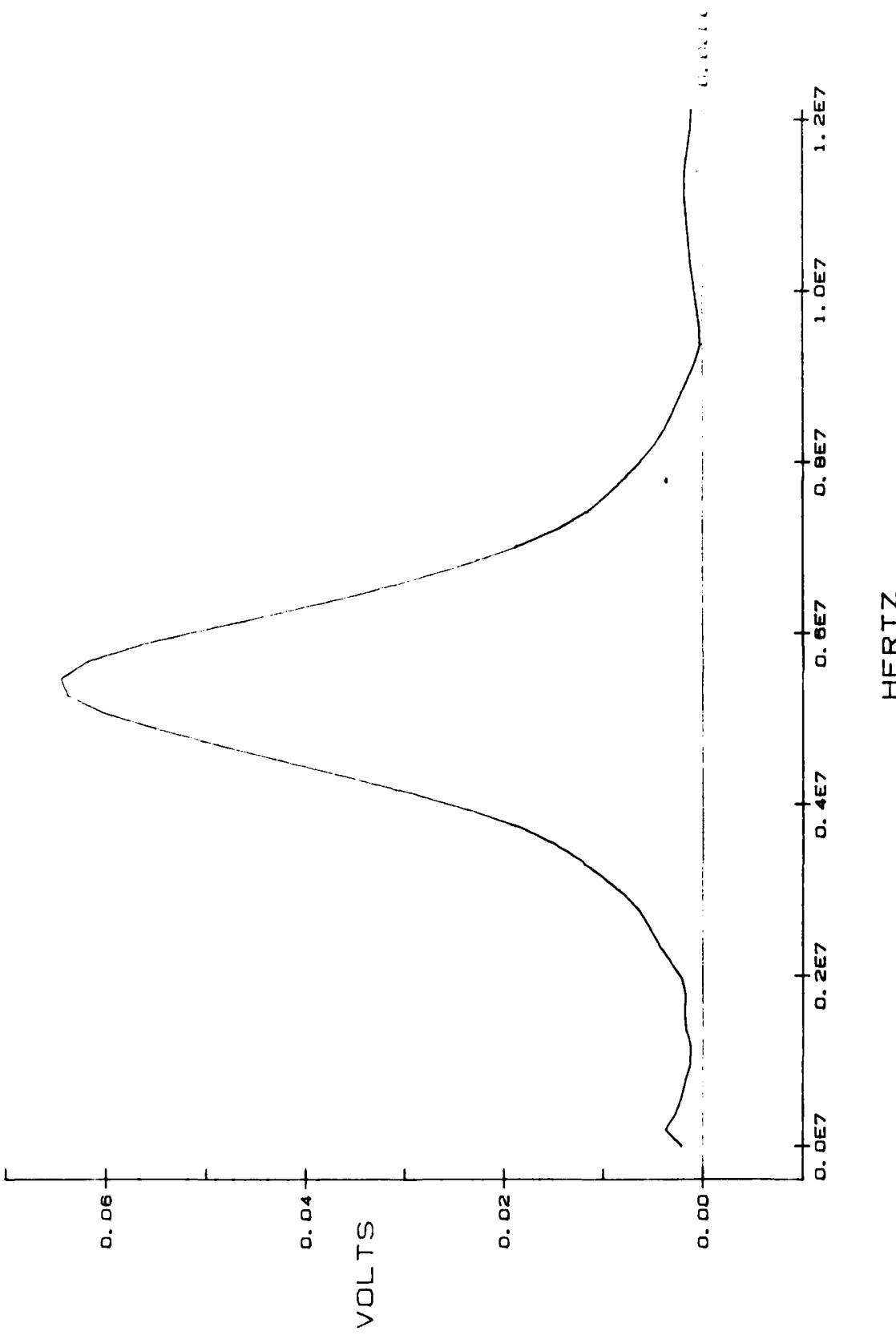


Fig. 16. FFT of the front-surface reflection from aluminum (Fig. 15)

five measurements are shown in Fig. 17; the reproducibility is $\pm 0.02\%$ i.e. two parts per ten thousand. Solid lines indicate the error bounds. Next, we studied the effect of removing, drying, and replacing the specimen (mimicing the corresponding events for an actual composite specimen) The results are shown in Fig. 18. The precision is reduced from 0.02% in Fig. 17 (specimen not removed) to 0.08% here, the hash marks indicate the error bounds.

The attention is now turned to a Graphite/Epoxy specimen (16-5). To study the "worst case" we took the most severely damaged specimen. Fig. 19 shows the time domain signal for the first two reflections. Note that due to dispersion of the wave the second pulse has "spilled over" into the first pulse. The operator judgement was used to place the cursor mark at the "end" of the first pulse. The FFT of the first signal is shown in Fig. 20. When the specimen was not removed from its position, the repeatability was found to be $\pm 0.02\%$ (Fig. 21). However, when the specimen is removed, dried and replaced the error increases by a factor of five to 0.1% (Fig. 22).

In conclusion, the present technique has been developed to the point where even for the worst-damage case the measurement error is claimed to be about 0.2% (using a factor of safety of two).

Work in Progress

Work is now in progress in which a specimen will be loaded monotonically to a certain load level and then unloaded. Following measurements will be made: (1) Longitudinal wavespeed;
(2) Axial stiffness
(3) Edge replication (crack density and total crack surface area)

ALUMINUM CALIBRATION (did not remove)

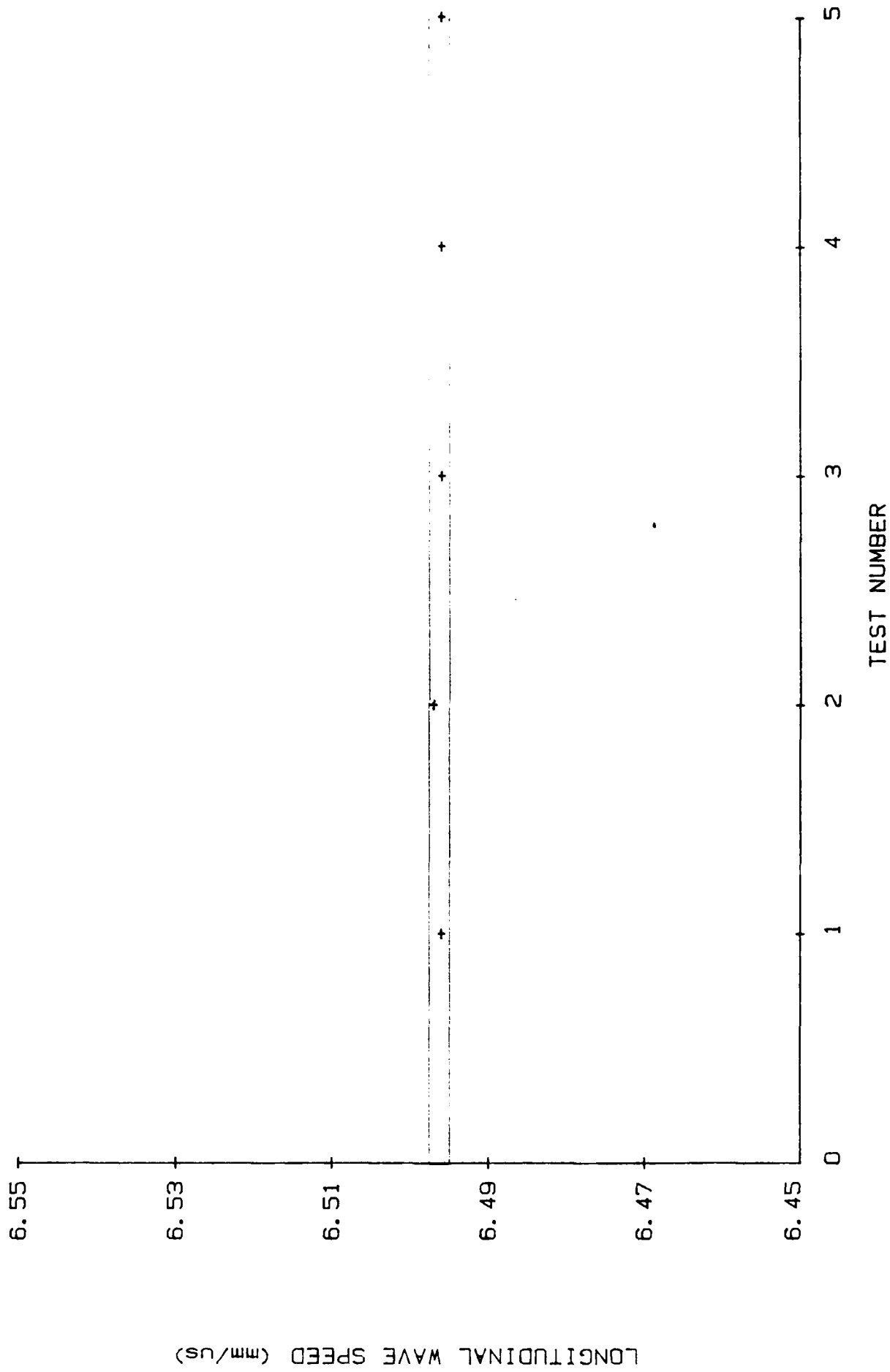


Fig. 17.

ALUMINUM CALIBRATION (replaced each time)

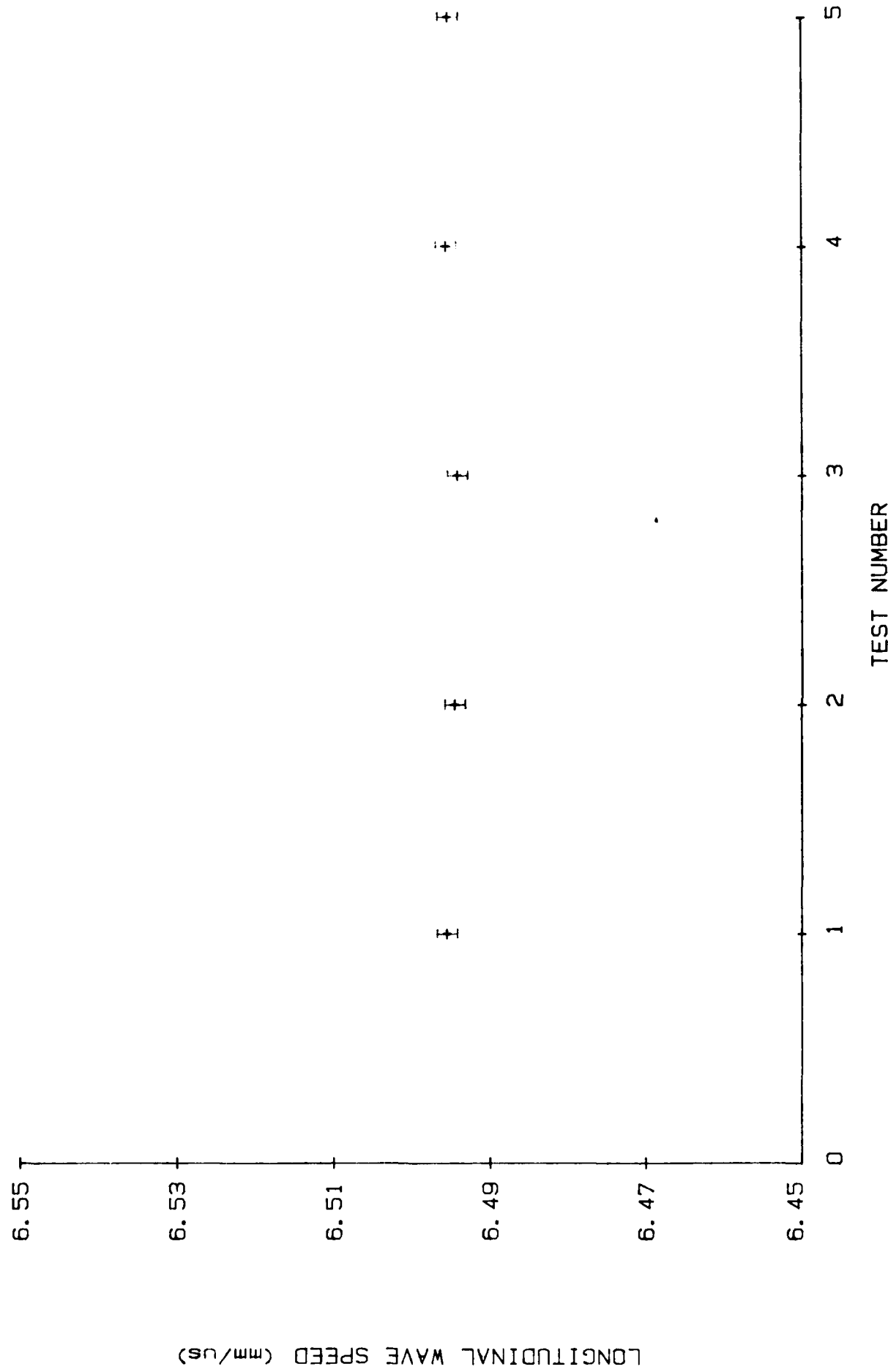


Fig. 18

AVG. A1

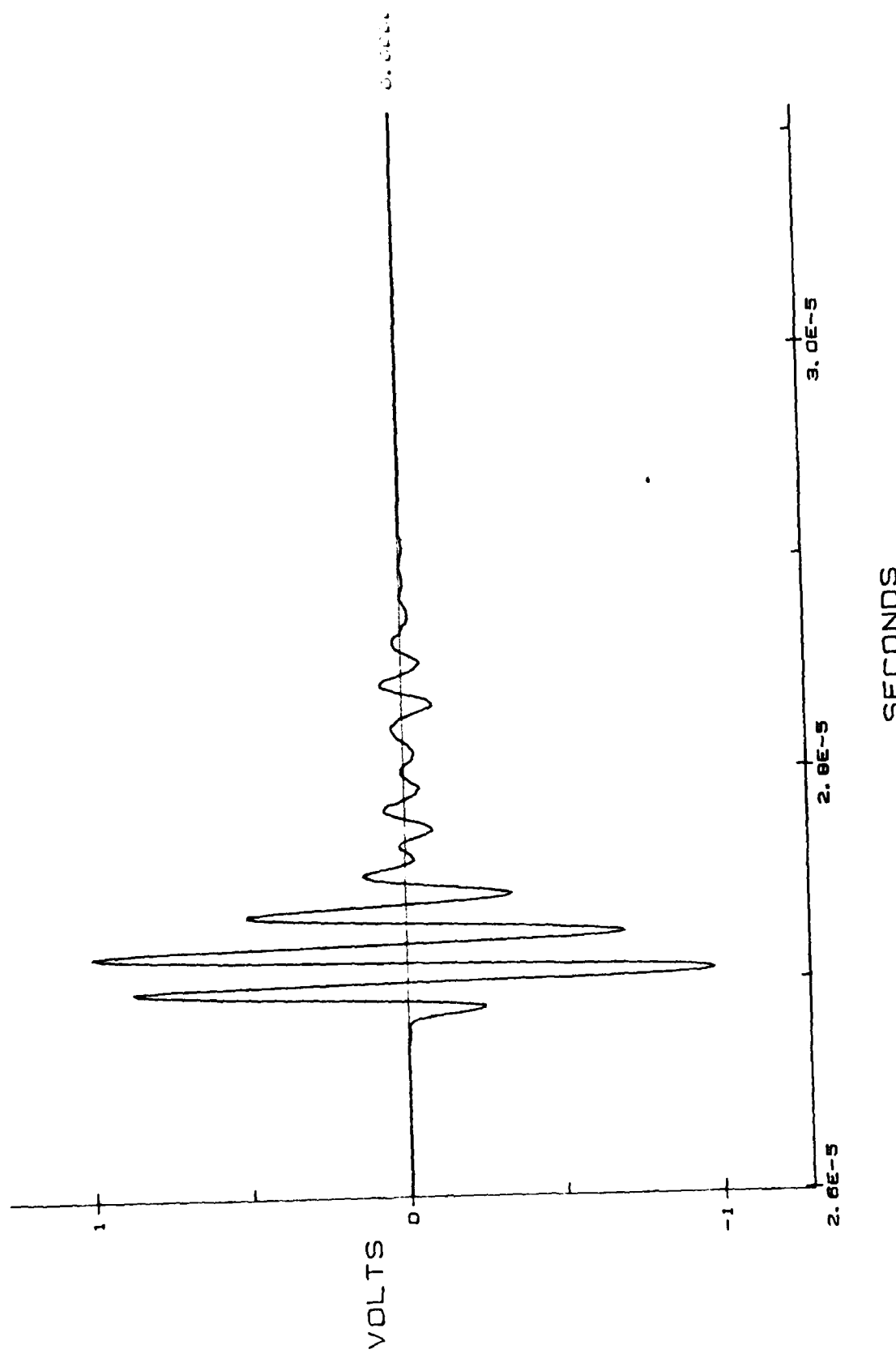


Fig. 19. Front-surface and back-surface reflections from a highly damaged composite specimen

MAGCA1

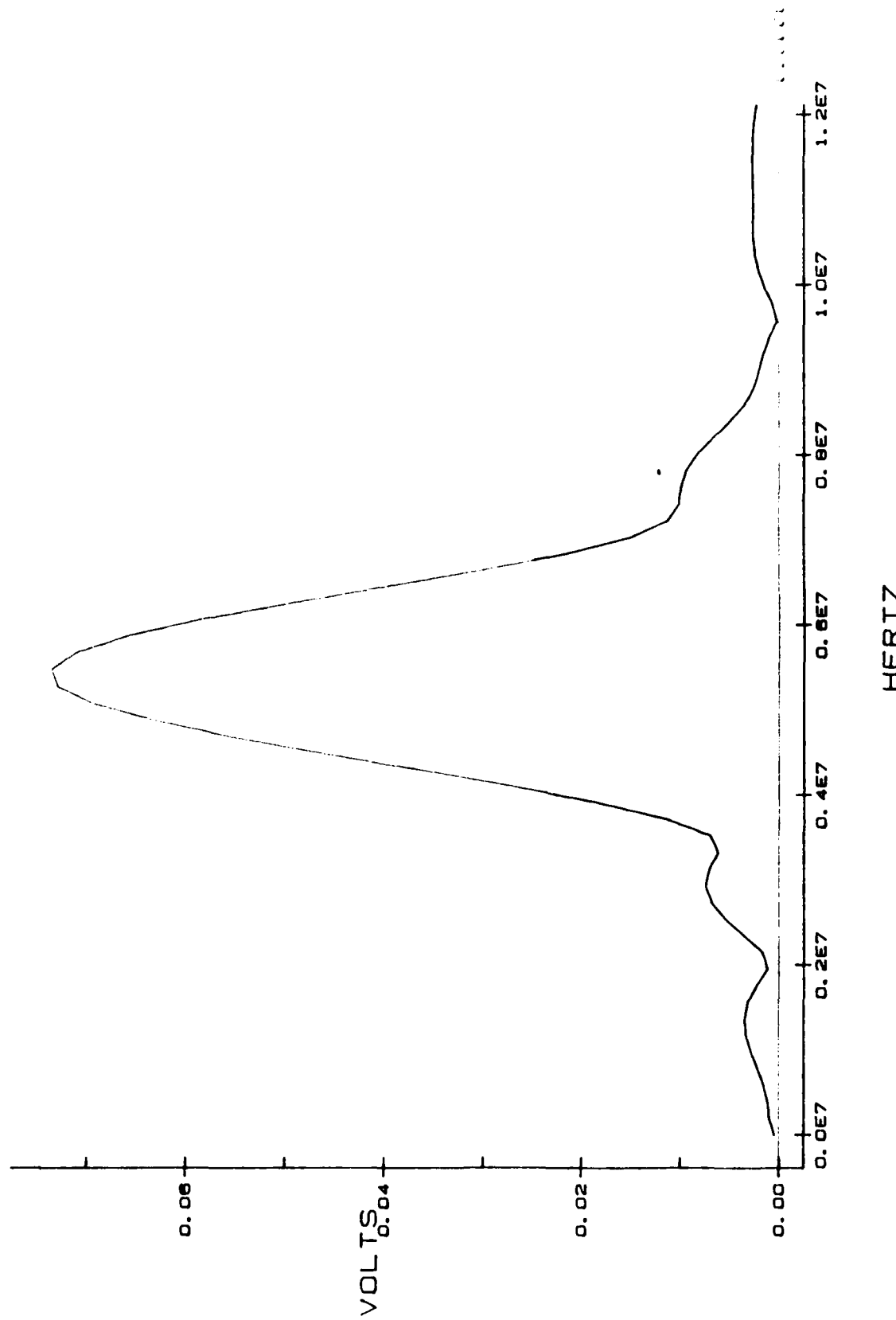


Fig. 20. FFT of the front-surface reflection from the composite; see Fig. 19.

SPECIMEN 16-5 (maximum damage)

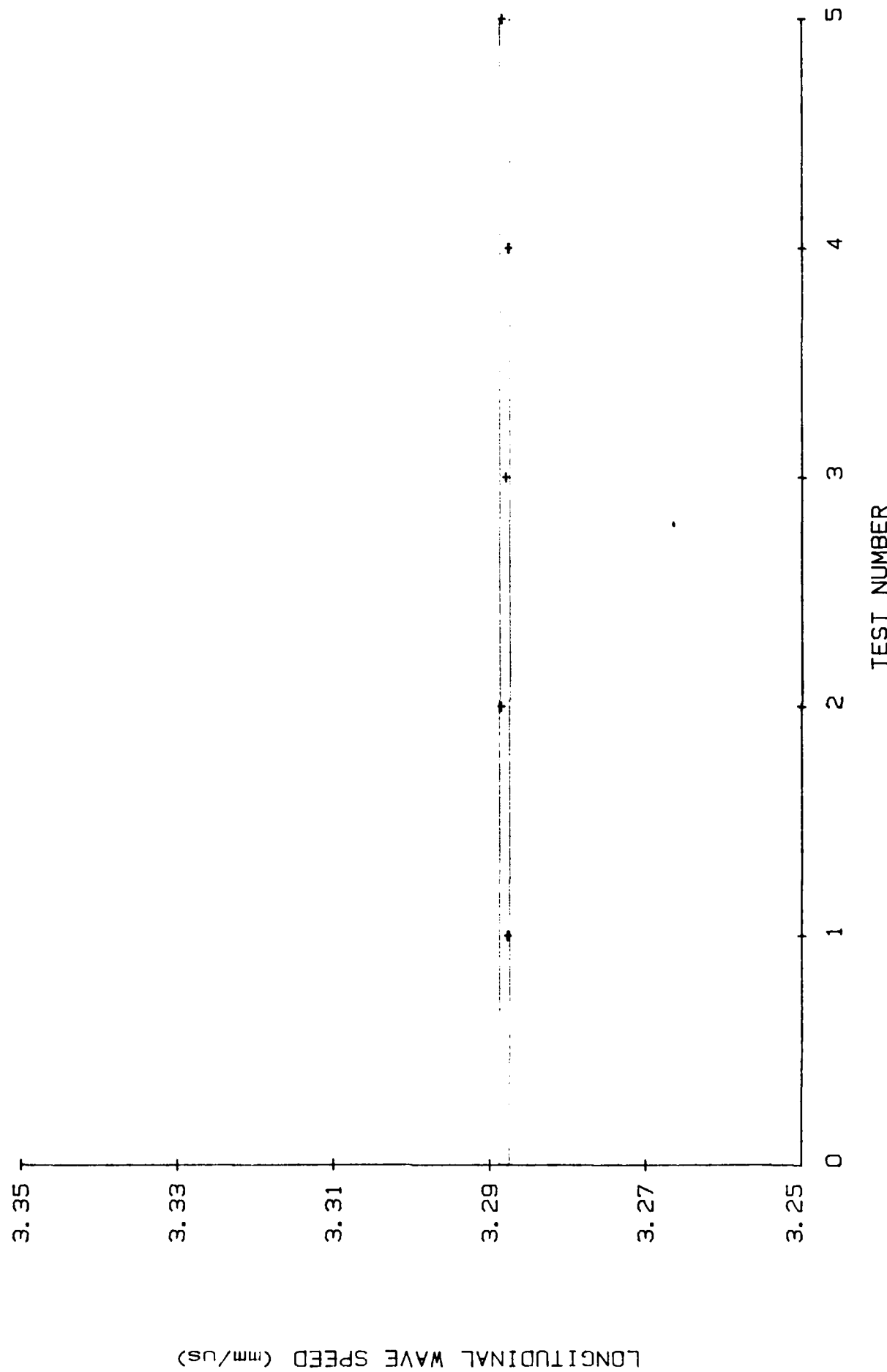


Fig. 21

SPECIMEN 16-5 (replaced each time)

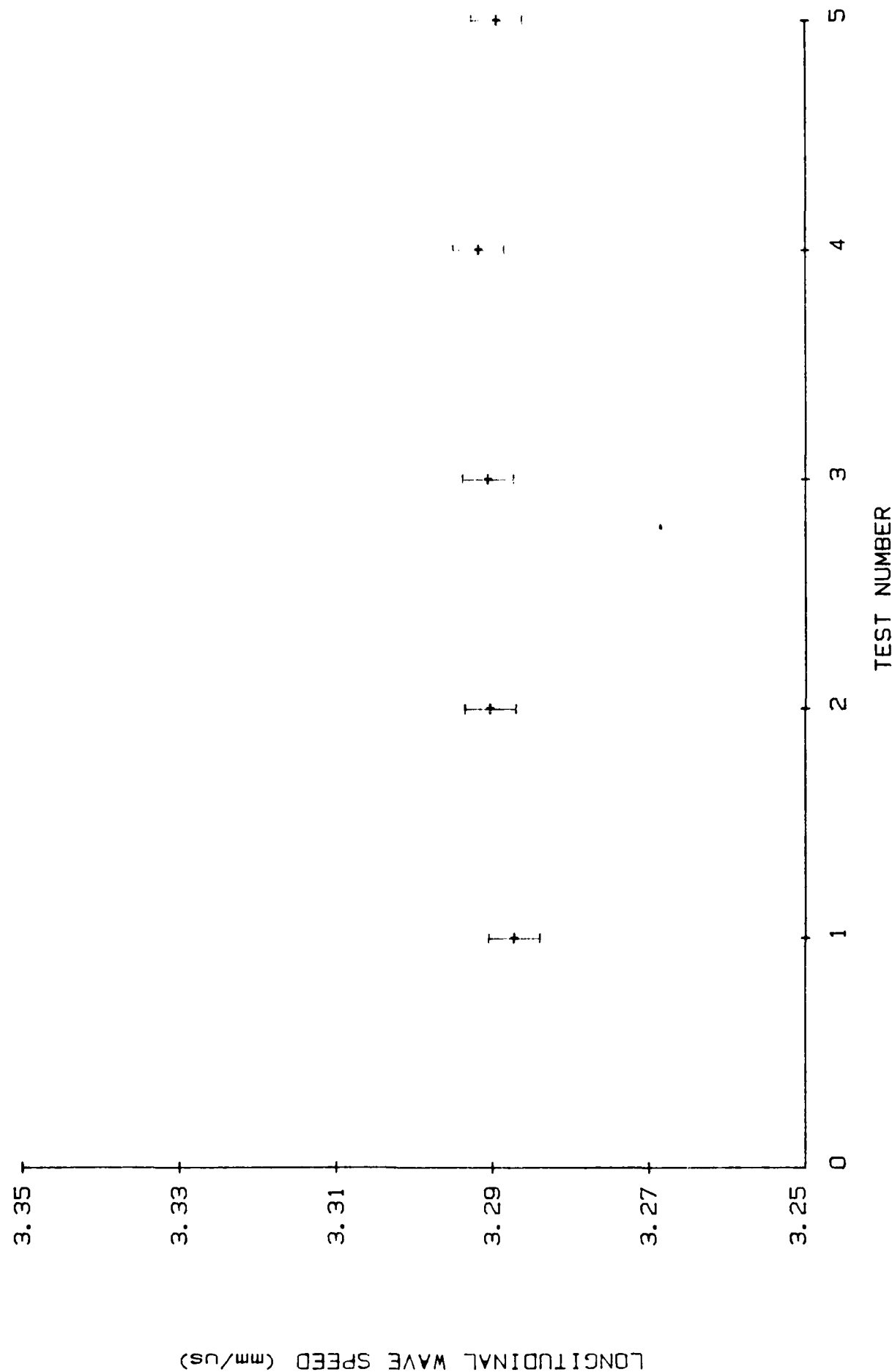


Fig. 22

The specimen is then reloaded to a higher load level and the sequence is repeated until the final failure occurs.

Some preliminary results have been obtained. But these are contrary to what was expected. These results are being carefully examined for some additional sources of error.

5. Professional Personnel

1. Dr. Vikram K. Kinra, Principal Investigator
2. Mr. J. Greg Eden, M.S. Student
3. Mr. Vinay Dayal, Ph.D. Student
4. Mr. Vasu Iyer, Ph.D. Student (Will replace Mr. Eden after he
finishes his M.S. in May/June 1985)
5. Mr. J. Grillo, Laboratory Technician-Mechanical
6. Mr. P. Patti, Laboratory Technician Electronics

6. Interactions

1. Attended "Vibration Damping Workshop", Long Beach, California February 1984.
2. Chaired a session, "Composites II" at the V International Congress on Experimental Mechanics, Montreal, June 1984.
3. Presented a paper at the Sixth International Conference on Fracture Mechanics, New Delhi, India, December 1984.
4. Organiser and Chairman of a session, "Ultrasonic Nondestructive Evaluation of Composites" at the forthcoming Spring conference of Society for Experimental Mechanics, Las Vega, June, 1985.
5. Will be presenting an invited review paper, "Some Experiments Concerning Multiple Scattering of Elastic Waves in Random Media" at a Symposium/Workshop, "Multiple Scattering of Waves in Random Media and by Random Rough Surfaces", The Pennsylvania State University, July 1985.
6. Held technical consultations concerning the project with technical staff of the following:
 - (a) Martin Marietta Aerospace, Denver
 - (b) Douglas Aircraft Corporation, Long Beach
 - (c) Hercules Corporation, Utah

Appendix I.

A Survey of Literature Concerning Ultrasonic Nondestructive Testing of Composite Materials.

A Survey of Literature Concerning Ultrasonic

Nondestructive Testing of Composite Materials

by

John Gregory Eden

The methods for detecting damage may be separated into two categories: 1) Destructive testing, and 2) Nondestructive Testing and Evaluation (NDTE). Destructive testing is self-explanatory. One such destructive test is the deply technique [4]. Composite test specimens are pyrolyzed after being impregnated with gold chloride diethylether solution. Upon unstacking, the laminate damage due to loading may be viewed with the use of a stereo microscope and fluorescent lamp. Destructive testing has one major drawback- the specimens are destroyed. Therefore, NDTE techniques are much more desirable from the viewpoint of field applications.

Reifsnider, et.al. [5] defines NDE as `...that activity associated with experimental schemes used to interrogate the state of stress and state of the material without influencing either of those states or altering the strength, stiffness, and life of the laminates being

evaluated'. A complete description and comparison of NDE techniques is given by Sendeckyj [6]. Nondestructive techniques such as surface replication, X-ray radiography, vibrothermography, holography, and liquid crystal coatings have been applied to composite materials by Stalnaker [7], Dance [8], Jones [9], Maddux [10], and Charles [11], respectively.

The main focus of the present research concerns the application of ultrasonics to assess damage in composite materials due to fatigue or monotonic loading. Much work has been done in the area of Acoustic Emission (AE). Whenever a failure mechanism takes place (ie., fiber breakage, matrix cracking, etc.) stress waves are emitted from the source. By monitoring a test specimen under loading with a triangular array of transducers one may locate the failure site by using the arrival times of the stress pulses received at the transducers. Bailey, Freeman, and Hamilton [12] used the above technique in conjunction with X-ray radiography to correlate AE signal amplitudes with different types of damage progression in fatigue loaded composite plates. R. Williams [13] has combined AE and thermography to monitor damage growth in Boron/epoxy and Boron/aluminum specimens subjected to fatigue loading. Arora and Tangri [14] used AE techniques to detect and continuously monitor subcritical crack growth in Zr-2.5% Nb. Block [15] tested a number of composite specimens and

determined that AE events generated by fiber fracture have substantially higher peak amplitudes than those generated by resin-controlled mechanisms. Ulman [16] observed that an increase in AE count rate coincided with the onset of matrix plasticity and also damage development at high loads in metal matrix composites.

As reported by Williams and Egan [17] AE results contained in much of the literature are largely qualitative even though quantitative measures are often presented. Comparison of AE research is almost impossible due to the insufficient reporting of the technique used. Also, due to the complexity of the problem, even within a single specimen a small change in stress may result in a number of AE events, some of which may initiate from different sources. Therefore, comparison of single AE events to one another will most likely not lead to source mechanism discrimination. However, by combining individual AE spectral densities to derive 'mean' normalized densities which in turn could be statistically analyzed, Williams and Egan were able to provide quantitative discrimination between AE from 10, 90, [$\pm 45, \pm 45$] degree specimens during tensile loading.

Another type of ultrasonic evaluation is the C-scan. Blake [18-21] has reported on the application of C-scan digital systems to NDE of composite materials. Analyzing the signature formed by digitally monitoring the amplitude

of a particular segment of a received ultrasonic waveform can lead to information regarding material discontinuities. Time domain representations of the wave form can be used to correlate discontinuities which appear similar in the amplitude signature. The technique involves coupling a transducer to the specimen and propagating longitudinal waves through the thickness direction. The same transducer is used to receive the reflected sound waves. The received signal may now be processed by analog or digitally. If by analog, the gated portion of the total waveform is peak-height analyzed. The peak output is quantized to ten discrete levels in 0.1 volt increments. Each increasing level corresponds to a darker shade of gray when transmitted to a pen amplifier. The pen burns the surface layers of an ink-impregnated, electrically conductive paper to produce a picture of the specimen's material integrity. Alternatively, one could digitize the received signal [18-21]. The digitized signal can then be processed by a computer. Peak data (voltage) is sent through a microprocessor which performs gray scale conversions and in turn sends this data to either a dot-matrix printer, an analog conductive paper system, or a color graphics system. Chang, et.al. [22,23] have developed an in-service inspection system (ISIS) which can produce hard-copy real time plots and post-inspection C-scans to be used in production hand scanning. Post-inspection flaw

magnification, flaw-amplitude listing, and RF (radio frequency) waveform digitization are the major advantages of the ISIS. Kiraly and Meyn [24] have developed a computer controlled scanning system to monitor the initiation and progression of local damage patterns in composite specimens under tensile loading. While scanning a specimen, a 16-level gray scale image is displayed on a CRT and stored on a floppy disk. The images may be stored in sequence of load step which can be played back to create a movie showing damage growth as a function of loading. Daniel [25] has conducted C-scan evaluations of fatigue loaded specimens with temperature and moisture variations to monitor flaw growth in graphite/epoxy laminates containing initial flaws. Liber [26] has used C-scan to determine damage behavior in flat and cylindrical composite specimens with pre-existing flaws. The limitation of the C-scan technique is that it only works with relatively large delamination flaws; it yields little information about other flaw types. However, the technique is qualified in that it provides a pictorial view of specimen quality.

In the work done by Dreumal and Speijer [27,28] a technique called Polar Scan was developed which can generate an image that is a unique fingerprint of a specific laminate. The technique involves rotating the particular specimen of interest between two transducers and monitoring the amplitude of the through transmitted

ultrasonic wave. In this way layer orientation and stacking sequence may be determined. In the same manner as C-scan, the signal is transformed into brightness modulation to be viewed on a video screen.

In a series of papers Vary and his co-workers [29-37] have studied the ultrasonic stress wave factor (SWF) and its relation to material characteristics. This technique works on the principle of energy dissipation in a material. During failure in composites stress waves are generated which interact with the different plies to promote microcracking and crack extension. The effect of the stress waves is restricted by the amount of scattering, dispersion, and reflections due to microstructure and boundary conditions of the specimen. Vary's technique involves a more qualitative approach to damage detection. Broad-band ultrasonic pulses are propagated at normal incidence to the specimen by a transducer. A stress wave is excited by the pulses and travels in the lengthwise direction where it is received by another ultrasonic transducer. The received signal consists of a great number of oscillations due to multiple reverberations in the specimen. In order to analyze the signal Vary defines the SWF as $E = (R) * (T) * (C)$. SWF is a measure of the efficiency of stress wave energy transmission. R is the pulse repetition rate, T is an interval of time predetermined for the receiver circuit reset timer, and C is the number of

ringdown oscillations exceeding a preset threshold voltage. Vary has shown that microvoid content, ultimate tensile strength, cure pressure, and interlaminar shear strength all effect the value of SWF. Also, the SWF was determined at various positions along specimens and the location of minimum values of SWF correlated with the actual failure sites when the specimens were loaded to failure.

Following Vary, Williams et.al. [38-42] have studied the effect of fatigue and impact loading on SWF and attenuation. In earlier works with metals, Truell and Hikata [43] established a relation between the attenuation and number of recorded fatigue cycles in aluminum. Joshi and Green [44] have successfully used attenuation to monitor fatigue damage in polycrystalline aluminum and steel specimens. Williams and Doll [38] have monitored attenuation and wave velocity in compression-compression fatigue loaded unidirectional composites in the frequency range of .5 to 2 MHz. Within $\pm 5\%$ accuracy no change in wave velocity as a function of fatigue was detected. However, initial attenuation above 1.5 MHz was found to be a good indicator of relative fatigue life. Williams and Lampert [42] determined that impact damage in graphite fiber composites can be assessed quantitatively using either the through-the-thickness attenuation or the SWF. Williams, Hashemi, and Lee [41] conducted a complete study of ultrasonic attenuation and velocity in AS/3501-6

composites. In the frequency range of .25 to 14 MHz they found the wave velocity to be frequency independent although attenuation was frequency dependent. Williams, Yuce, and Lee [39] measured the attenuation at 4 MHz through composite specimens which varied in cure temperature and pressures and found good correlation with the number of fatigue cycles to failure and an increase in attenuation. Hayford, et.al. [45] determined correlations between initial attenuation and shear strength in graphite polyimide composites. Henneke, et.al. [46] have also studied the relation between SWF and fatigue life in composite materials. Talreja [47] has applied spectral frequency analysis and observed close agreement between spectral density and stiffness changes. Nimmer [48] has used attenuation and wave velocity to monitor damage accumulation in composite flywheel disks. Hemann [49] has conducted a study of the effect of stress on ultrasonic pulses in fiberous composites. The velocities were found to be frequency dependent, but weakly dependent on the stress in the specimen.

The anisotropy of composite materials can greatly complicate the interpretation of the received ultrasonic signal. Kriz, et.al. [50-52] and Kinra and Eden [53] have applied the solutions of the Christoffel [54] equations to graphically depict stiffness, longitudinal wave velocity, and shear wave velocity variations in specified planes for

graphite epoxy laminates. Deviations between wave propagation direction and energy propagation were found to be as large as 60 degrees. This has some rather interesting implications concerning the interpretation of received ultrasonic pulses. Kriz [51], Tauchert and Guzelsu [55,56] have experimentally determined elastic moduli by relating wave velocity measurements in various propagation directions to stiffness.

The previous velocity measurements in composites have relied on monitoring the time delay for a through transmitted pulse. This technique works well if the specimen is thick. If too thin, then multiple reflections within from the front and back surfaces may interfere with the received wave packet. In order to alleviate this problem a new technique , Spectroscopy, has been investigated. Spectroscopy utilizes the frequency contents of the reflected signals instead of the time domain data. Chang, et.al., have utilized the connection of resonance and frequency to determine wave velocities in thin composite specimens within $\pm 2\%$ [57]. Since Spectroscopy techniques reley on signal processing of digitized waveforms, which has only recently been established, the amount of published articles is few. However, much work is currently being done in this area.

REFERENCES

1. K.L. Reifsnider and R. Jamison, "Fracture of Fatigue-Loaded Composite Laminates," Int. J. of Fatigue, Oct., 1982, p.187-197.
2. J.D. Achenbach, Wave Propagation in Elastic Solids, North-Holland Publishing Company, 1973, p.30.
3. H. Kolsky, Stress Waves in Solids, New York Dover Publications, Inc., 1963, p.17.
4. W.M. Pless, S.M. Freeman, and C.P. Bailey, "Advanced Methods for Damage Analysis in Graphite-Epoxy Composite," 14th National SAMPE Technical Conference, Oct.12-14, 1982.
5. K.L. Reifsnider, H.G. Henneke, W.W. Stinchcomb, and J.C. Duke, "Damage and NDE of Composite Laminates," Engineering Science and Mechanics Dept., Virginia Polytechnique Institute (VPI).
6. G.P. Sendeckyj, "NDE Techniques for Composite Laminates," AGARD Conference Proceedings No. 355, Papers presented at the 56th meeting of the Structures and Materials Panel in London, United Kingdom, April 12-14, 1983, p2-1.
7. D.O. Stalnacker and W.W. Stinchcomb, "Load History-Edge Damage Studies in Two Quasi-Isotropic Graphite Epoxy Laminates," American Society for Testing and Materials, ASTM STP-674, p.620-641.
8. W.E. Dance and J.B. Middlebrook, "Neutron Radiographic Nondestructive Inspection for Bonded Composite Structures," Nondestructive Evaluation and Flaw Criticality for Composite Materials, ASTM 696, R.B. Pipes, Ed., American Society for Testing and Materials, 1979 pp.57-71
9. T.S. Jones and E.G. Henneke, "Detection of Damage in Composite Materials by Vibrothermography," Non-destructive Evaluation and Flaw Criticality for Composite Materials, ASTM 696, R.B. Pipes, Ed., American Society for Testing and Materials, 1979, pp.83-95.
10. G.E. Maddux and G.P. Sendeckyj, "Holographic Techniques for Defect Detection in Composite Materials," Nondestructive Evaluation and Flaw Criticality for Composite Materials, ASTM 696, R.B. Pipes, Ed., American Society for Testing and Materials, 1979,

pp.83-95.

11. J.A. Charles, "Liquid Crystals for Flaw Detection in Composites," Nondestructive Evaluation and Flaw Criticality for Composite Materials, ASTM 696, R.B. Pipes, Ed., American Society for Testing and Materials, 1979, pp.72-82.
12. C.D. Bailey, S.M. Freeman, and J.M. Hamilton, "Acoustic Emission Monitors Damage Progression in Graphite Epoxy Composite Structure," Materials Evaluation, Vol.38, Aug., 1980, p.21.
13. R.S. Williams and K.L. Reifsnider, "Real-Time Nondestructive Evaluation of Composite Materials During Fatigue Loading," Materials Evaluation, Vol. 35, Aug., 1977, p. 50.
14. A. Arora and Tangri, "Acoustic Emission: A Means of Measuring Crack Growth at Elevated Temperatures," Experimental Mechanics, Vol. 21, No. 7, July, 1981, p.261.
15. Joachim Block, "Monitoring of Defect Progression by Acoustic Emission," AGARD Conference Proceedings No. 355, Papers presented at the 56th meeting of the Structures and Materials Panel in London, United Kingdom, April 12-14, 1983, p3-1.
16. David A. Ulman, Edmund Henneke, J.C. Duke, K.L. Reifsnider, and W.W. Stinchcomb, "Nondestructive Evaluation in Metal Matrix Composites," Dept. of Engineering and Mechanics, VPI. Final Report, June 1, 1982.
17. J.H. Williams and D.M. Egan, "Acoustic Emission Spectral Analysis of Fiber Composite Failure Mechanisms," Materials Evaluation, Vol. 37, No. 1, Jan., 1979, p.43.
18. Robert A. Blake, "Digital Nondestructive Evaluation of Composite Materials," Micro-Delcon, March, 1982.
19. Robert A. Blake, "Digital Dot Matrix C-Scan," Center for Composite, University of Delaware, Newark, Delaware.
20. Robert A. Blake, "Ultrasonic Image Histogram Evaluation and Enhancement," IEEE 1983 Proceedings of the Sixth Annual Micro-Delcon Conference.
21. Robert A. Blake and Hans S. Hartmann, "Computer-Aided

Ultrasonic Evaluation of Fiber FP Metal Matrix Composites," Composites Technology Review, Vol. 6, No.3, Sept., 1984, pp.118-123.

22. F.H. Chang, J.R. Bell, A.H. Gardner, C.P. Fisher, and R.W. Haile,"A Laboratory Mock-Up Ultrasonic Inspection System for Composites," Materials Evaluation, Vol. 40, No. 7, June, 1982, pp.756-761.
23. F.H. Chang, J.R. Bell, A.H. Gardner, G.P. Handley, and C.P. Fisher,"In-Service Inspection of Advanced Composite Aircraft Structures," General Dynamics, Fort Worth Division, Report AFML-TR-79-4087, Feb., 1979.
24. Louis J. Kiraly and Erwin H. Meyn,"Ultrasonic Scanning System for Imaging Flaw Growth in Composites," Twenty-Eighth Int. Instrumentation Symposium, Instrument Society of America, May 3-6, 1982.
25. I.M. Daniel, S.W. Schramm, and T. Liber,"Fatigue Damage Monitoring in Composites by Ultrasonic Mapping," Materials Evaluation, Vol. 39, No. 9, August, 1981, pp.834-839.
26. T. Liber, I.M. Daniel, and S.W. Schramm,"Ultrasonic Techniques for Inspecting Flat and Cylindrical Composite Specimens," Nondestructive Evaluation and Flaw Criticality for Composite Materials, ASTM 696, R.B. Pipes, Ed., American Society for Testing and Materials, 1979, pp.5-25.
27. W.H.M. van Dreumel and J.L. Speijer,"Nondestructive Composite Lamineate Characterization by Means of Ultrasonic Polar-Scan," Materials Evaluation, Vol. 39, No. 10, Sept., 1981, pp.922-924.
28. W.H.M. van Dreumel and J.L. Speijer,"Polar-Scan, A Non- destructive Test Method for the Inspection of Layer Orientation and Stacking Order in Advanced Fiber Composites," Materials Evaluation, Vol. 41, No. 9, August, 1983, pp.1060- 1062.
29. A. Vary and K.J. Bowels,"Ultrasonic Evaluation of the Strength of Unidirectional Graphite/Polyimide Composites," Proceedings of the Eleventh Symposium on Nondestructive Testing, Columbus, and Southwest Research Institute, San Antonio, 1977, pp.242- 258.
30. A. Vary,"A Review of Issues and Strategies in Nondestructive Evaluation of Fiber Reinforced Composites," Proceedings of the Eleventh National SAMPE Technical Conference: New Horizons-Materials and

Processes for the Eighties, Vol. 11, Society for the Advancement of Material and Process Engineering, Azusa, CA., 1979, pp.166-177.

31. A. Vary,"Correlations between Ultrasonic and Fracture Toughness Factors on Metallic Materials," Fracture Mechanics, American Society for Testing and Materials, ASTM STP-677, Philadelphia, 1979, pp.563-578.
32. A. Vary and K.J. Bowles,"An Ultrasonic-Acoustic Technique for Nondestructive Evaluation of Fiber Composite Quality," Polymer Engineering and Science, Vol. 19, No. 5, 1979, pp.373-376.
33. A. Vary and R.F. Lark,"Correlation of Fiber Composite Tensile Strength with the Ultrasonic Stress Wave Factor," J. of Testing and Evaluation, Vol. 7, No. 4, 1979, pp.185-191.
34. A. Vary,"Concepts and Techniques for Ultrasonic Evaluation of Material Mechanical Properties," Mechanics of Nondestructive Testing, Plenum Press, New York, 1980, pp.123-141.
35. A. Vary,"Ultrasonic Measurements of Material Properties," Research Techniques in Nondestructive Testing, Vol. 4, Academic Press, London, 1980, pp.159-204.
36. A. Vary and D.R. Hull,"Interrelation of Material Microstructure, Ultrasonic Factors and Fracture Toughness of a Two Phase Titanium Alloy," Materials Evaluation, Vol. 41, 1983, pp.309-314.
37. A. Vary,"Correlations Among Ultrasonic Propagation Factors and Fracture Toughness Properties of Metallic Materials," NASA Technical Memorandum, NASA TM X-71889, 1976.
38. J.H. Williams and B. Doll,"Ultrasonic Attenuation as an Indicator of Fatigue Life of Graphite Fiber Epoxy Composite," Materials Evaluation, Vol. 38, No. 5, May, 1980, pp.33-37.
39. J.H. Williams, H. Yuce, and S.S. Lee,"Ultrasonic and Mechanical Characterizations of Fatigue States of Graphite Epoxy Composite Laminates," Materials Evaluation, Vol. 40, No. 5, April, 1982, pp.560-565.
40. J.H. Williams and S.S. Lee,"Stress-Wave Attenuation in Thin Structures by Ultrasonic Through-Transmission," J. of Nondestructive Evaluation, Vol. 1, No. 4, 1980,

pp.277-286.

41. J.H. Williams, Hamid Nayeh-Hashemi, and S.S. Lee, "Ultrasonic Attenuation and Velocity in AS/3501-6 Graphite Fiber Composite," J. of Nondestructive Evaluation, Vol. 1, No. 2, 1980, pp.137-148.
42. J.H. Lampert and N.R. Lampert, "Ultrasonic Evaluation of Impact-Damaged Graphite Fiber Composite," Materials Evaluation, Vol. 38, No. 12, Dec., 1980, pp.68-72.
43. R. Truell and A. Hikata, "Fatigue and Ultrasonic Attenuation," Symposium on Nondestructive Testing, Los Angeles, CA., Sept. 17, 1956, American Society for Testing and Materials, ASTM STP-213, Philadelphia, PA., 1957, pp.63-69.
44. Narayan R. Joshi and Robert E. Green, "Ultrasonic Detection of Fatigue Damage," Engineering Fracture Mechanics, Vol. 11, 1972, pp.577-583.
45. D.T. Hayford, E.G. Henneke, and W.W. Stinchcomb, "The Correlation of Ultrasonic Attenuation and Shear Strength in Graphite-Polyimide Composites," J. of Composite Materials, Vol. 11, Oct., 1977, pp.429-444.
46. E.G. Henneke, J.C. Duke, W.W. Stinchcomb, A. Govada, and A. Lemascon, "A Study of the Stress Wave Factor Technique for the Characterization of Composite Materials," NASA Contractor Report 3670, Grant NSG-3-172, Feb., 1983.
47. Ramish Talreja, Anil Govada, and E.G. Henneke, "Quantitative Assessment of Damage Growth in Graphite Epoxy Laminates Acoustic-Ultrasonic Measurements," Materials Response Group, Dept. of Engineering Science and Mechanics, VPI.
48. R.P. Nimmer, "Progressive Matrix Damage in Laminated Fiber-Epoxy Flywheel Disks," General Electric Corporate Research and Development, Schenectady, New York, March, 1980.
49. John H. Hemann and George Y. Baaklini, "The Effect of Stress on Ultrasonic Pulses in Fiber Reinforced Composites," NASA Contractor Report 3724, 1983.
50. R.D. Kriz and H.M. Ledbetter, "Elastic Representation Surfaces of Unidirectional Graphite/Epoxy Composites," Fracture and Deformation Division, National Bureau of Standards, Boulder, Colorado, 80303, USA.

51. R.D. Kriz and W.W. Stinchcomb, "Elastic Moduli of Transverse Isotropic Graphite Fibers and Their Composites," Experimental Mechanics, Vol. 19, No. 2, Feb., 1979, pp.41-49.
52. R.D. Kriz, "Monitoring Elastic Stiffness Degradation in Graphite/Epoxy Composites," Fracture and Deformation Division, National Bureau of Standards, Boulder, Colorado, 80803, USA.
53. V.K. Kinra and J.G. Eden, "Propagation of Elastic Waves in Unidirectional Fiber-Reinforced Composites," Dept. of Aerospace Eng., Texas A&M, MM4875-84-19, Aug., 1984.
54. M.P.J. Musgrave, Crystal Acoustics, Holden-Day Inc., San Francisco, CA., 1970.
55. T.R. Tauchert and A.N. Guzelsu, "An Experimental Study of Dispersion of Stress Waves in a Fiber-Reinforced Composite," J. of Applied Mechanics, Vol. 39, March, 1972, pp.98-102.
56. T.R. Tauchert, "Measurements of the Elastic Moduli of Laminated Composites Using an Ultrasonic Technique," J. of Composite Materials, Vol. 5, Oct., 1971, pp.549-552.
57. F.H. Chang, J.C. Couchman, and B.G.W. Yee, "Ultrasonic Resonance Measurements of Sound Velocity in Thin Composite Laminates," J. of Composite Materials, Vol. 8, October, 1974, pp.356-363.

Appendix II.

Propogation of Elastic Waves in Undirectional Fiber-Reinforced Composites



**Mechanics and Materials Center
TEXAS A&M UNIVERSITY
College Station, Texas**

**PROPAGATION OF ELASTIC WAVES IN
UNIDIRECTIONAL FIBER-REINFORCED COMPOSITES**

J.G. EDEN
V.K. KINRA

AIR FORCE OFFICE OF SCIENTIFIC RESEARCH
OFFICE OF AEROSPACE RESEARCH
UNITED STATES AIR FORCE
CONTRACT No. F49620-83-C-0067

MM 4875-84-19

AUGUST 1984

INTRODUCTION

The present work is a part of an overall effort to devise experimental techniques for Nondestructive Testing and Evaluation of fiber-reinforced composite materials. A clear understanding of the nature of wave propagation in anisotropic media is a necessary prerequisite for a correct interpretation of the experimental data. In the following, we explore some concepts which are unique to composite materials: velocity surfaces, slowness surfaces, and deviations of group velocity vector and particle displacement vector from the wave normal vector.

RESULTS AND DISCUSSIONS

The anisotropic nature of fiber-reinforced composites give rise to some rather interesting behavior patterns when plane waves are propagated through them. The solutions to the equations of Christoffel [1] are:

$$(C_{ijkl} N_j N_l - \rho v^2 \delta_{ik}) p_k = 0$$

where C_{ijkl} is the 6x6 stiffness matrix, \hat{n} a unit vector normal to the wavefront, ρ is the density, v is the phase velocity, δ_{ik} is the Kronecker delta, and \hat{p} is a unit particle displacement vector. These equations yield three characteristic eigen-velocities with which are associated with three corresponding eigen-vectors. As the wave normal takes on all possible values, $v(n)$ will trace out a velocity surface of three sheets. A computer program was written to solve the above equations for the most general composite material. The numerical values presented here are, however, only for the case of a unidirectional composite which has been modelled as a transversely isotropic material. The five independent elastic constants required to describe such a material are presented in Table 1. These are: Young's modulii E_1 and E_2 , shear modulus G_{12} , and Poisson's ratios ν_{12} and ν_{23} . Figure 1 defines all angles to be used in the following sections. Figures 2-6 show plots of the three velocity sheets for each material as well as the particle displacement vector, \hat{p} . Because of symmetries of a transversely isotropic material only a quarter of the intersection of the velocity surfaces with the X_1-X_3 plane needs to be plotted. From Figs. 2-6 it is obvious that along one branch the phase velocity increases greatly in the direction of the fibers (X_1 denotes the fiber direction while X_3 is normal to the fibers). Since on this surface the particle displacement at $\theta = 0^\circ, 90^\circ$ is purely longitudinal this velocity surface will be denoted as the longitudinal (L) velocity sheet. The velocity surface which has the particles moving transversely in the X_1-X_3 plane will be called the transverse (or shear) vertical (SV) and the last surface

with the particles moving transversely in the X_2 -direction will be referred to as the transverse (or shear) horizontal (SH). As expected Figs. 2-6 indicate that as stiffness in the 1, 2, or 3 direction increases or decreases the corresponding velocity in those directions will follow the same trend. It may also be observed that for the stiffer materials the \tilde{p} -vector rotates much faster towards the direction of highest stiffness when θ is increased.

The next set of figures (7-11) show the deviation (α) of the particle displacement vector from what it would be in the case of an isotropic material. For the longitudinal branch the \tilde{p} -vector is parallel to the wave-normal whereas for the SV and SH branches the \tilde{p} -vector is perpendicular to the wave-normal. These figures show only two curves each, but actually three curves exist. The L and SV deviations are exactly identical while the SH indicates no deviation from the isotropic case. It is often common to define a particular branch on the basis of the direction of particle displacement. That is, if the angle between the \tilde{p} -vector and wave normal is between 0° and 45° the branch should be called quasi-longitudinal and if the angle is between 45° and 90° it would be called quasi-transverse (0° = purely longitudinal, 90° = purely transverse). Figures 7-11 indicate that these labels may be misleading due to the tendency for α to increase beyond 45° for the L branch and then decrease. It is for the above reason that the previously defined L, SV, and SH labels were based upon $\theta = 0^\circ$, 90° \tilde{p} -vector directions. As the material stiffness increase so does the deviation angle which again indicates the preference of particle motion in the direction of greater stiffness for the L branch and in the direction of higher shear strength for the SV branch.

Slowness is defined as the inverse of the velocity. Figures 12-16 show plots of the slowness surfaces for each composite. Also on the plots are the directions of the energy propagation vector F_i given by [1]

$$F_i = \frac{1}{2} c^2 w^2 C_{ijkl} p_j p_k s_l$$

without loss of generality the factor $\frac{1}{2} c^2 w^2$ was set equal to one for our case, since c and w are constants. C_{ijkl} is the stiffness matrix, \tilde{p} is the particle displacement vector, and \tilde{s} is the slowness vector defined as $s_l = n_l/v$. As expected the normal to the slowness surface coincides with the direction of the energy vector F_i [1]. The plots also show that for the L branch the energy velocity direction moves rapidly towards the fiber direction as the wave normal angle (θ) is increased from 0° to 20° . This interesting phenomenon is shown explicitly in Figs. 17-21 where the deviation angle (Δ) between the energy vector and wave normal is plotted. The plots also show an interesting feature along the SV branch. The energy initially shows a preference to propagate in the direction of the fibers for small values of θ . However, as θ is further increased there is a cross-over point beyond which the energy prefers to propagate away from the fiber-direction. At this time we have no reasonable explanation for this phenomenon.

CONCLUSIONS

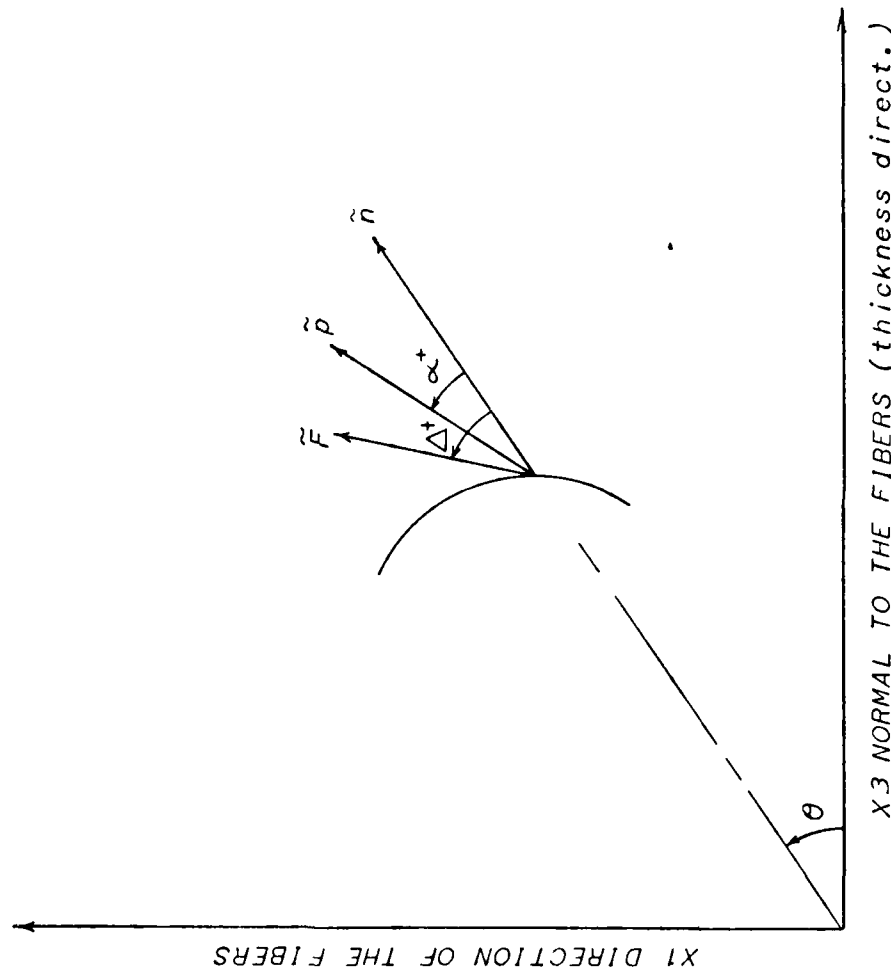
In conclusion, the dynamic response of unidirectional fiber-reinforced composites has been studied in some detail. This study has revealed several interesting features which are peculiar to anisotropic media. For example, the deviation between the energy vector and the wave propagation direction may be as large as 60° in some cases. This has some obviously rather interesting implications concerning excitation and detection of elastic disturbances in composite materials using piezoelectric crystals. This study is a prelude to Ultrasonic Nondestructive Testing of composite materials.

TABLE #1
Composite Properties

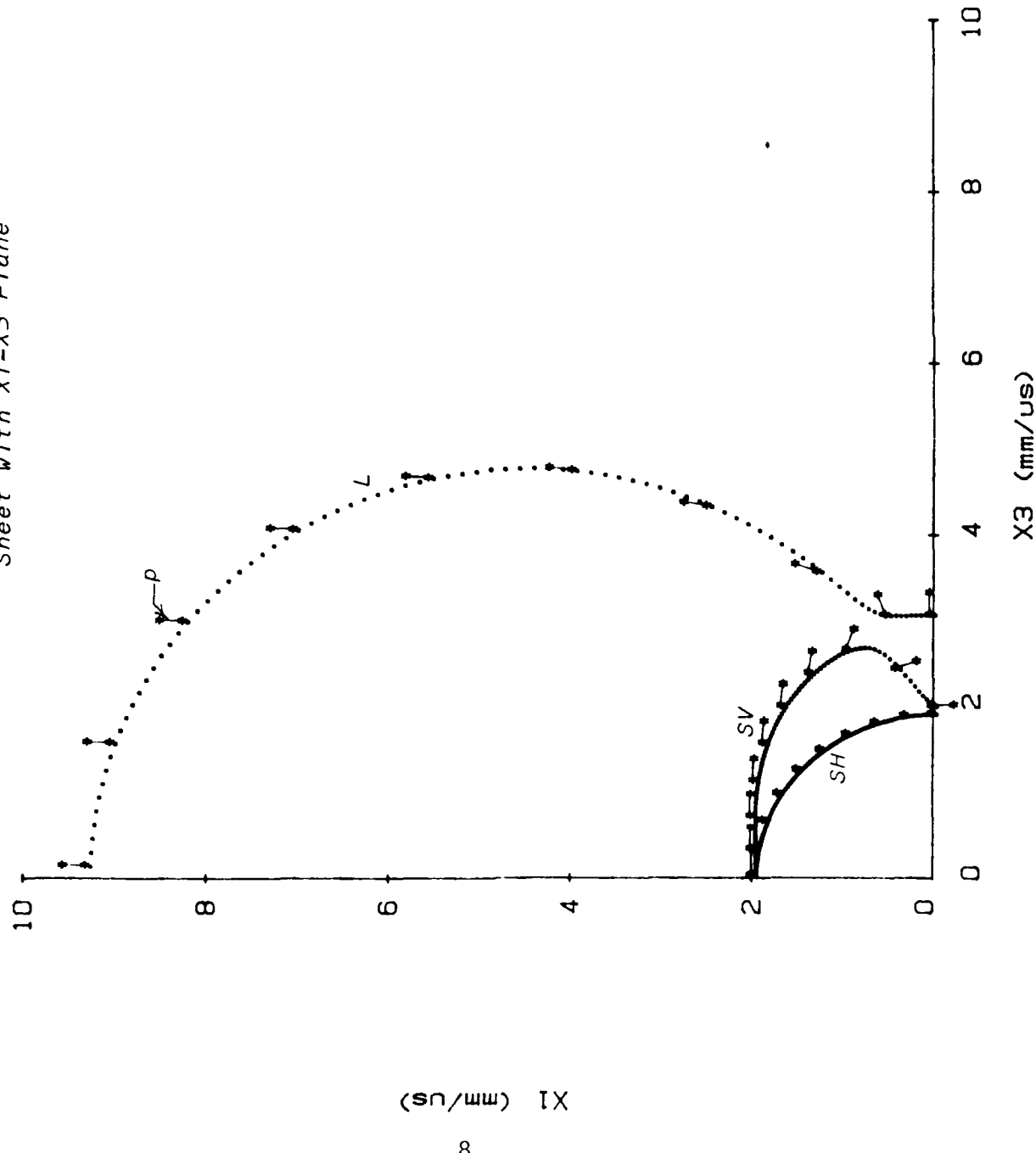
	A	B	C	D	E	F
Property	Graphite/ Epoxy	Graphite/Epoxy AS/3501	GY 70/ Epoxy	E Glass/ Epoxy	Boron/Epoxy	Graphite/ Aluminum
E_1	20×10^6	21×10^6	42×10^6	6.2×10^6	30×10^6	18.0×10^6
E_2	2.1×10^6	1.4×10^6	1.0×10^6	1.7×10^6	2.1×10^6	3.6×10^6
r_{11}	0.21	0.30	0.30	0.27	0.21	0.30
G_{11}	0.95×10^6	0.6×10^6	0.95×10^6	0.6×10^6	0.8×10^6	3.2×10^6
S_{11}	5.00×10^{-6}	4.76×10^{-6}	2.38×10^{-6}	1.61×10^{-6}	3.33×10^{-6}	5.56×10^{-6}
S_{12}	-1.05×10^{-6}	-1.43×10^{-6}	-7.14×10^{-6}	-4.35×10^{-6}	-7.00×10^{-6}	-1.67×10^{-6}
S_{22}	4.76×10^{-6}	7.14×10^{-6}	1.00×10^{-6}	5.88×10^{-6}	4.76×10^{-6}	2.78×10^{-6}
S_{33}	1.18×10^{-6}	1.67×10^{-6}	1.05×10^{-6}	1.67×10^{-6}	1.25×10^{-6}	3.13×10^{-6}
Q_{11}	2.01×10^6	2.11×10^6	1.29×10^6	6.33×10^6	3.07×10^6	1.83×10^6
Q_{22}	4.43×10^6	4.23×10^6	3.07×10^6	4.68×10^6	4.42×10^6	1.10×10^6
Q_{33}	2.11×10^6	1.40×10^6	1.02×10^6	1.73×10^6	2.11×10^6	3.67×10^6
Q_{12}	9.50×10^6	9.600×10^6	9.50×10^6	6.000×10^6	8.00×10^6	3.20×10^6
ρ	1.5×10^{-4}	1.5×10^{-4}	1.5×10^{-4}	—	1.9×10^{-4}	2.5×10^{-4}

E_1 , E_2 , r_{11} , G_{11} , S_{11} , S_{12} , S_{22} , S_{33} , Q_{11} , Q_{22} , Q_{33} , Q_{12} in lb/in² and ρ in lb/in³. For SI units: 1 lb/in² = 6.895×10^6 N/m²; 1 lb/in³ = 2.721×10^{-9} m³.

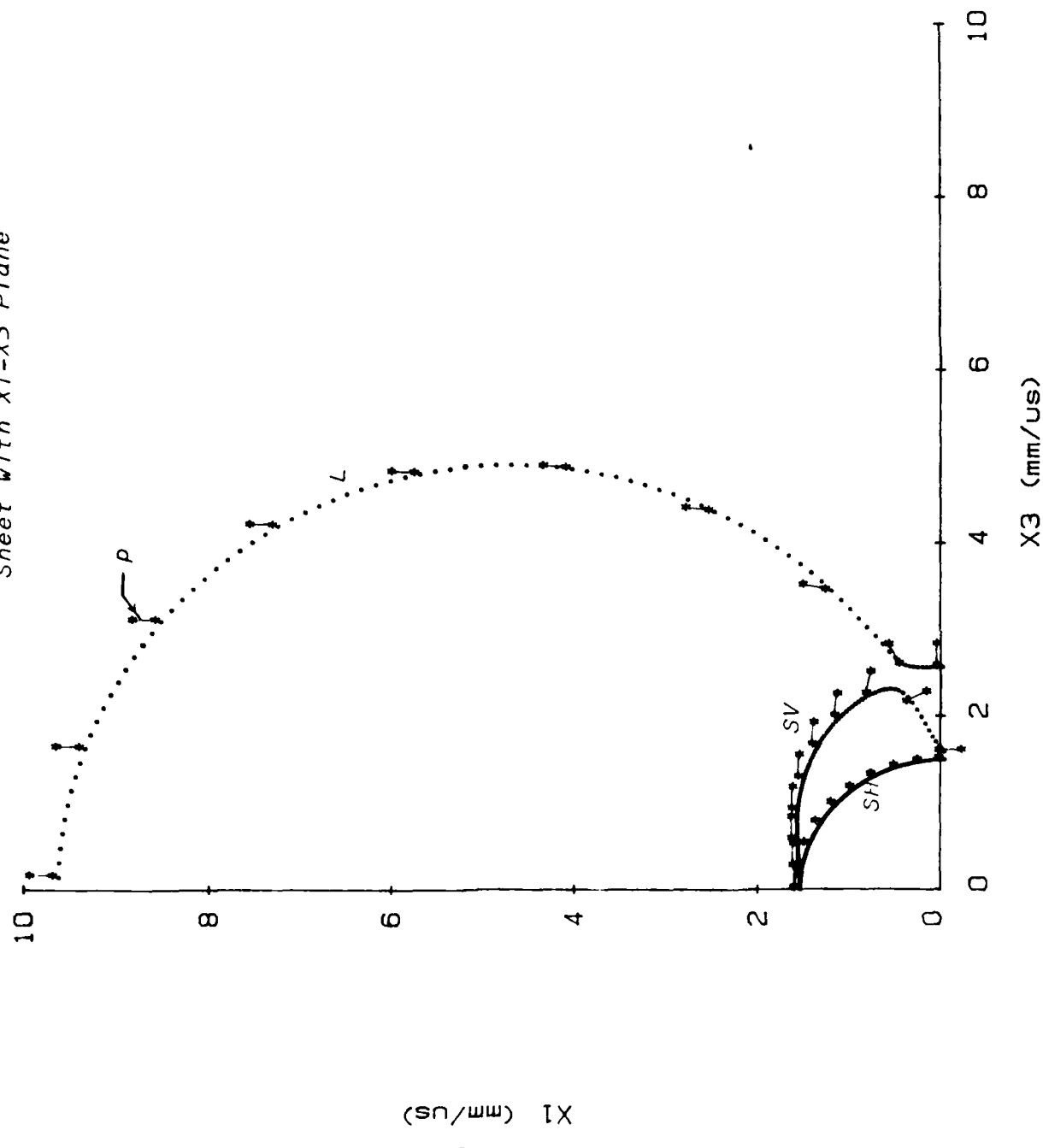
Figure 1: Angle Descriptions



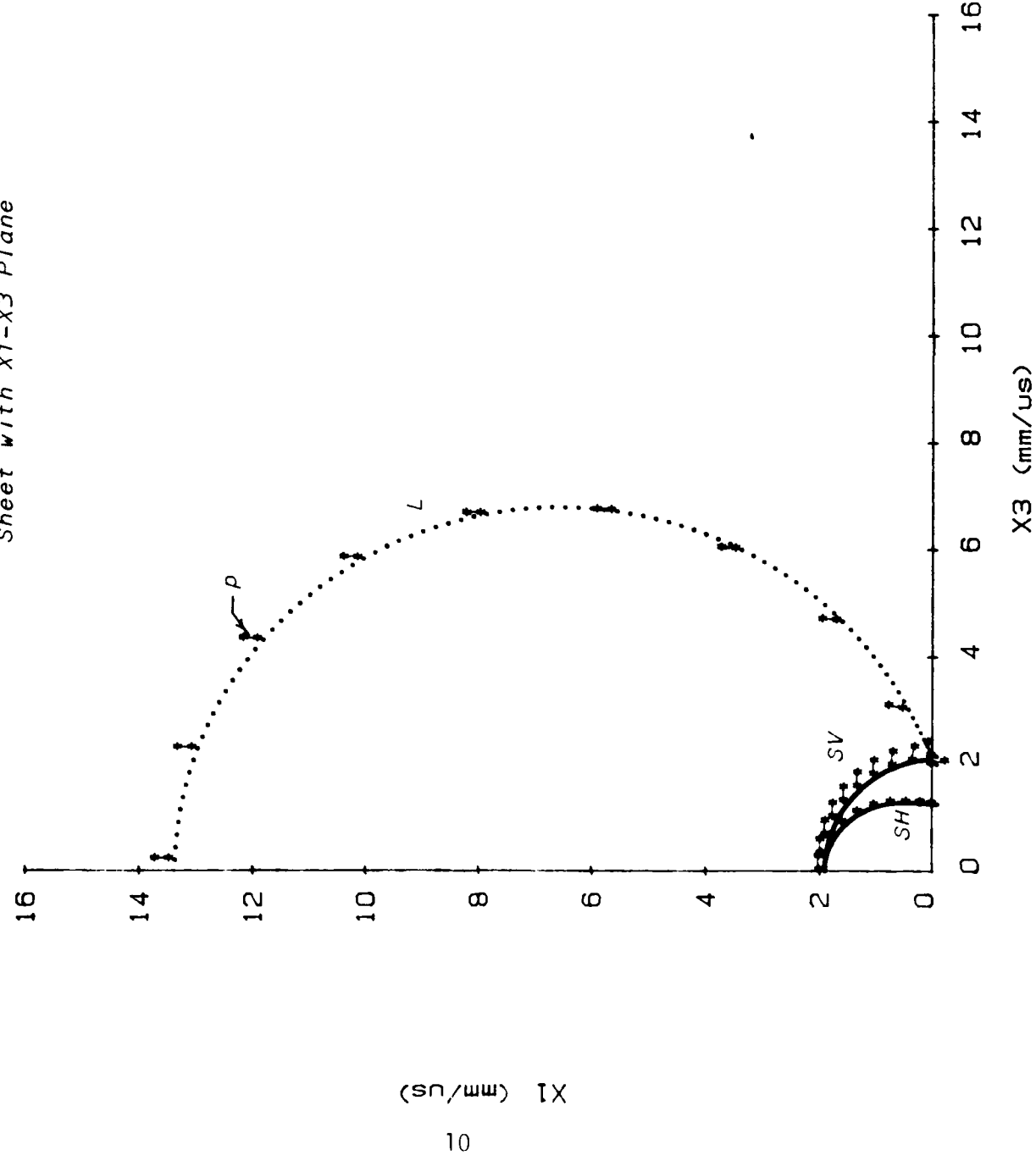
O DEG. GRAPHITE/EPOXY
Figure 2: Intersection of Velocity
Sheet with x_1-x_3 Plane



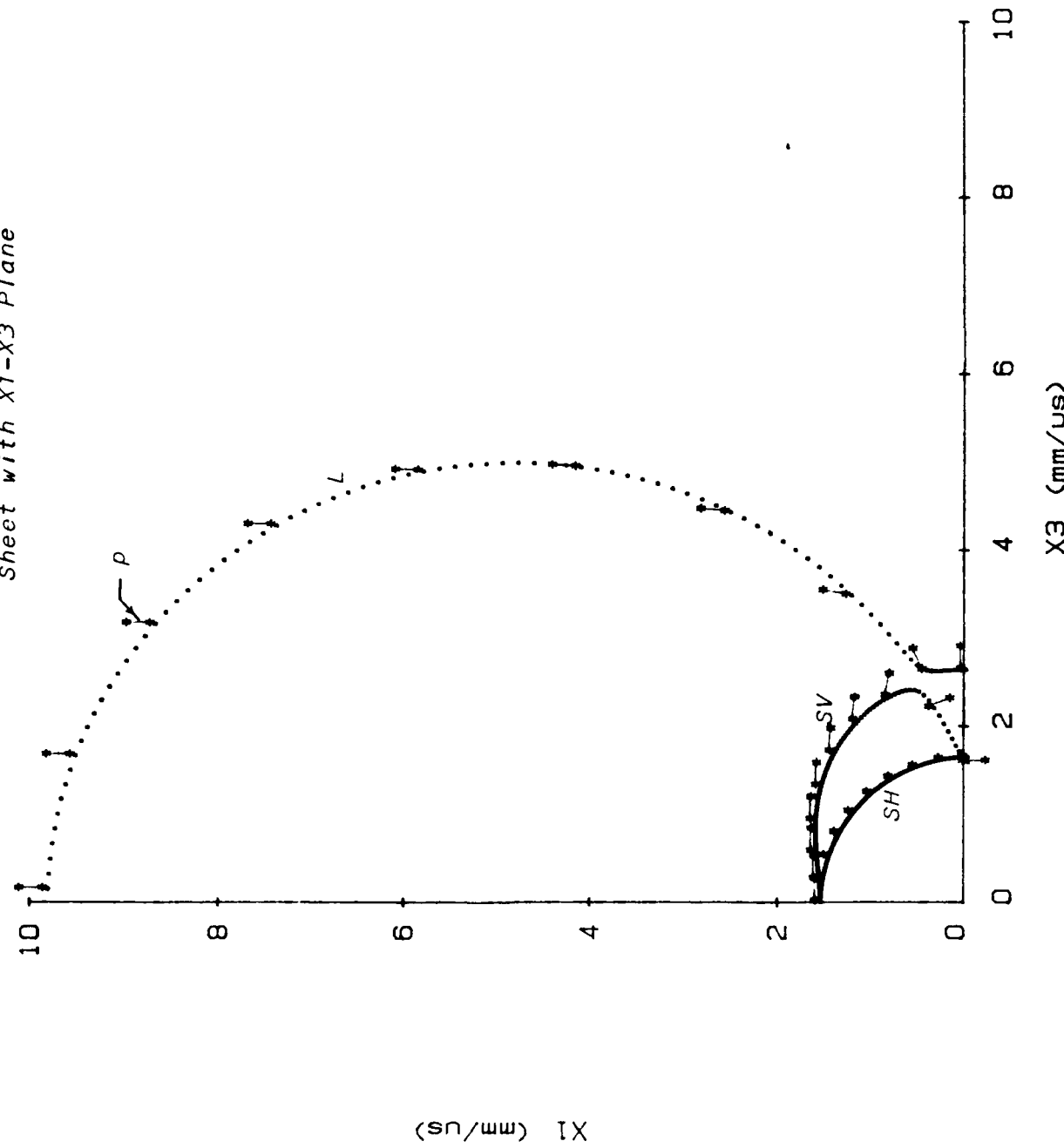
0 DEG. AS/3501
Figure 3: Intersection of Velocity
Sheet with X_1 - X_3 Plane



0 DEG. GY-70/EPOXY
Figure 4: Intersection of Velocity
Sheet with X_1 - X_3 Plane

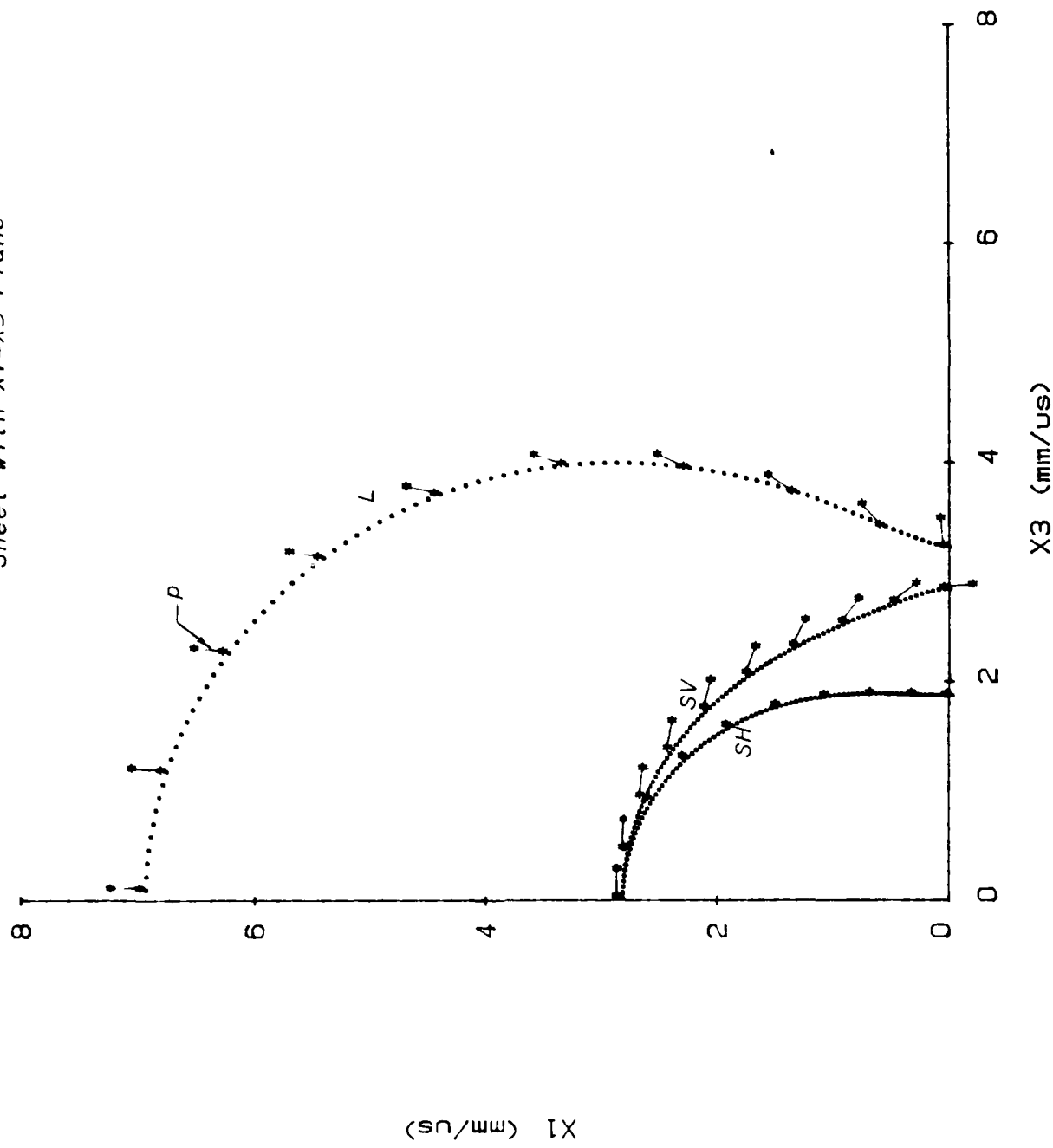


0 DEG. BORON/EPOXY
*Figure 5: Intersection of Velocity
Sheet with X₁-X₃ Plane*



X_1 (mm/us)

0 DEG. GRAPHITE/ALUMINUM
Figure 6: Intersection of Velocity
Sheet with X_1 - X_3 Plane



0 DEG. GRAPHITE/EPOXY

Figure 7: P -vector Deviation from Isotropic P -vector
versus Angle of Wave Front Normal (theta)

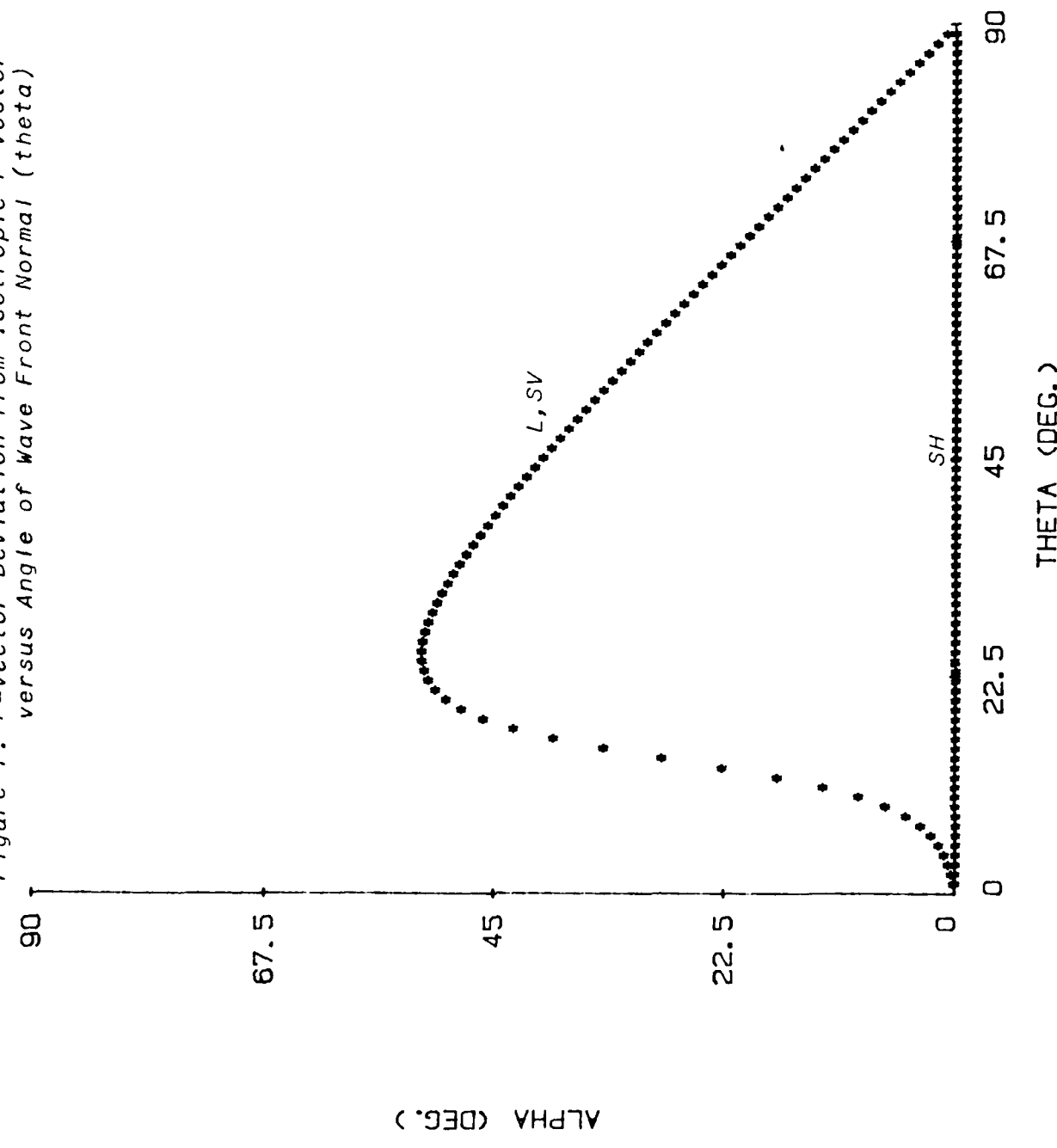
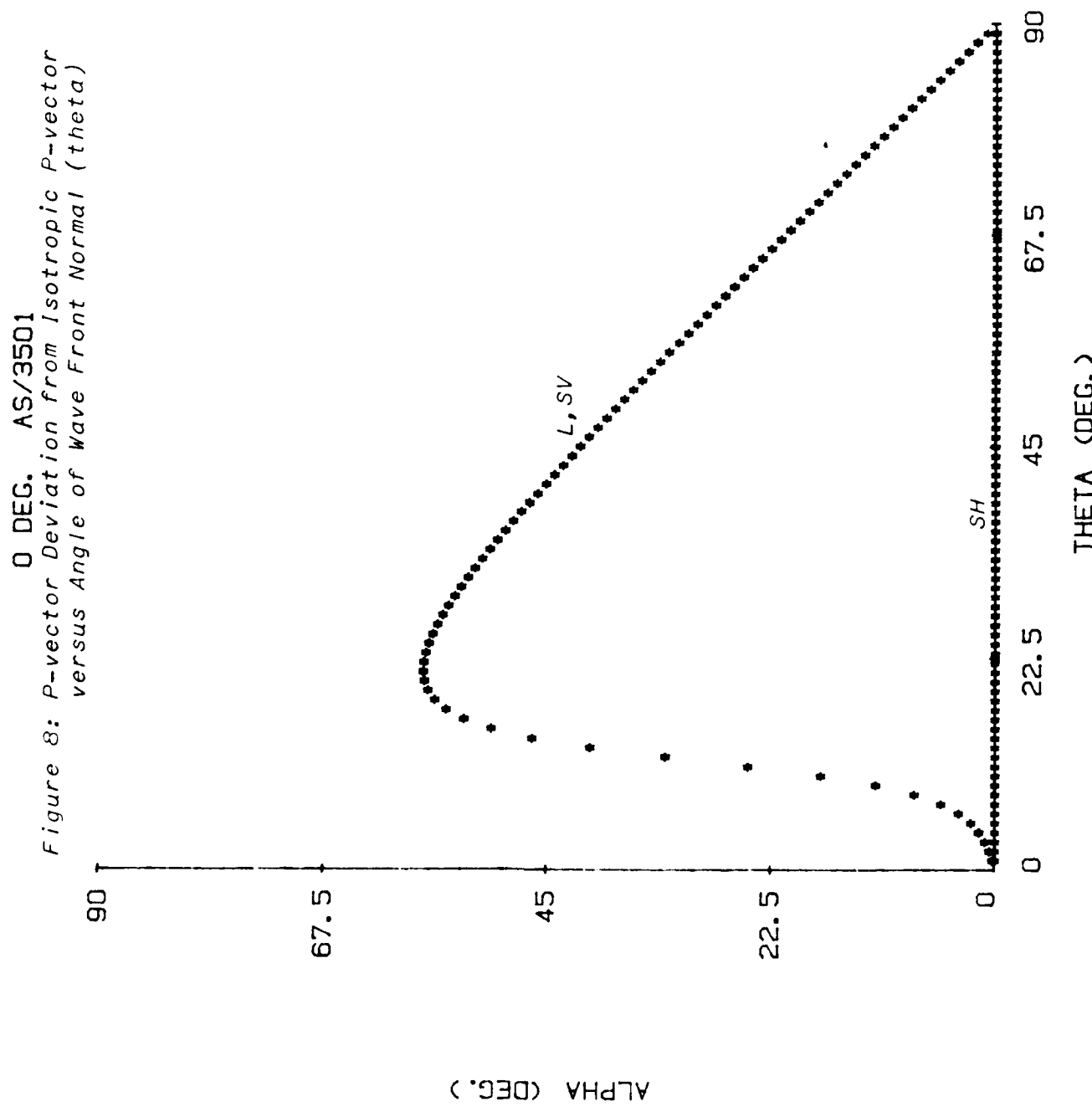
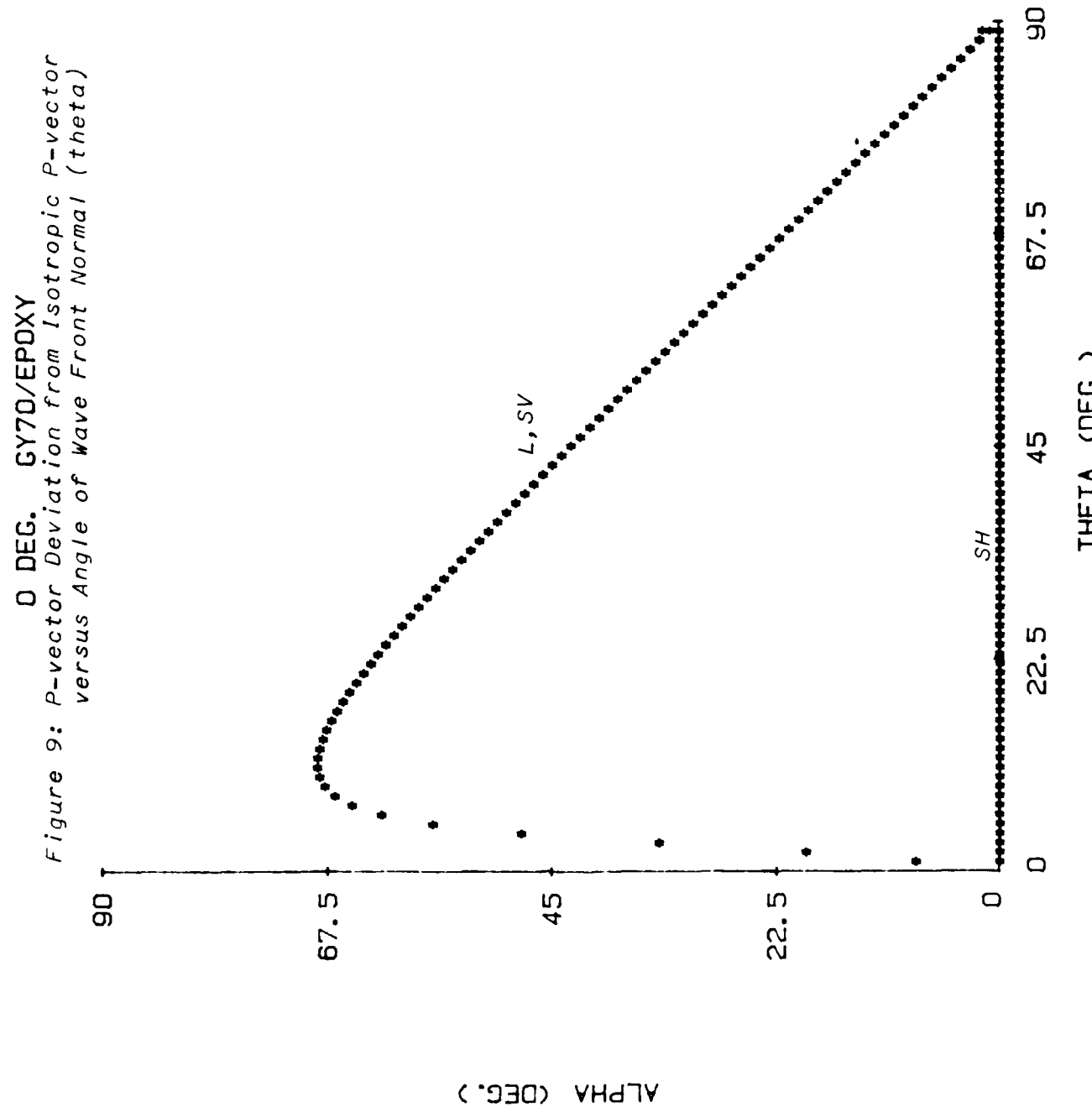
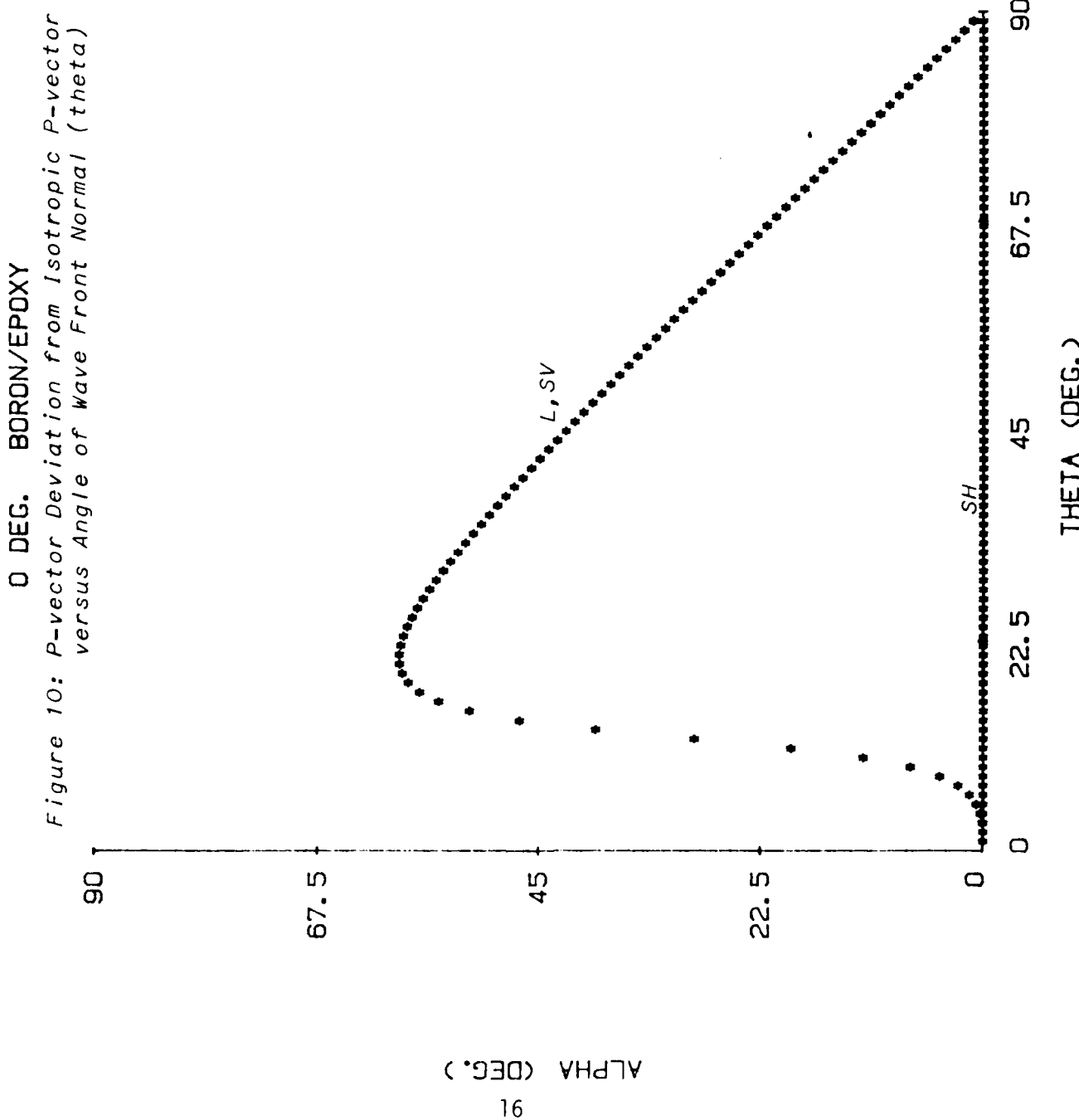


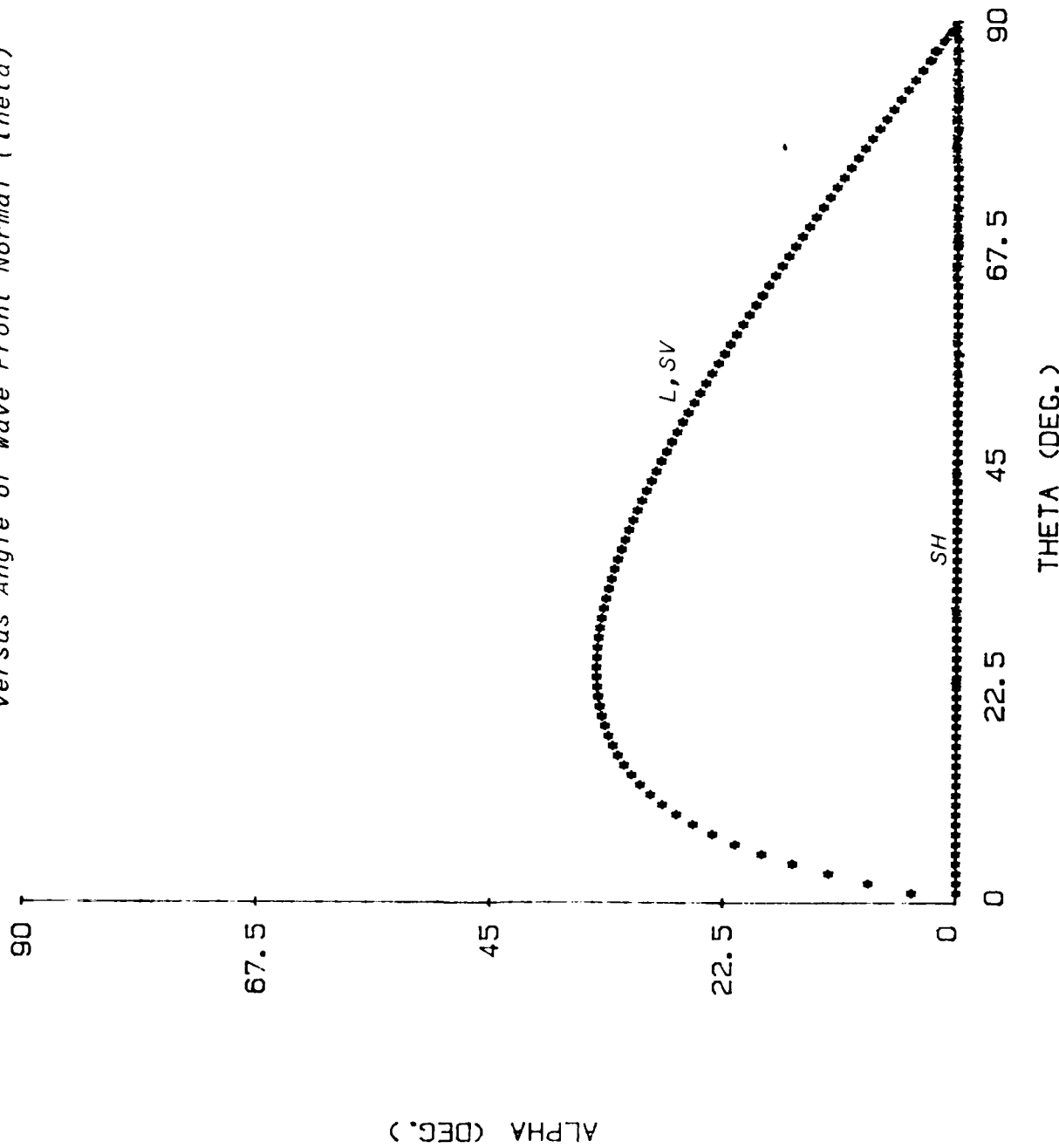
Figure 8: P-vector Deviation from Isotropic P-vector
versus Angle of Wave Front Normal (theta)



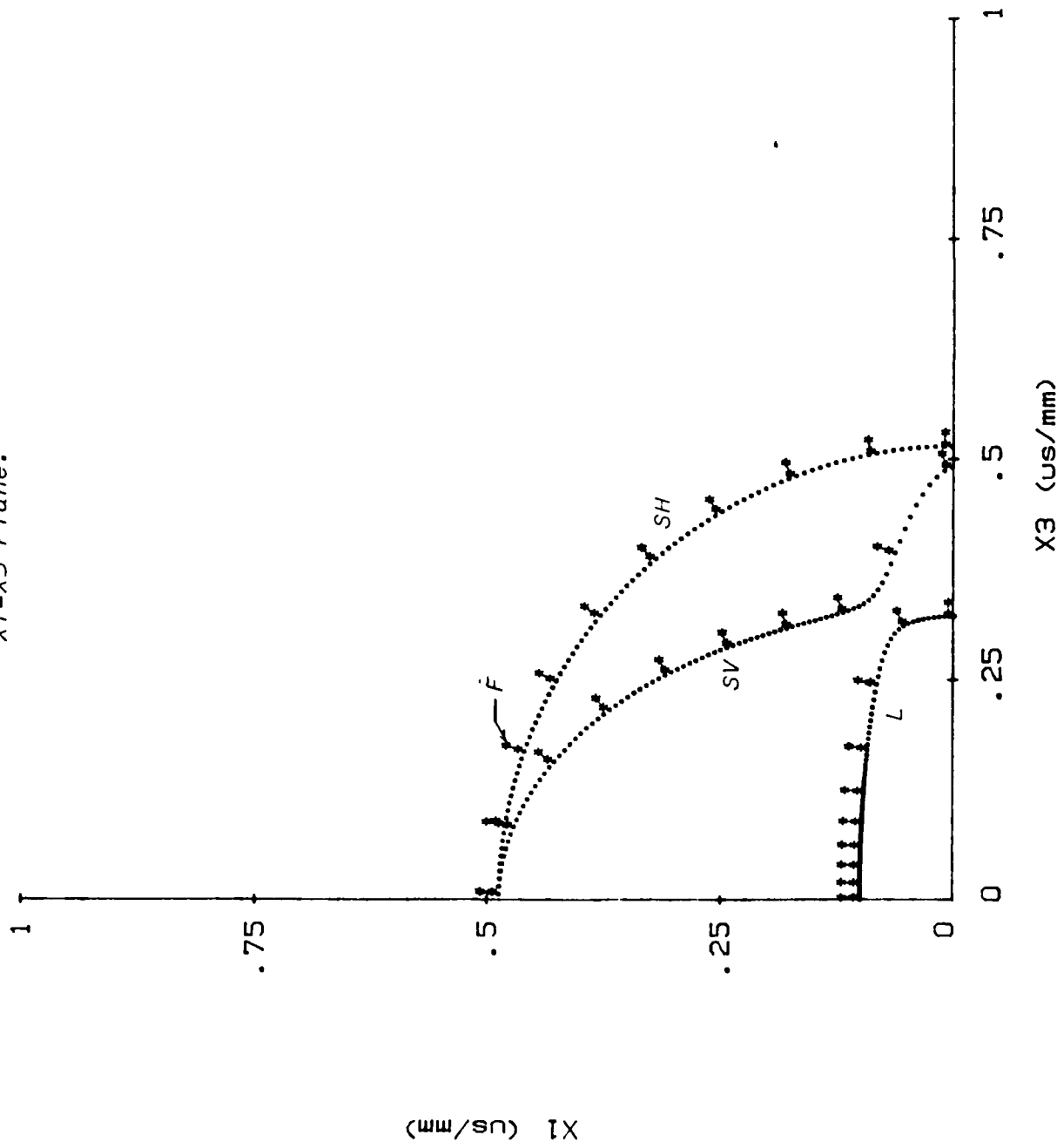




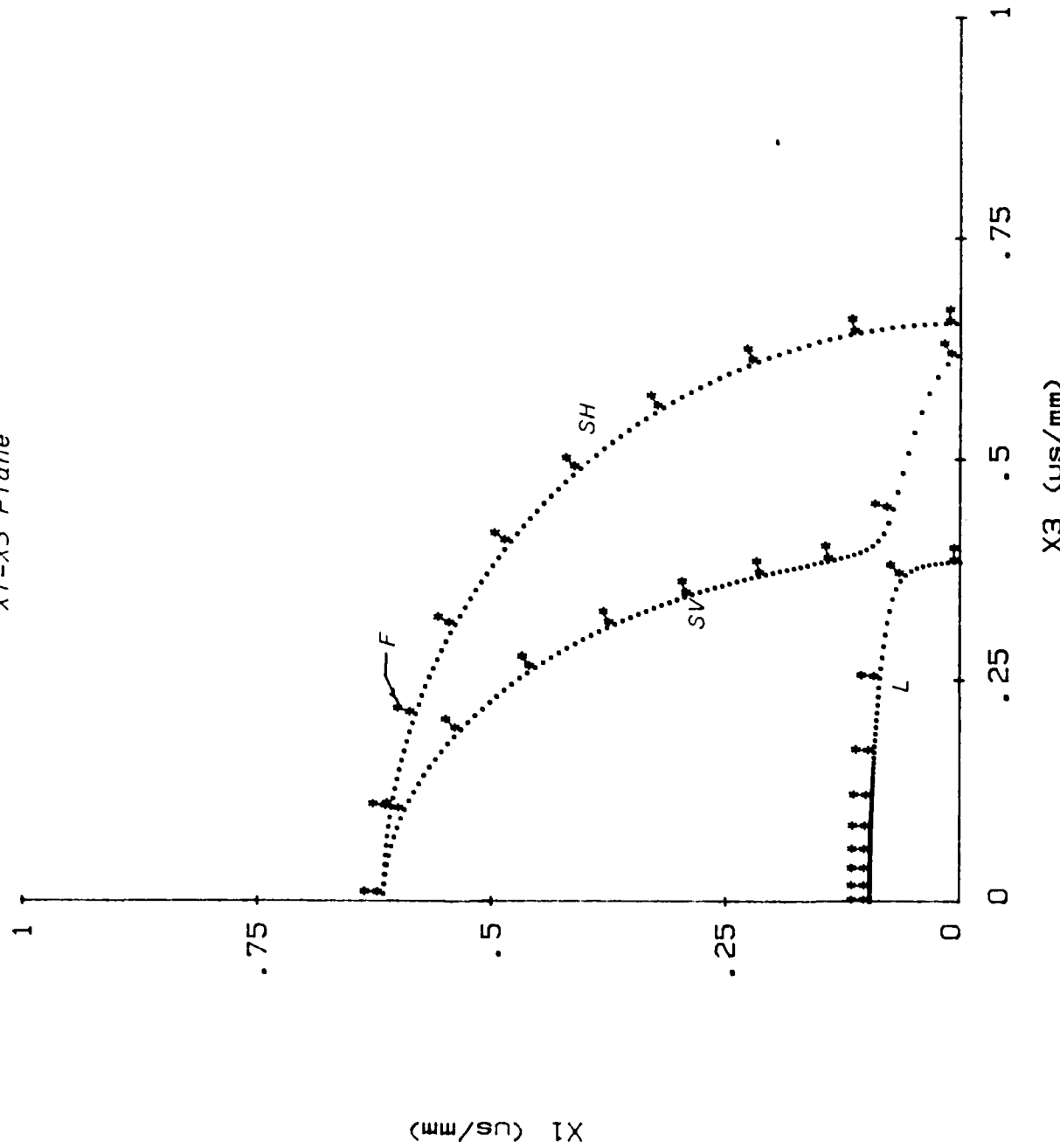
O DEG. GRAPHITE/ALUMINUM
Figure 11: ρ -vector Deviation from Isotropic ρ -vector
versus Angle of Wave Front Normal (θ)



SLOWNESS SURFACES- 0 DEG. GRAPHITE/EPOXY
Figure 12: Slowness Sheet Intersection with
 X_1-X_3 Plane.

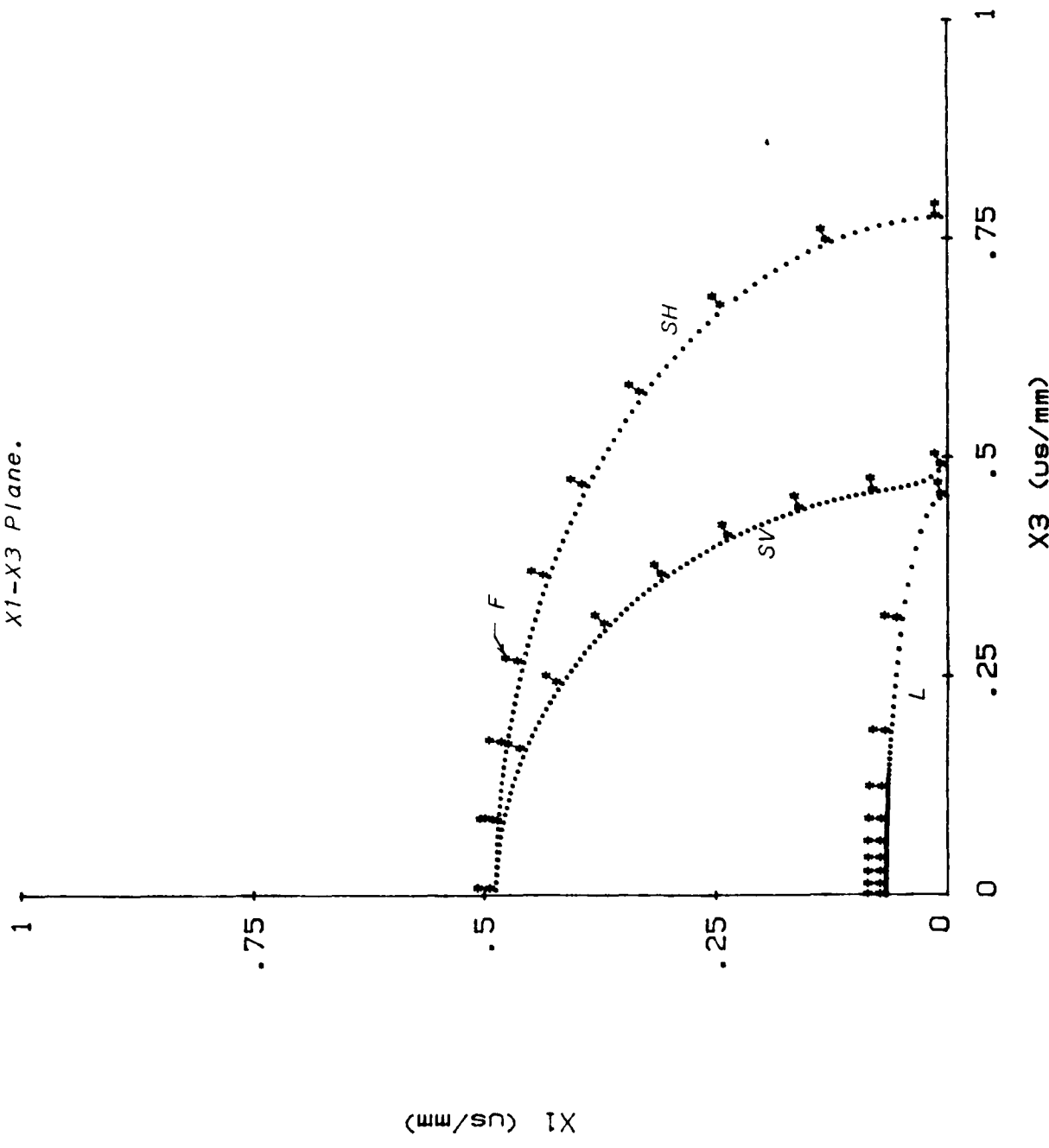


SLOWNESS SURFACES- 0 DEG. AS/3501
Figure 13: Slowness Sheet Intersection with
 X_1-X_3 Plane



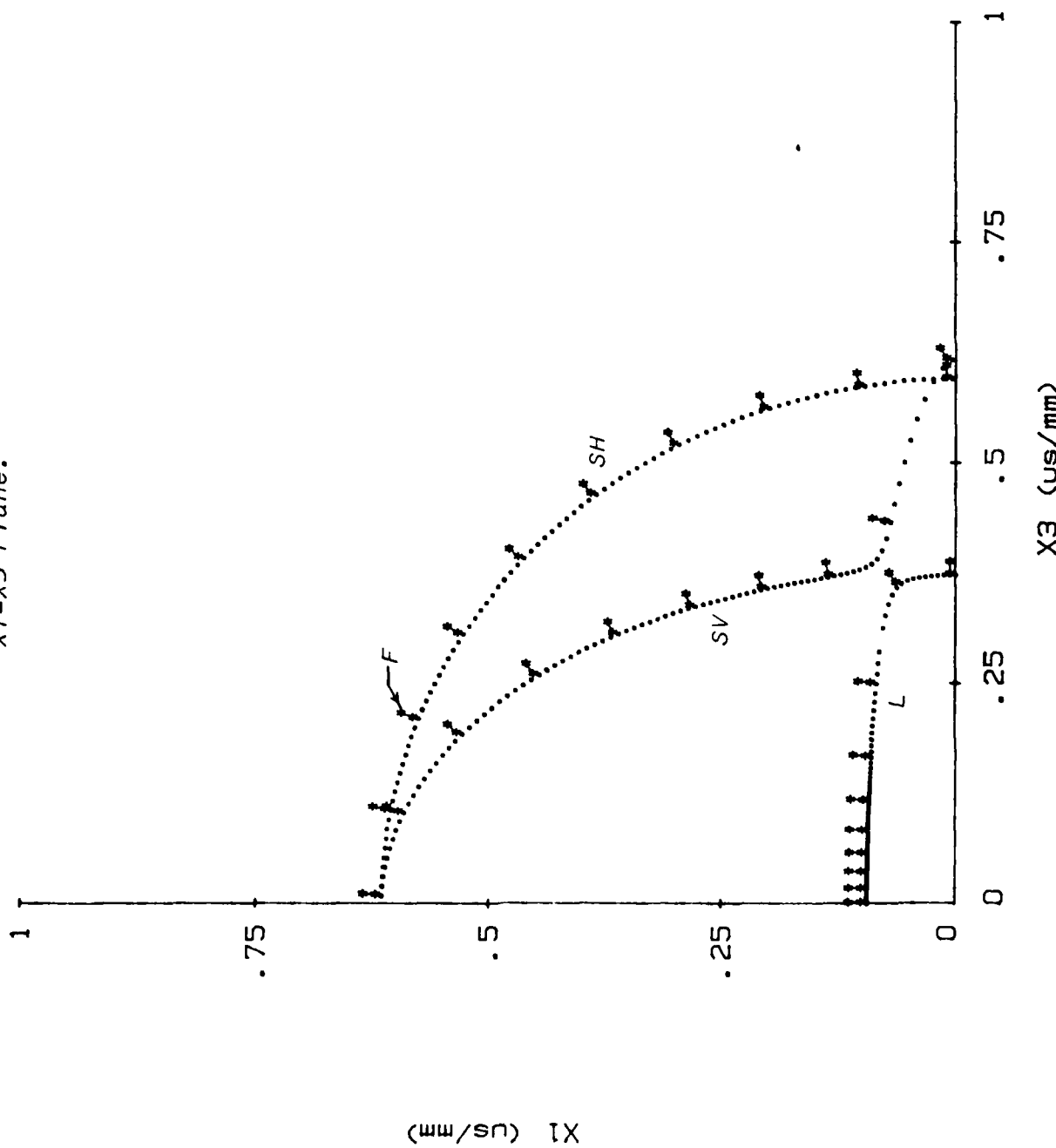
SLOWNESS SURFACES- 0 DEG. GY70/EPOXY

Figure 14: Slowness Sheet Intersection with
 X_1-X_3 Plane.



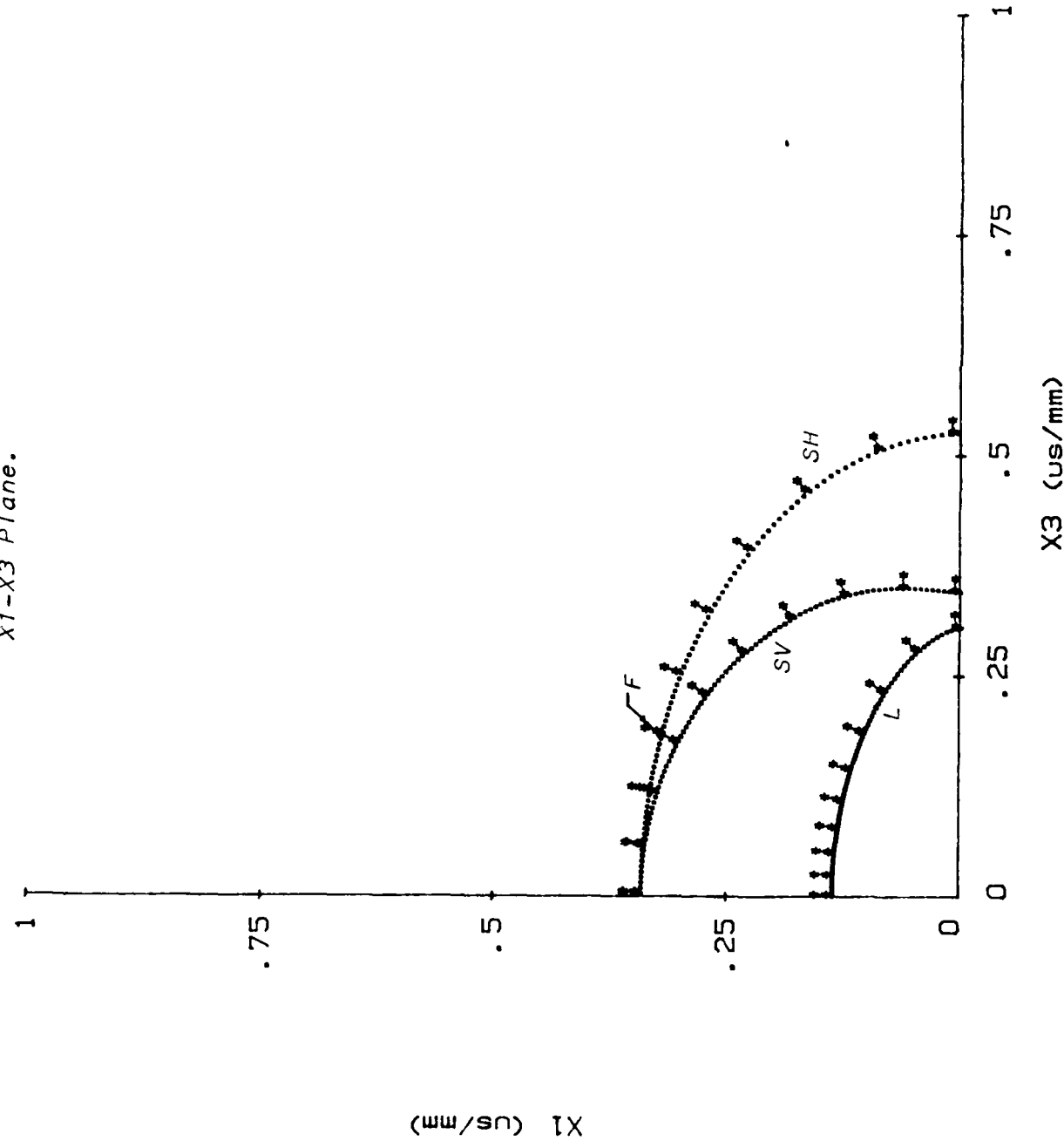
X_1 (us/mm)

SLOWNESS SURFACES- 0 DEG. BORON/EPOXY
*Figure 15: Slowness Sheet Intersection with
X1-X3 Plane.*



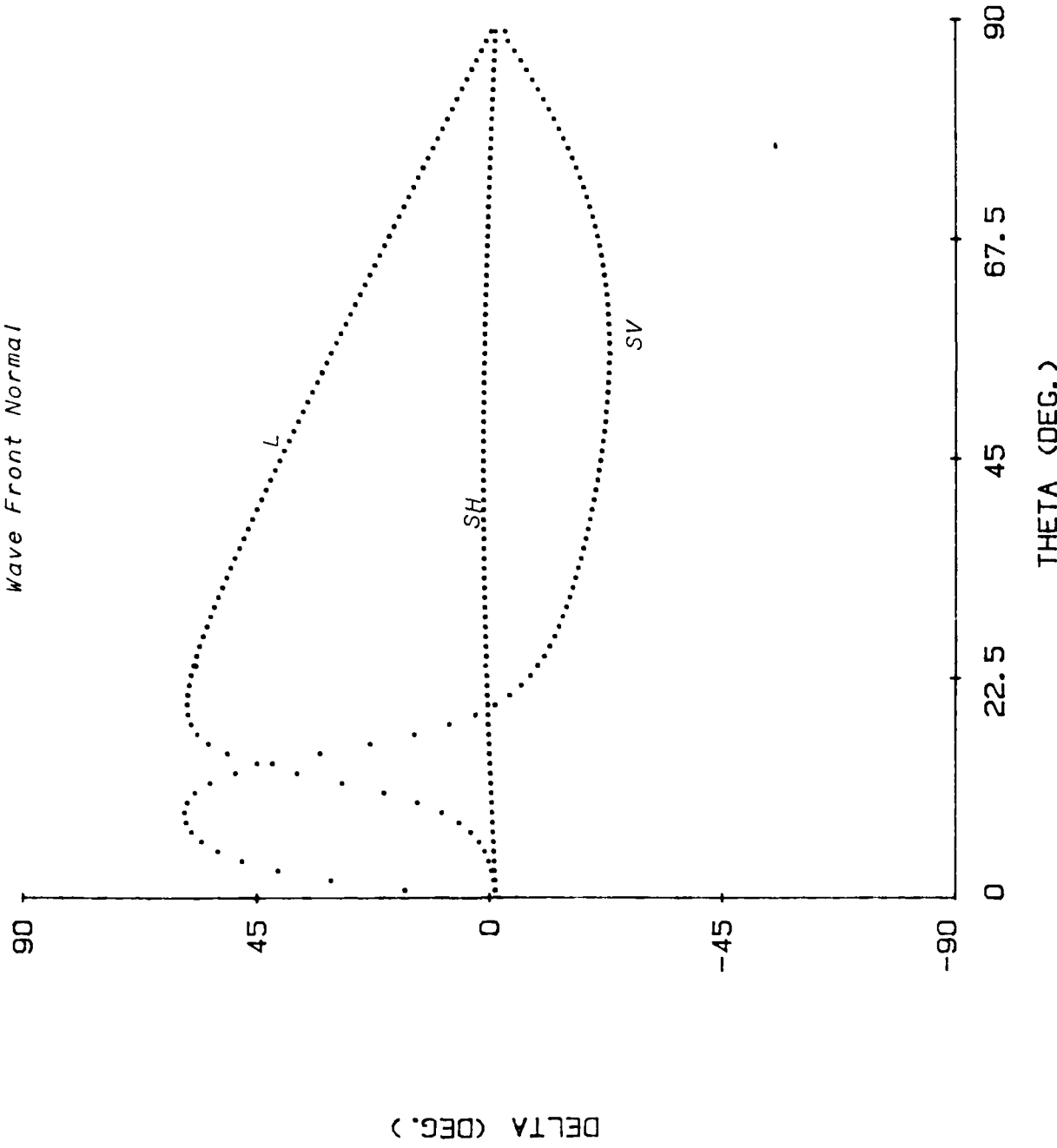
(μs/mm) X1

SLOWNESS SURFACES- 0 DEG. GRAPHITE/ALUMINUM
Figure 16: Slowness Sheet Intersection with
 X_1-X_3 Plane.



0 DEG. GRAPHITE/EPOXY

Figure 17: Energy Vector Deviation from Wave Front Normal



O DEG. AS/3501
*Figure 18: Energy Vector Deviation from
Wave Front Normal*

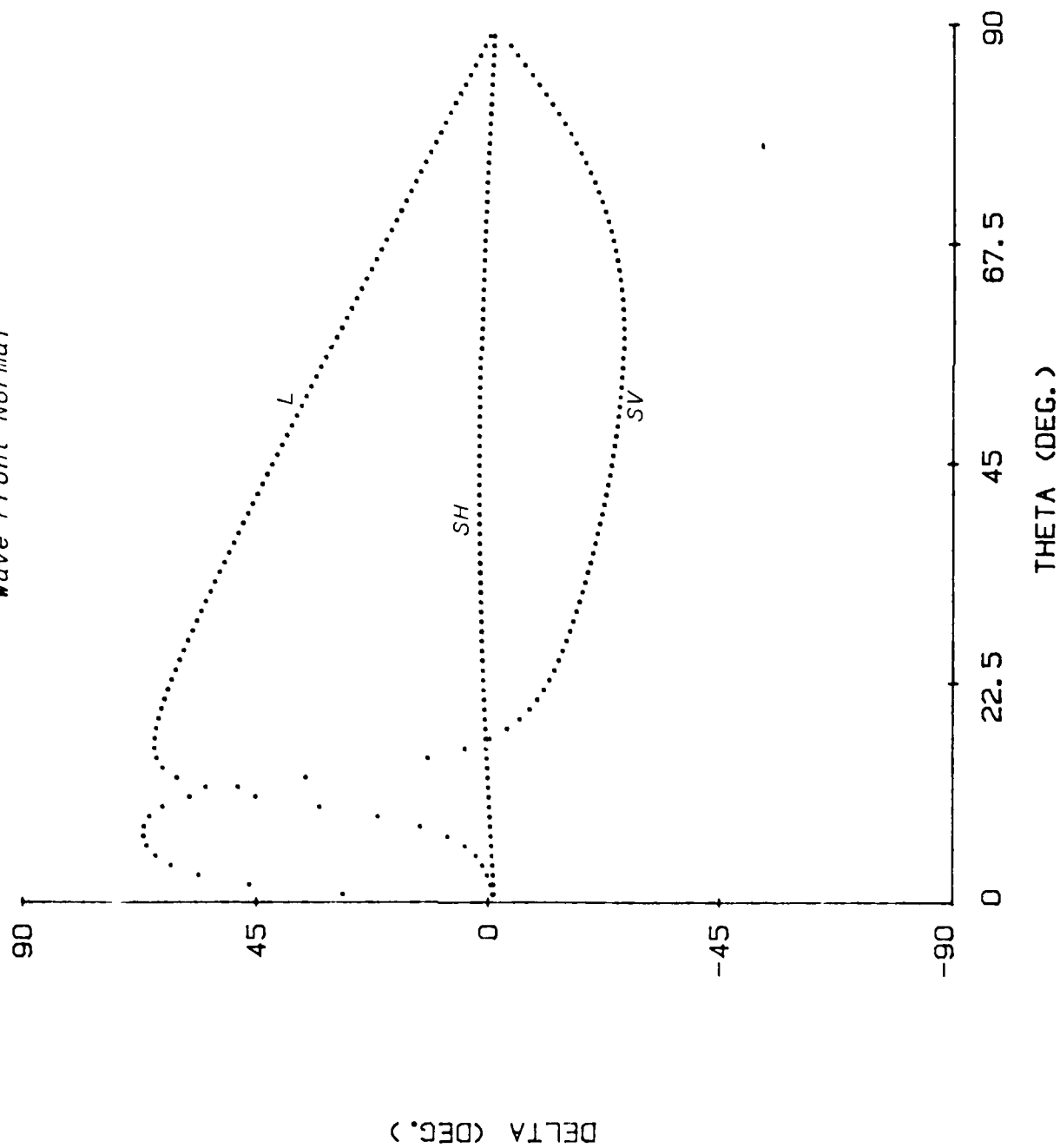
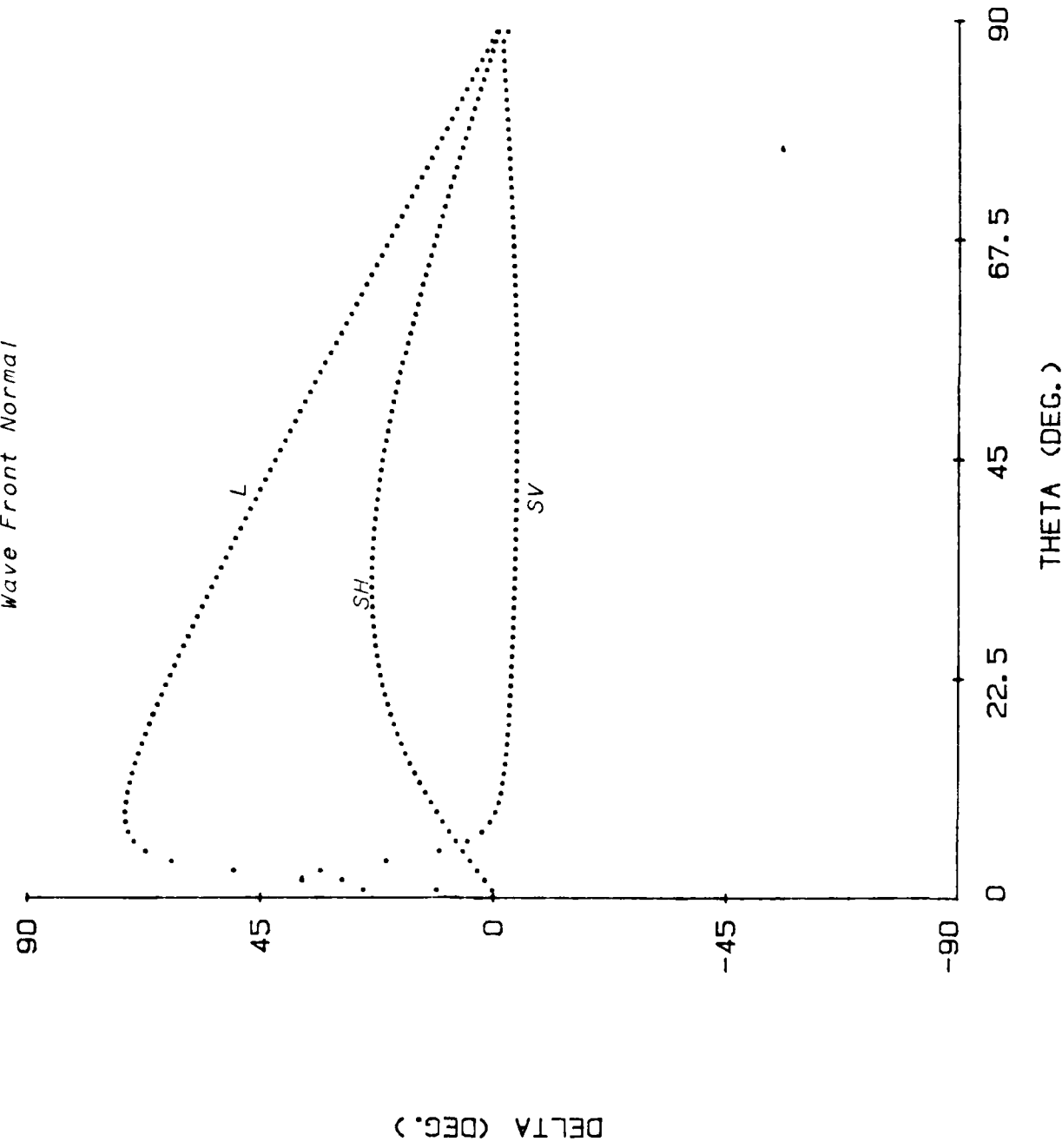
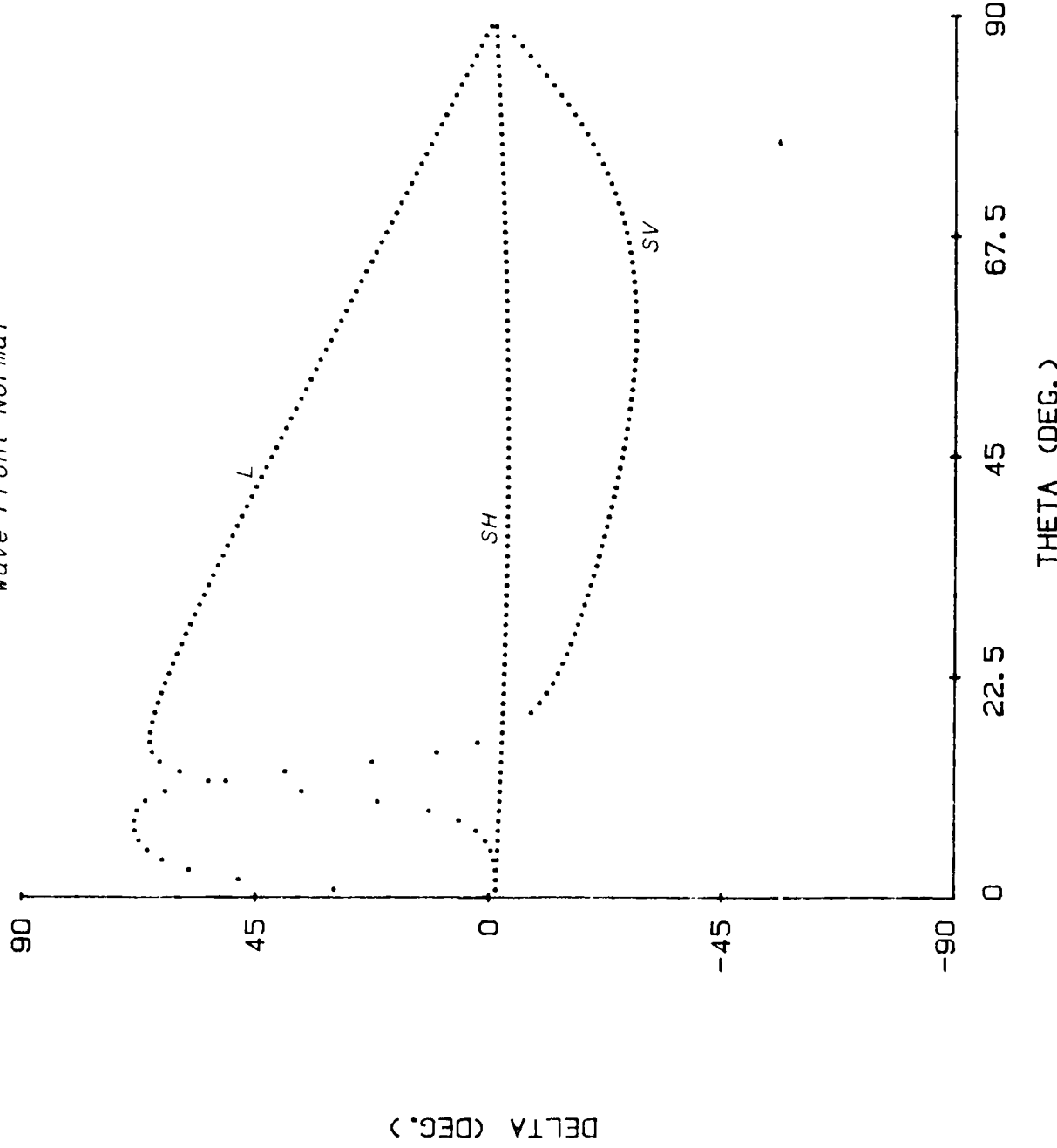


Figure 19: Energy Vector Deviation from Wave Front Normal
0 DEG. GY70/EPOXY

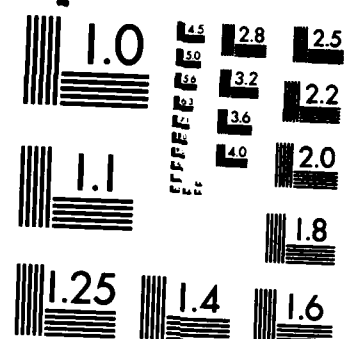


0 DEG. BORON/EPOXY
Figure 20: Energy Vector Deviation from
Wave Front Normal



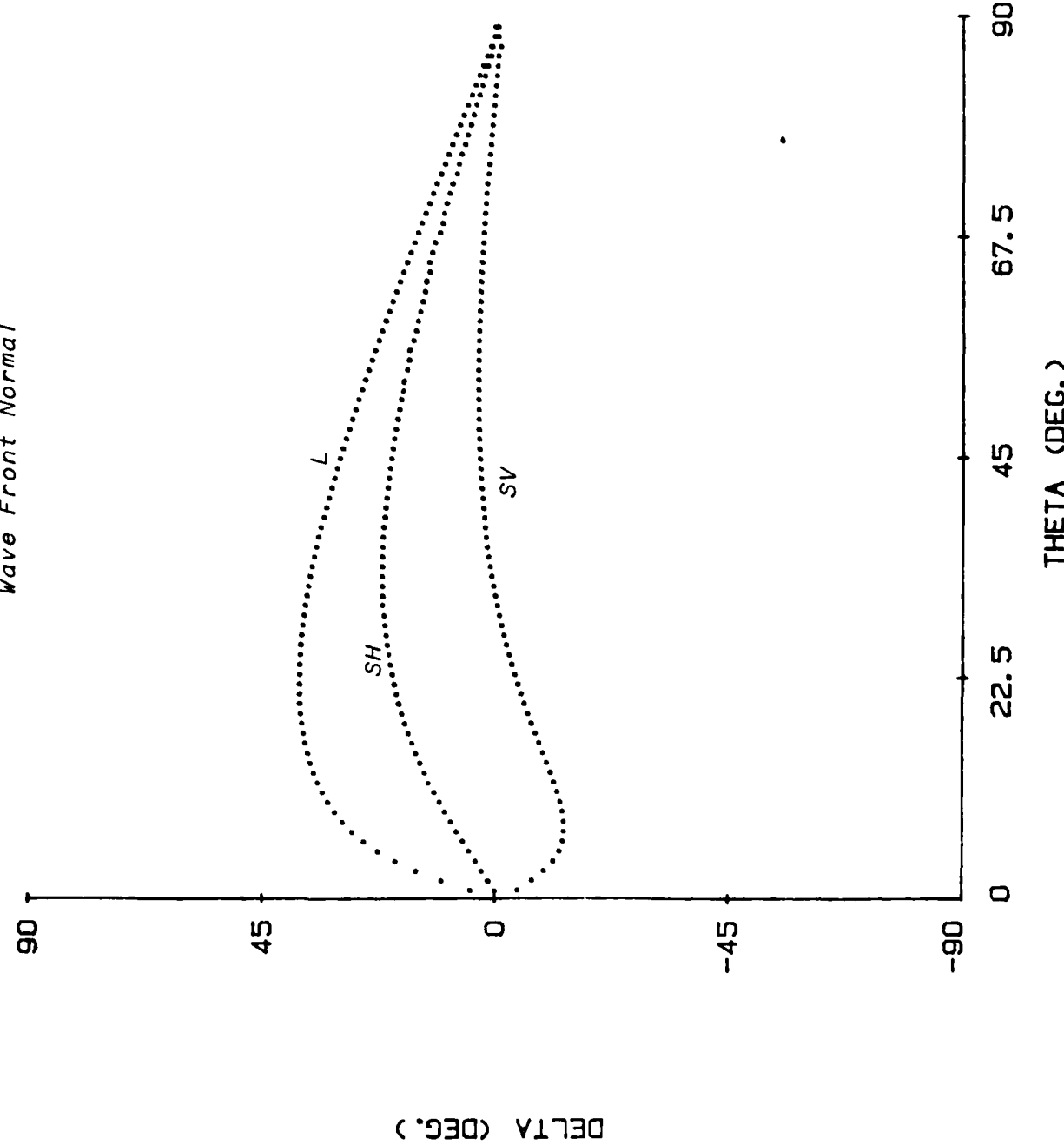
AD-A164 056 ULTRASONIC NONDESTRUCTIVE EVALUATION OF DAMAGE IN 2/2
CONTINUOUS FIBER COMPOS (U) TEXAS A AND M UNIV COLLEGE
STATION MECHANICS AND MATERIALS RE V K KINRA APR 85
UNCLASSIFIED MM-5024-85-7 AFOSR-TR-85-1227 AFOSR-84-0066 F/G 11/4 NL





MICROCOPY RESOLUTION TEST CHART
NATIONAL BUREAU OF STANDARDS-1963-A

0 DEG. GRAPHITE/ALUMINUM
*Figure 21: Energy Vector Deviation from
Wave Front Normal*



DELTA (DEG.)

Reference 1. Musgrave, M. J. P., "Crystal Acoustics", Holden-Day, Inc., 500
Sansome Street, San Francisco, California, 1970.

END

FILMED

3 - 86

DTIC